TAMPEREEN TEKNILLINEN YLIOPISTO
TAMPERE UNIVERSITY OF TECHNOLOGY

VILLE RAATIKAINEN

CONNECTIVITY MEASURES FOR IN VITRO NEURONAL CELL NETWORKS

Master's of Science thesis

Examiners: Professor Jari Hyttinen
and Dr. Jarno Tanskanen
Examiners and topic approved by the
Faculty Council of the Faculty of Computing
And Electrical Engineering on 7 November
2012

TIIVISTELMÄ

TAMPEREEN TEKNILLINEN YLIOPISTO
Sähkötekniikan koulutusohjelma
RAATIKAINEN, VILLE: Konnektiivisuusmitat in vitro mitatuille neuroniverkoille
Diplomityö, 59 sivua, 16 liitesivua
Toukokuu 2013
Pääaine: Lääketieteellinen fysiikka
Tarkastaja: professori Jari Hyttinen, tohtori Jarno Tanskanen
Avainsanat: kantasolut, MEA, hermosoluverkot, konnektiivisuusmitat, vaihelukitusarvo, yleistetty osittaiskohdennettukoherenssi, siirtoentropia

Sähköisesti aktiivisten solujen, kuten hermo- ja sydänsolujen aktiivisuus sisältää paljon fysiologisesti ja patofysiologisesti tärkeää informaatiota. Tämän vuoksi onkin tärkeää tutkia kuinka nämä hermosolut toimivat hermoverkkotasolla, jotta voimme ymmärtää kaikkia niiden toimintoja. Mikroelektrodi array –teknologian (MEA) avulla hermosolupopulaatioiden aktiivisuutta voidaan mitata in vitro –tutkimuksessa kasvattamalla samanaikaisesti soluja kasvualustalla, jossa on mittauselektrodeja. Tarvitsemme kuitenkin luotettavia menetelmiä, joiden avulla tätä MEA:lla mitattua informaatiota hermosoluverkkojen aktiivisuudesta voitaisiin tulkita.

Tässä diplomityössä tarkastellaan erilaisia konnektiivisuusmittoja, ja arvioidaan samalla kuinka käyttökelpoisia ne ovat MEA datan analysointiin. Kirjallisuusselvityksen pohjalta valitsemme kolme menetelmää käytännöntestaukseen. Valitut menetelmät ovat vaihelukitusarvo (eng. Phase Lock Value, PLV), yleistetty osittaiskohdennettukoherenssi (eng. generalized Partial Directed Coherence, gPDC) sekä siirtoentropia (eng. Transfer Entropy, TE) –menetelmät. Tutkimusdatana käytimme MEA:lla mitattuja signaaleja hermosoluverkoista, jotka oli muodostettu ihmisten alkiokantasoluista. Käytännön tutkimus jakaantuu kahteen osaan: simuloidun konnektiivisuuden sekä aitojen monikanavaisten verkkovasteiden analysointiin. Simuloitujen yhteyksien tutkimiseen valitsimme kaksi aitoa MEA:lla mitattua signaalia, joilla on hyvä signaali-kohina-suhde. Näistä signaaleista muodostimme muutaman signaalikombinaation käyttämällä alkuperäisiä signaaleja, ja luoden simuloituja yhteyksiä viivästäen ja summaten alkuperäisiä signaaleita. Lopuksi tarkastelemme lyhyesti menetelmien antamia tuloksia aidoille monikanavaisille verkkovasteille vertailemalla 6-kuoppaisen MEAn tuloksia kahden farmakologisen välittäjäaineen; bicuculline (eksitoiva) ja cnqx+dap5 (inhiboiva) tapauksessa. Tässä työssä keskityimme käsittelemään paikallisia kenttäpotentiaaleja.

Simuloitujen yhteyksien tutkimus viittaa siihen, että PLV-menetelmä tunnisti luotettavasti yhteydet, kun taas gPDC-menetelmä antoi epäluotettavia tuloksia. TE-menetelmä tarjosi monipuolisimmat tulokset, mutta tuloksissa oli muutamia epätarkkuuksia. Simulaatiotulosten pohjalta TE- ja PLV-menetelmät vaikuttavatkin potentiaalisilta lisätutkimuksia varten. Aidon MEA datan analyysi antoi kuitenkin hieman ristiriitaisia tuloksia. Esimerkiksi PLV-menetelmä tulkitsi yhteyksiä aidon datan tapauksessa myös niiden signaalien välille, joilla sitä ei kuulunut olla. Lisätutkimus onkin tarpeen, jotta tiedämme johtuvatko nämä väärät analyysitulokset mittausympäristöstä vai menetelmästä itsestään, vai onko kyse erityisesti 6-kuoppaisen MEAn signaalien laatuongelmasta. Tarvitsemme myös lisätutkimusta, jotta voimme määrittää kuinka eri parametrit kuten signaalien laatu, hermosolujen aktiivisuuden määrä ja signaalien keskinäiset viiveet vaikuttavat menetelmien toimivuuteen ja luotettavuuteen.

ABSTRACT

TAMPERE UNIVERSITY OF TECHNOLOGY
Master's Degree Programme in Electrical Engineering
RAATIKAINEN, VILLE: Connectivity Measures for In Vitro Neuronal Cell Networks
Master of Science Thesis, 59 pages, 16 Appendix pages
May 2013
Major: Medical Physics
Examiners: Professor Jari Hyttinen, Dr. Jarno Tanskanen
Keywords: stem cells, MEA, local field potentials, neuronal cell networks, Phase Lock Value, Partial Directed Coherence, Transfer Entropy

Network activity of electrically active cells such as neuronal cells and heart cells underlies fundamental physiological and pathophysiological information. To be able to understand all these functions, it is essential to study how neuronal cells work in concert in neuronal network level. With microelectrode array (MEA) technology, the electrical activity of the neuronal cell population can be measured while the cells grow *in vitro* on a growth plate with embedded recording electrodes. In order to interpret the measured information with MEAs, we need reliable methods and measures to analyse the connectivity properties of neuronal cell networks. This thesis examines different connectivity measures and evaluates how applicable they are for MEA data analysis.

Different connectivity measures are reviewed in detail in order to investigate what kind of information they provide, what are the advantages and limitations of them. Based on the literature review comparison, we selected three methods; Phase Lock Value (PLV), generalized Partial Directed Coherence (gPDC) and Transfer Entropy (TE). The selected methods were tested and evaluated with the data from human embryonic stem cell derived neuronal cell (hESC) networks which are cultured on MEAs. The analysis is divided into two parts: simulated connectivity signal studies and real MEA data analysis. The simulated connectivity signal study is performed in such a way that first two measured real signals with good signal-to-noise ratio are selected. Secondly, few combinations of three signals are created from the selected signals by making modifications such as adding delays and summing signals together. In real MEA data analysis, we explore and compare the results of the same well in the case of two different pharmacological measurements: bicuculline (excitative) and cnqx+dap5 (inhibitive) based on the findings of simulation study. All analysis is done with local field potentials frequencies below 300 Hz.

The simulation study indicates that PLV method correctly recognized the connections, while gPDC provided unreliable results. TE provided the most detailed results only with few inaccuracies. Based on the simulation results, TE and PLV seem potential for further research on MEA signals. However, incoherent results were obtained in real MEA data analysis. For example, PLV claimed connections between signals measured from different wells. Based on the results, further research is needed in order to assess whether the incoherencies are influenced by the measurement environment, the methods themselves, or by the quality problem of signals in 6-well MEA. Further research is also needed in order to investigate how certain parameters such as noise level, spikes and interaction delay affect the applicability of the methods.

PREFACE

This master's thesis work has been done at the Department of Electronics and Communications Engineering at Tampere University of Technology and BioMediTech where I have worked since May 2012. This work was done for the 3DNeuroN project called Biomiking the Brain – towards 3D Neuronal Network Dynamics.

Firstly, I would like to thank especially my supervisor and employer Prof. Jari Hyttinen who gave me this great opportunity to work with this new and interesting project. This interesting topic was a great motivator to me on those situations when it seemed that the work was progressing very slowly. Great thanks also to my second supervisor Dr. Jarno Tanskanen. He gave especially good advices relating to the structure and content of the thesis. Both of my supervisors were always eager to help when I needed. I have obtained much new valuable information during this work.

Special thanks also to my colleagues here at our department. You provided a great atmosphere to work with. Moreover, I'd like to thank those many scientists abroad whom I have emailed with. Especially Prof. Michael Wibral from Goethe University, Frankfurt, gave a great help when I was learning new software relating to this work.

Finally, I would like to thank my dear life partner Maria. You have encouraged me and been always there to listen. Without you, this would have felt much more difficult. Thanks also to my nearest relatives and friends who have cheered me up during this journey.

In Tampere 10.05.2013

Ville Raatikainen

Contents

ABBREVIATIONS AND SYMBOLS

ADTF	Adaptive Directed Transfer Function.
AIC	Akaike Information Criterion
ACF	Auto-correlation function
AMVAR	Adaptive multivariate autoregressive
BCI	Brain computer interface
BSSM	Bilinear state space model
CC	Cross-correlation
cISI	Cross-inter-spike-intervals
CM	Connectivity matrix
CMOS	Complementary metal-oxide-semiconductor
CNS	Central nervous system
DC	Direct current
DCM	Dynamic Causal Modeling
dDTF	Direct directed transfer function
DTF	Directed transfer function
ECoG	Electrocorticography
EEG	Electroencephalography
ERP	Event-related potential
ESC	Embryonic stem cell
ffDTF	Full frequency directed transfer function
FDR	False discovery rate
FFT	Fast Fourier Transform
fMRI	Functional magnetic resonance imaging
GABA	Gamma-aminobutyric acid
GC	Granger Causality
GUI	Graphical user interface
gPDC	Generalized Partial Directed Coherence
hESC	Human embryonic stem cell
hiPSC	Human induced pluripotent stem cell
iPSC	Induced pluripotent stem cell
JE	Joint-Entropy
LFP	Local field potential
MEA	Microelectrode array or multielectrode array
MEG	Magnetoencephalography
MI	Mutual Information
ML	Maximum likelihood
MVAR	Multivariate autoregressive model
PET	Positron emission tomography
PDC	Partial Directed Coherence
PLV	Phase Lock Value

ROI	Region of Interest
SEM	Structural Equation Modeling
TE	Transfer Entropy
TiN	Titanium nitride
TRENTOOL	The Transfer Entropy Toolbox
$\mathbf{\Lambda}(f)$	Matrix of model coefficients
$\Phi(t)$	Instantaneous phase of the signal
$\boldsymbol{\theta^2_{ij}(f)}$	The Directed Transfer Function (DTF)
$\boldsymbol{\gamma^2_{ij}(f)}$	Normalized Directed Transfer Function
$\boldsymbol{\pi_{ij}(f)}$	Partial Directed Coherence (PDC)
$\boldsymbol{\eta^2_{ij}(f)}$	The full frequency DTF (ffDTF)
$\boldsymbol{\delta_{ij}(f)}$	Direct DTF (dDTF)
$\mathbf{Z}$	Vector of equation errors (random disturbances)
$\mathbf{\Gamma}$	Matrix of coefficients of the exogenous variables
T	Time lag or time shift
$\mathbf{B}$	Matrix of coefficients of the endogenous variables
Ca^{2+}	Calcium ions
cISI	Cross-inter-spike-intervals
$\mathbf{e}(t)$	Vector of multivariate zero-mean uncorrelated noise
$\mathbf{H}(f)$	Inverse of the frequency-transformed coefficient matrix
$\mathbf{I}$	Identity matrix
JE	Joint-Entropy
$k_{ij}(f)$	Coherence
K^+	Potassium ion
$\mathbf{L}$	Lead field matrix
Na^+	Sodium ion
MI	Mutual Information
P	Model order
PLV	Phase Lock Value
s(t)	Time series signal
$\hat{s}(t)$	Hilbert transform of the signal *s(t)*
$\mathbf{S}(f)$	Power spectra
Δt	Temporal interval between two time samples
TE	Transfer Entropy
U	Prediction time
$\mathbf{V}$	Variance matrix
V_m	Plasma membrane voltage
$\mathbf{X}$	Vector of independent (exogenous) variables
$\mathbf{x_t^{dx}}$	Delay vector
$\mathbf{X_{ij}}(f)$	Partial Coherence
$\mathbf{Y}$	Vector of dependent (endogenous) variables

$\mathbf{y}_t^{dy}$	Delay vector
$\mathbf{y}(t)$	Data vector
$z(t)$	Analytical signal
$\mathbf{Z}$	Matrix of the observed variables

1 INTRODUCTION

Network activity of electrically active cells such as neuronal cells and heart cells is based on fundamental physiological and pathophysiological phenomena. Despite the known properties of single neuronal cells, ion channels and synapses, it is believed that only a collective effort of many cells create what is commonly called as self-awareness. Especially, a wide range of pathophysiological conditions such as Parkinson's disease, Alzheimer's disease and epilepsy have been shown to rely on many neuronal cells to form these conditions. Moreover, all higher brain functions such as spatial awareness, associative learning, and pattern and speech recognition, memory acquisition and retrieval depend on synchronized activity of many neuronal cells in space and time.

To be able to understand all these functions, it is essential to study how neuronal cells work in concert in neuronal network level. Microelectrode array (MEA) technology provides us a way to measure the electrical activity of a neuronal system at the network level. With MEAs, the electrical activity of neuronal cell populations can be measured while the cells grow *in vitro* on a growth plate with embedded recording electrodes [1]. MEA recordings provide information about the temporal and spatial distribution of electrical activity which is generated by neuronal cell populations near the recording electrodes. The neuronal cell cultures can be examined for long periods of time, observing network development from the stage of isolated neuronal cells into the fully connected neuronal cell networks. Despite the simplified level of cell culture organization on MEA, the system reveals essential knowledge regarding to developmental changes in the activity patterns, electrophysiological properties and basic learning mechanisms of the nervous system. The human embryonic stem cells (hESCs) are excellent for these studies as they have nearly unlimited developmental capacity and can continue to replicate and maintain their ability to differentiate into any cell type of human body even after months of growth [2]. In addition to hESCs studies, MEAs have been used for several studies in order to investigate the behaviour of cultured neuronal networks [3]-[5].

Although the neuronal cell populations and MEA technologies provide an excellent platform to study the properties of neuronal cell networks, we still need the tools to interpret the information contained in the measured on MEA signals. Connectivity measures are mathematical tools that describe relationships between signals. Connectivity can be considered at different levels: from neuronal cells, via neuronal cell microcircuits to brain structures. Among the estimators of connectivity, there are non-linear, linear, bivariate and multivariate measures which provide different kinds of information. Some provide causal information, while some don't and some allow

directional information flow to be studied while the others do not. Numerous studies have been performed with different connectivity measures such as Phase-Lock Value (PLV) [6], Multivariate Autoregressive Models (MVARs) [7]-[11], Statistical Methods [12]-[13] and Information Theory based methods [14]-[15]. Despite the numerous studies of connectivity measures being made, most of the studies have been made for electroencephalography (EEG) [6]-[8],[12],[13] electrocorticography (ECoG) [6],[9], magnetoencephalography (MEG) [13],[15], whereas the studies of connectivity of MEA signals have aroused less attention [14].

In this master's thesis, different connectivity measures are reviewed. Few connectivity measures, Phase Lock Value (PLV), generalized Partial Directed Coherence (gPDC), and Transfer Entropy (TE) are chosen for a deeper analysis. PLV is a bivariate measure that gives undirectional information whereas gPDC and TE offer directional information. PDC is the most widely accepted method of Multivariate Autoregressive models so we decided to use the enhanced and generalized form of it – gPDC. In the study made by Garofalo et al. [14] it was suggested that TE provides the best and most reliable results of Information Theoretic measures. In that study, they extracted dissociated cortical neuronal cells from rat embryos and plated then on 60-channel MEAs. We were also interested in comparing results between PDC and TE, as PDC analysis requires the use of a linear stochastic model, whereas TE does not require a model of the interaction. The selected methods were tested and evaluated with the data from human embryonic stem cell derived neuronal cell (hESC) networks which are cultured on MEAs. The analysis is divided into two parts: simulated connectivity signal studies and real MEA data analysis. In real MEA data analysis, we explore and compare the results of the same well in the case of two different pharmacological measurements: bicuculline (excitative) and cnqx+dap5 (inhibitive). In this study, we concentrate on local field potentials which here are taken to occur on the frequencies below 300 Hz [16], excluding direct current (DC).

2 NEURONAL CELLS AND NETWORKS

2.1 Anatomy of a neuronal cell

There are different types of neuronal cells in a human body. Generally, they can be categorized into three different groups: 1) sensory neuronal cells, which convey sensory information, 2) motor neurons, which convey motor information and 3) inter neurons, which convey and process information between different types of neuronal cells. [17] The fundamental task of neuronal cells is to receive, conduct and transmit signals. They carry signals from the sense organs towards the central nervous system (CNS) which consists of spinal cord and brain. In the CNS the signals are interpreted and analysed by a system of neuronal cells, which then produce an output response. The response is then sent by neuronal cells back for action to glands and muscle cells. [18]

Different neuronal cell types differ by shapes and size, but they all have some common features as presented in Figure 1. The four morphologically defined regions are the cell body, dendrites, axon, and presynaptic terminals. The cell body, or soma, contains the nucleus and other cell organelles such as endoplasmic reticulum and mitochondria. The branches of dendrites receive signals from other neuronal cells, whereas an axon conducts signals away from the cell body. [18] A neuronal cell may have many thousands of dendrites, but it will have only one axon [17]. The most of the axons in vertebrates are sheathed in myelin, which is formed by either two types of glial cells: oligodendrocytes insulating those of the central nervous system and Schwann cells sheathing peripheral neuronal cells. The myelin sheath allows much faster action potential propagation than possible in unmyelinated neuronal cells. The presynaptic terminals are the distinct parts of neurons that contain neurotransmitters. These are the chemical media which transfer signals from one neuronal cell to the next at chemical synapses. [17] The combined number of neuronal cells and glial cells in the human body is estimated to be around 10^{12}. The length of an axon varies from less than 1 mm to 1 m meter depending on the type of neuronal cell, and the diameter varies between 0.1 µm and 20 µm. [18]

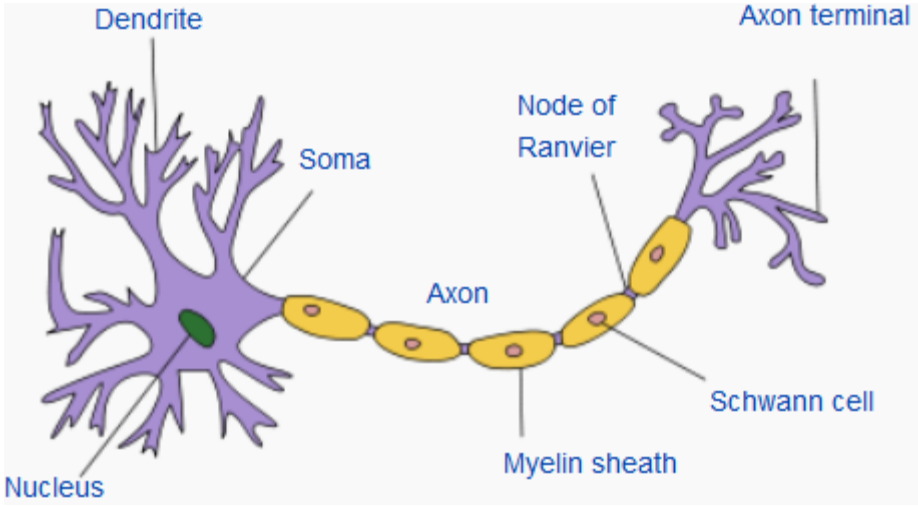

Figure 1. *The structure of a neuronal cell. [19]*

2.2 Neuronal signalling

To support the general function of the nervous system, neuronal cells have evolved to possess unique capabilities both for communication between cells (intercellular signalling) and within the cell (intracellular signalling). Action potentials propagating along neuronal cells enable fast communication over long distances. [17] The traveling action potential wave has a speed up to 100 m/s depending on the cell type [18]. This mechanism how the body of the cell communicates with its own terminals via its own axon is called conduction. Whereas, the mechanism how the neuronal cells communicate with other neuronal cells at synapses is called the neurotransmission. [17]

To begin with conduction, an action potential is generated at a location in the soma, called axon hillock. The action potential is triggered, if the combined electrical stimulus at the hillock exceeds a certain threshold. Normally the resting potential of the cell membrane rests at around -70 mV. A decrease in the membrane potential is called depolarization, whereas an increase in the membrane potential is called hyperpolarization. Depolarization causes action potential if certain membrane potential threshold is exceeded, whereas the hyperpolarization tends to block action potential generation. Hence, a hyperpolarizing signal is inhibitory and a depolarizing signal is excitatory. [18]

A sudden depolarization of the plasma membrane is caused in many cases by ionic current, which results from stimuli by neurotransmitters released to the dendrites from other neuronal cells. The voltage-gated channels in the plasma membrane are affected when the depolarization exceeds a certain threshold level (for example from -65 mV to -55 mV). First, the sodium channels at the site open, which leads to the situation that the higher Na^+ concentration on the outside of the axon drives these ions to move into the axon. Thus, the sodium ions flow along the electrochemical gradient from outside to inside the axon. This flow of positive ions into the axon further strengthens the depolarization, so that the voltage V_m of the plasma membrane continues to increase. [18] When the voltage is still negative but continues to increase, the potassium channel

at the site begins to open up, which enables the positive K^+ ions to flow out along the electrochemical gradient. However, as long as the sodium channels are still open the voltage nevertheless continues to increase. Soon the sodium channels start to shut down and remain in that state for a period of time called refractory period. While the sodium channels are closed in the refractory period, the potassium channels remain open so that the membrane potential (which typically arises to +50 mV) starts to decrease, eventually going to its initial depolarized position. The propagation of the action potential is illustrated in Figure 2. In this way, step-by-step, the action potential moves along the membrane without a significant weakening. [18]

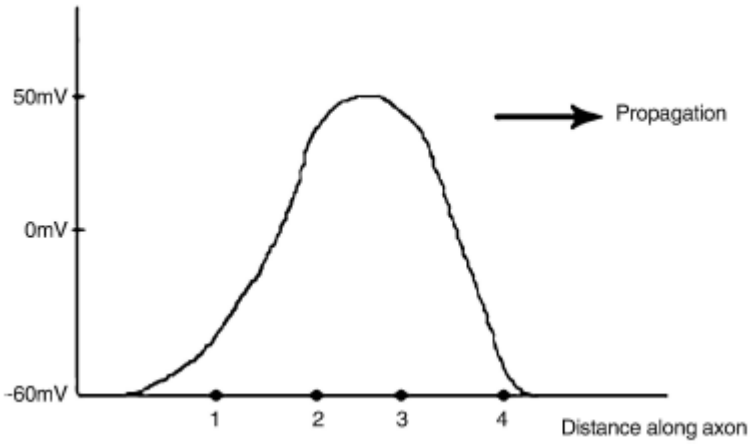

Figure 2. *Propagation of the action potential. 1: Na^+ channels open, 2: K^+ channels open, 3: Na^+ channels close, 4: K^+ channels close. [18]*

As the action potential arrives to neural terminal, it allows the communication between neuronal cells via neurotransmission. The other cell where the signal will be transmitted might be another neuronal cell or muscle cell. The spacing through which the signal will be transmitted is called a synaptic cleft. The synaptic transmission can be achieved in two different ways, either by chemical or electric transmission. Figure 3 shows a chemical synaptic transmission. It involves several steps: the voltage-gated Ca^{2+} channels near the synaptic end start to open up when the action potential arrives at the presynaptic axon. Then calcium ions begin to flow into the presynaptic region and cause the vesicles containing the neurotransmitters to fuse with the cytoplasmic membrane and release their content into the synaptic cleft. The released neurotransmitters will bind then to the specific protein receptors on the postsynaptic membrane after they have diffused across the synaptic cleft. This binding will trigger the protein receptors to open (or close) channels, thereby changing the membrane potential to a depolarizing (or a hyperpolarizing) state. [18]

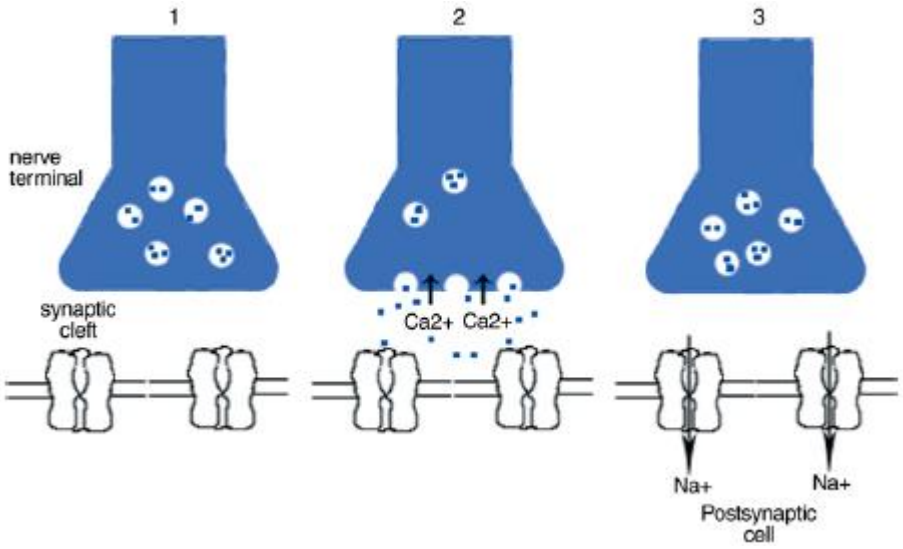

Figure 3. *Synaptic transmission at chemical synapses. 1. The action potential arrives. 2. Ca^{2+} flows in, vesicles fuse to cytoplasm membrane, and release their contents to the synaptic cleft. 3. Postsynaptic (for example Na^{+}) channels open and Ca^{2+} ions return to vesicles. [18]*

When the action potential makes direct electrical contact with the postsynaptic cell, this process is called electrical transmission. The gap junction in electrical transmission is very narrow, being only around 3.5 mm. In contrast to chemical transmission, electrical transmission incurs no time delay, no variability, is bidirectional between two neuronal cells, and requires no threshold. [18] Whereas, the chemical transmission incurs time delay and some variability due to the associated diffusion processes, it is a unidirectional, and it requires a threshold of the action potential.

2.3 Neuronal cell networks

When neuronal cells evolve, they start to develop connections to other neuronal cells and form neuronal cell networks. A neuronal cell network is composed of a group or groups of functionally associated or chemically connected neuronal cells. Like stated before, connections called synapses are usually formed from axons to dendrites which enables electrical signalling but there are also other forms of signalling that arise from neurotransmitter diffusion. Some signals act as inhibitions and others as excitations to a neuronal cell firing. Dendrites feed the action potentials to the soma of the neuronal cell, which collects the potentials and determines whether their sum exceeds a threshold. If the threshold is exceeded, the neuronal cell fires and electrical impulses are generated via axon to other connected neuronal cells in the network. Series of action potentials is called spike train. [18]

Neuronal cell networks typically consist of numerous different neuronal cells. It has been estimated that there are around hundred billion (100,000,000,000) neuronal cells in the human brain, each connected to as many as 1 000 other neuronal cells [20]. Neuronal cell networks typically compose of layers, which connect different group of

neuronal cells together. A simplified version of the structure of neuronal cell network is presented in Figure 4. The input layers refers to the input where the incoming signals are generated, whereas the hidden layer describes the groups of neuronal cells which conduct and process the information (signals) and finally, the output layer describes the response of neuronal signalling.

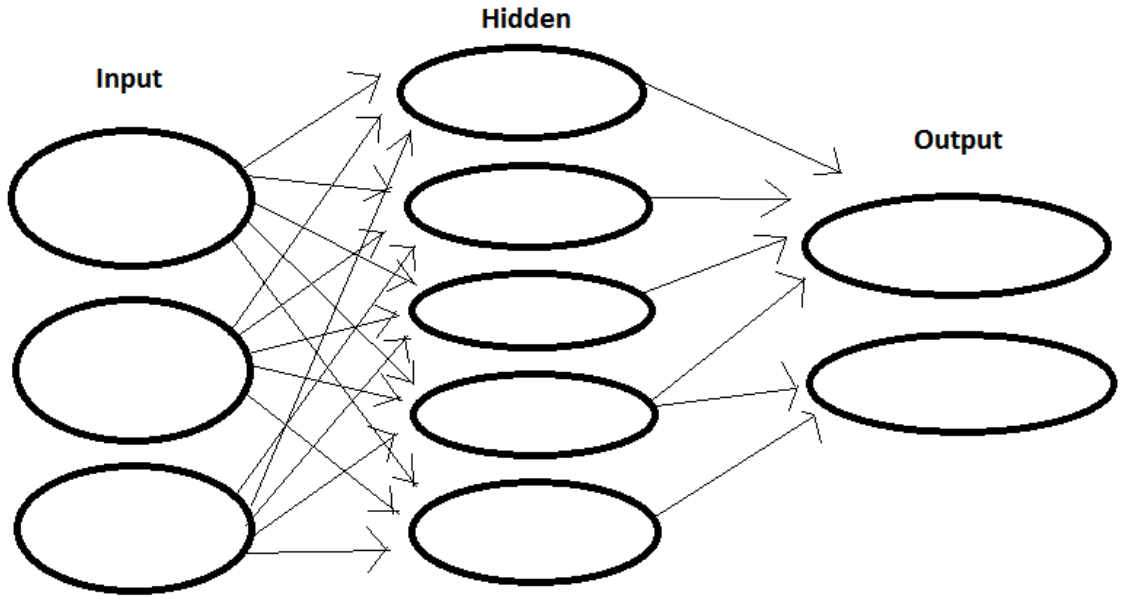

Figure 4. *A simplified version of neuronal cell network.*

Neural oscillation is repetitive or rhythmic activity in neural tissue. Neural tissue can generate oscillatory activity in multiple ways, driven either mechanisms localized within individual neuronal cells or by interactions between different neuronal cells. Oscillatory activity in groups of neuronal cells typically arises from feedback connections between neuronal cells that result in the synchronization of their firing patterns. The oscillations can occur at different frequency than the firing frequency of individual neuronal cells based on the interaction between neuronal cells.

Neural oscillations are observed throughout the neural tissue and at all levels, e.g., local field potentials, spike trains and large-scale oscillations. Neuronal cells can generate rhythmic patterns of action potentials or spikes. Bursting is another type of rhythmic spiking. It is an extremely diverse and general phenomenon of the activation patterns of neuronal cells where periods of rapid spiking are followed by silent, quiescent periods. Oscillations can be characterized by their amplitude, phase and frequency. Information is thought to be encoded in terms of the frequency of the action potential, called firing or spiking rate (i.e., rate coding), as well as in the timing of action potentials (i.e., temporal coding) [21].

Neural oscillations can be analysed using mathematics. There are different class of models which try to emphasize the behaviour of neural dynamics at different levels. The neural models can be divided into different categories such as single neuron model,

spiking model and neural mass model. Single neuron models are mathematical descriptions of the properties of neuronal cells that are designed to accurately predict and describe its biological processes [21]. Spiking models describe larger population of physically interconnected neuronal cells or a group of disparate neuronal cells whose inputs define a recognizable circuit. These models aim to describe how the dynamics of neural circuitry arise from interactions between individual neuronal cells. Neural mass models are another tool in studying neural oscillations and variables such as mean firing rate in space and time [21]. Instead of modelling individual neuronal cells, this approach approximates a group of neuronal cells by its average interactions and properties.

2.4 Stem cells

Stem cells have specific properties as they can divide in an undifferentiated stage and differentiate then into a specific cell or cells depending on their differentiation capacity. Stem cells can be divided into three categories based on their differentiation capacities: 1) totipotent cells can form a new individual such as fertilized egg and very early embryo; 2) pluripotent cells can differentiate into any organ or cell type; and 3) multipotent cells have more limited capacity in their differentiation (for example fetal and adult stem cells). [22]

Human embryonic stem cells (hESCs) belong to the pluripotent stem cells which have nearly unlimited developmental capacity. They can continue to replicate and maintain their ability to differentiate into any cell type of human body even after months of growth [2]. Due to these unique properties and their huge potential in medical and pharmacologic applications, they can be widely used for transplantation therapies or in different *in vitro* models, such as developmental, toxicological and drug screening models [23], [24]. Much effort has been applied to optimize hESC culture conditions.

Induced pluripotent stem cells (iPSCs) are one of the newest pluripotent stem cell types. Gene transduction is used to revert these cells from fibroblasts to the stem cell stage [22]. The behaviour of these reprogrammed cells is very similar to hESCs, but much more information is needed about their pluripotent gene-silencing and behaviour during differentiation before they can be used in clinical studies [25]. Both human induced pluripotent stem cell – differentiated (hiPSC) and hESC-differentiated cells, however, show line-specific differences in their differentiation potential [25]. Nevertheless, both of these pluripotent stem cell types have been differentiated into neuronal cell types, including electrically functionally oligodendrocyte and astrocyte neuronal cells.

Multipotent stem cells (including fetal stem cells) have also a high potential for different clinical applications since they carry a smaller risk of tumour formation compared to cells which have embryonic stem cell (ESC) origin [26], [27]. Fetal stem cells have ethical complexities and limited availability, whereas adult stem cells can be harvested from bone marrow, cartilage, fat tissue, blood and placenta. However,

production of sufficient amounts of neuronal cells for transplantation therapies is very challenging, since these cells have a limited differentiation capacity. [22]

2.5 Cell culturing

Cell culture refers to the removal of cells from their natural environment (for example from animal) and growing them in a favourable artificial environment. The cells can be removed from the tissue and disaggregated by mechanical or enzymatic means before cultivation, or they can be derived from a cell strain or cell line that has already been established. [28] In practise, the term cell culture refers to the culturing of cells which are derived from eukaryotic cells, especially from animal cells. The term may also, however, refer to the culturing of other cells like plants, fungi and microbes, including viruses, bacteria and protists. The culture allows the cells to act as independent units, much like micro-organism such as a bacterium. The cells can grow in size and divide unless their behaviour is controlled with some culture variable such as nutrient depletion. [29]

When the cells are derived from donor tissue, they can be maintained in a number of different ways. A simple fragment of tissue can be adhered to the growth surface either spontaneously or by mechanical means. These mechanical means can be a plasma clot or an extracellular matrix constituent such as collagen, which will usually give rise to an outgrowth of cells. [29] Initially, cultures were prepared on glass for ease of observation, but cells may also be cultured on many different charged surfaces including many polymers and metals. The scaffolds have the same requirements as conventional substrates in terms of low toxicity and ability to promote cell adhesion. In generally, scaffolds should be made of clinically approved biocompatible materials. The structure of scaffold determines the transport of nutrients, regulatory molecules and metabolites to and from the cells, whereas the scaffold chemistry may have an important role in cell differentiation and attachment. [29]

Cell culture is one of the major tools used in molecular and cellular biology. It provides excellent model systems for studying the normal biochemistry and physiology of cells, for example aging and metabolic studies. It also provides model systems for studying the effects of toxic compounds and drugs, and carcinogenesis and mutagenesis. It is also used in drug screening and development, and large scale manufacturing of biological compounds. The major advantage of using cell culture is the reproducibility and consistency of results that can be obtained using a batch of cells. However, the disadvantage is that, after the cells have grown some certain period, cell characteristics can change and may differ from those found in the starting population. Cells may also adapt to different culture environments like different nutrients and temperatures by varying the activities of their enzymes. [28]

3 MICROELECTRODE ARRAYS (MEAS)

3.1 Measurement principle

The electric properties of the neuronal cells can be measured either extracellularly or intracellularly. In extracellular measurements, the local differences of extracellular space ion concentrations for example potential are measured. Extracellular measurements are also used to detect the local field potentials of the neuronal networks. The frequency range of local field potentials is difficult to define precisely but some authors have defined them to occur in the frequencies below 300 Hz [16]. Extracellular methods are concentrated on network and thus the most important measured parameters are spontaneous activity of the neuronal network, excitability of the neuronal network, plasticity of the neuronal network, and responses to pharmaceutical and electrical stimulation [30]. In intracellular recordings, the electrical potential across the membrane is measured. In these methods, the most important measured parameters are passive membrane potential, cell excitability, and ion channel kinetics [30].

Patch clamp and MEAs are used in the measurements of electrical activity of the cell so it is convenient to state the main differences of these two. Patch clamp method is used for both intracellular and extracellular measurements, but usually for intracellular measurements. It allows measuring the electrical activity of individual cells. It provides excellent information about membrane potential, excitability and the ion channel composition of the cells. Patch clamp method can be further divided into current clamp and voltage clamp techniques. [30]

Whereas patch clamp method is used invasively to provide information of the electrical activity of an individual cell, MEA measurements are used to examine network activity. With MEA, the activity of neuronal cell network can be non-invasively measured *in vitro* for long periods of time, and the real-time monitoring can be performed and cultures can be stimulated at the same time. MEA provides a method for analysing spatiotemporal signalling activity at the neuronal network level, where both stimulated and spontaneous activity can be measured. The stimulation can be either electrical or pharmacological stimulus. MEAs also provide information about developmental changes in activity patterns, electrical properties, and basic learning mechanisms of the nervous system. They can also be used to in long-term studies to examine the development of the neuronal network. The analysis of MEA signals is not straightforward as MEA measures the network level activity, and one electrode can detect signals from several neuronal cells. [22]

3.2 MEA measurement system

3.2.1 MEA system

Microelectrode arrays (MEAs) or multielectrode arrays are devices that contain multiple electrodes through which neural signals can be delivered or obtained, serving as interfaces that connect neuronal cells to electronic circuitry. They can be classified into two general classes of MEAs: non-implantable MEAs, used *in vitro*, and implantable MEAs, used in vivo. Primary cell preparations or cell lines are cultivated directly on MEA. Various studies have been made concerning the neuronal cell cultures on MEA [1], [31].

Several factors affect to the size and shape of recorded signal: the nature of interface between the cells and the MEA electrode (for example. area of contact and tightness); the nature of the medium in which the cell or cells are located (for example the medium's capacitance, homogeneity and conductivity); the nature of MEA electrode itself (its impedance, geometry and noise); the properties of filter and amplifier (the system's bandwidth, gain, and behaviour outside of cut-off frequencies), and finally the data sampling properties (digital signal processing, sampling rate, resolution).[32] Figure 5 shows the diagram, which parameters are involved in shaping the signal.

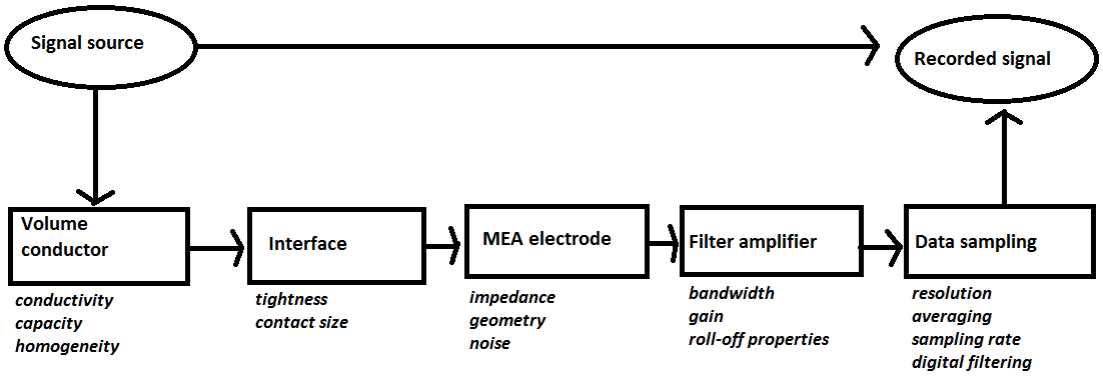

Figure 5. *A pathway that presents which parameters affect the recorded signal.*

MEA system consists of MEA chip, recording and stimulation electrodes, amplifier, stimulating system, recording device, probes and computer for signal processing. MEA chips are typically constructed either from silicon substrate or glass substrate. The data acquisition capabilities depend mainly on the properties of MEA type, for example the electrode diameter, the inter electrode distances of the electrodes and insulating material. [32]

3.2.2 MEA layouts

There are several types of MEA layouts available for different kinds of multichannel recordings. The type of application determines the selection of MEA type being used. Typical applications for MEAs are in the fields of neurobiology and cardiac

electrophysiology. MEAs differ in the geometry, i.e., electrode size and inter electrode distances. The materials used for the carrier and the recording area are also different between MEA types. The inter electrode distances and the electrode size are used for categorizing MEAs: the first number refers to the inter electrode distance (for example 100 µm) and the second number refers to the electrode size (for example 10 µm), which results in the standard MEA type 100/10, for example. [33]

Depending on the MEA type, the diameters of the electrodes typically vary between 10 and 100 µm and inter electrode distance between 30 and 500 µm. The noise level is typically less than ± 10 µm, when measured with a 30 µm electrode. Typical electrode material is Titaniuem nitride (TiN). Figure 6 A and 6 B present example images of two different MEA layouts of Multichannel systems (8x8 standard MEA and 6-well MEA). [22]

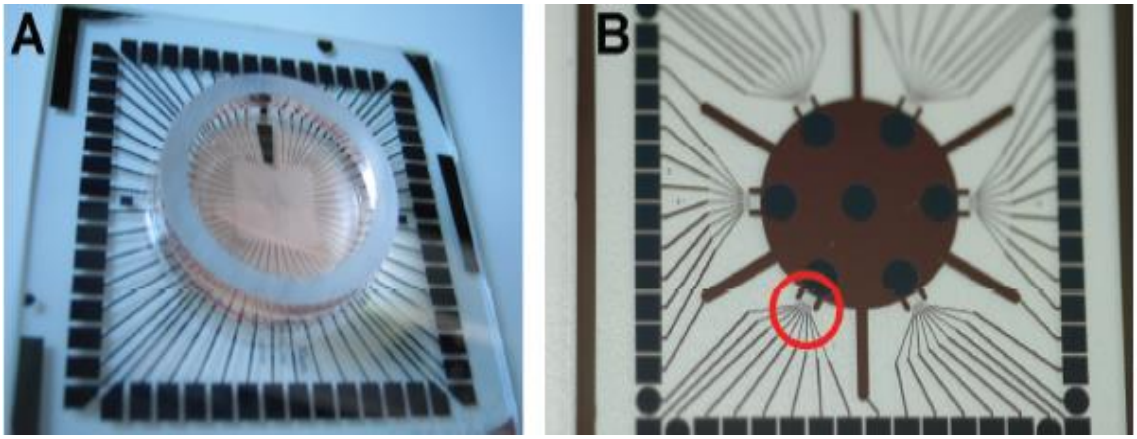

Figure 6. *Example of two different MEA layouts. Figure 6A shows the standard 8x8 electrode layout on MEA plate with glass ring. Figure 6B presents the 6-well MEA layout without culturing chamber. [22]*

Next, different MEA types of Multichannel systems are briefly listed and described. [33]

- **Standard MEAs** have 60 electrodes in an 8 x 8 layout grid with electrode diameters of 10 µm or 30 µm, and inter electrode distances of 100 µm or 200 µm. The MEAs with an inter electrode distance of 500 µm are arranged in a 6 x 10 layout.

- **HighDenseMEAs** with the highest spatial resolution and a double recording field of 5x6 electrodes each. The size of electrodes is 10 µm and the inter electrode spacing is 30 µm.

- **HexaMEAs** have a hexagonal layout and are perfect for recording from retina. In electrode layouts of 60HexaMEA-Ti and 60HexaMEA-ITO there are varying electrode diameters (10, 20, 30 µm) and inter electrode distances (30, 60, 90

µm). In 60HexaMEA40/10iR-ITO the electrodes are configured with invariable inter electrode distance of 40 µm, and TiN electrodes of 10 µm diameter.

- **ThinMEAs** with a thickness of only 180 µm are ideally suited for high-resolution imaging. Like on standard MEAs, 59 electrodes and one reference electrode are arranged in an 8 x 8 layout grid with electrode diameters of 10 µm and 30 µm, and inter electrode distances of 100 µm or 200 µm (60ThinMEA100/10-ITO, 60ThinMEA200/30iR-ITO). 60ThinMEAs are also available in a double 5 x 6 layout grid with 10 µm TiN electrodes and 30 µm inter electrode distance.

- **Stimulation MEAs** are available in 8 x 8 standard MEA layouts with additional 16 stimulation electrodes. Eight pairs of the stimulation electrodes are big and squared and they have the same size as the recording electrodes (30 µm).

- Very robust cost efficient **EcoMEAs** on glass of PCB (printed circuit board) are suited for applications with lower spatial resolution and higher throughput, especially for established cardiomyocyte cultures, large slices, or whole-heart preparations. The electrodes on EcoMEAs have a diameter of 100 µm and an inter electrode distance of 700 µm.

- **Perforated MEAs** allow perfusing the acute slice from up- and downside. They are identical in function and size to the standard MEAs, so the electrodes are arranged either in 8 x 8 or 6 x 10 layout grids.

- **6 well MEAs** feature a round MEA layout, and are separated in six segments of 3x3 electrodes. They are especially suited for drug application in screening experiment. The diameter of the electrodes is 30 µm and the inter electrode distance is 200 µm.

- **Square MEAs** have 60 TiN electrodes in an 8 x 8 layout grid with square electrode of 50 x 50 µm size and inter electrode distances of 200 µm.

- **Quadrant MEAs** whose electrode layout is organized in four quadrants with a centre line. The electrode diameter is 30 µm, and the inter electrode distance varies: Inside the quadrants the distance is 200 µm, from quadrant to quadrant the distance is 1000 µm, and to the centre line it is 500 µm.

- **256MEAs** have 252 recording electrodes in a 16 x 16 layout grid. The spacing of the electrodes in the 16 x 16 grid averages 60, 100 or 200 µm between the electrodes and the diameter of the electrodes is 30 µm.

- **9 well MEAs** which have 256 electrodes in nine blocks of 26 recording, 2 stimulation and reference electrodes each. The spacing between the electrodes averages 300 µm between the electrodes and the diameter of the electrode is 30 µm.

- **FlexMEAs** are made of flexible polyimide foil, which is perfect for in vivo and specific *in vitro* applications. The FlexMEA biosensor is only 12 µm thick and weighs less than 1 g. The FlexMEAs are available with 32 (64) recording electrodes plus two (four) indifferent reference electrodes and two (four) ground electrodes in a 6 x 6 (8 x 9) electrodes grid. The respective diameter of the electrode is 30 µm (100 µm) and inter electrode distance of 300 µm (625 µm or 750 µm).

- **EcoFlexMEAs** are made of flexible polyimide (Kapton). The EcoFlexMEA is available with 24 or 36 electrodes, two internal reference electrodes, and two ground electrodes. The diameter of the electrodes is 50 µm and the distance between the electrodes from centre to centre is 300 µm.

4 NEURONAL CONNECTIVITY ANALYSIS

The importance of estimating structural, effective and functional connectivity at different scale of complexity (from a few cells to organized tissue or whole brain) has been recently addressed in many works and has reached its momentum in neuroscientific society. It is fundamental to study functional and effective interconnections among neuronal cells and possibly to identify directionality and synaptic pathways. Therefore, it becomes essential to have reliable methods to investigate how single or groups of neuronal cells are connected as dynamically interacting neuronal populations represent functional blocks on which complex behaviour such as memory and learning are based. Thus a number of different neuronal connectivity measures, methods and analysis software have been developed in order to study and investigate neuronal networks.

In scientific papers the connectivity measures are commonly classified either by the concept of effective and functional connectivity or by the data type (i.e. continuous time series data or spike train data). The effective connectivity is defined as the simplest brain circuit which would produce the same temporal relationship as observed experimentally between cortical sites, whereas functional connectivity is defined as a temporal correlation between spatially remote neurophysiologic events [34]. Functional connectivity is often evaluated among all the elements of a system, regardless whether these elements are connected by directed structural links. Moreover, it is model-free, measures statistical interdependence without explicit reference to causal effects. Effective connectivity, on the other hand, describes the set of causal effects of one neuronal system over another one, either indirectly or directly. Some techniques for extracting effective connectivity require the specification of a model while others such as Transfer Entropy are completely model free. In general, effective connectivity measures are more complex to implement and computationally more challenging than the measures of functional connectivity.

Other common method to classify neuronal connectivity methods is the data type classification, i.e., either continuous time series or spike train data. Spike train data refers to the data storage where the time stamps (and the corresponding signal strength) of the peak of the signals (based on some threshold value) are recorded whereas continuous time series refers that each sample between the whole recording interval is used. Based on that classification, from the methods presented in this section, Phase Lock Value (PLV), Multivariate Autoregressive models (MVARs), Structural Equation Modeling (SEM) and Dynamic Causal Modeling (DCM) can be divided to time series type of analysis methods, whereas Cross-Correlation (CC), Mutual Information (MI),

Joint-Entropy (JE) and Transfer Entropy (TE) are usually classified as the methods of spike train data [14]. However, Transfer Entropy can also be calculated from time series data.

4.1 Phase Lock Value (PLV) based analysis

Analysis of phase locking has revealed information about cortico-muscular and cortico-cortical coupling of signals (Gross, et al., 2001, Fell, et al., 2001, Gross, et al., 2000, Lachaux, et al., 1999, Tass, et al., 1998) [35]. Measurement of phase locking (or phase coupling) of EEG or MEG, instead of formerly used spectral coherence has been used for examining of brain networking. The general procedure for detecting and quantifying the phase locking is based on the following steps. Given two signals, their instantaneous phases (across different frequency bands) are estimated by convolution with Hilbert transform or by a complex wavelet. The phase differences between the signals usually fluctuate along time or around a constant value across trials. Therefore it is needed to further test for synchrony in a statistical way. It provides a reliable measurement of phase coupling. The PLV measurement has been used for example as EEG features of motor imagery in BCI applications [36]. For our knowledge, no studies of PLV have been made with MEAs. Next, the mathematical background of PLV calculation will be explained.

Given $s_x(t)$ and $s_y(t)$ the signals over two electrodes x and y, and $\Phi_x(t)$ and $\Phi_y(t)$ their instantaneous phases, phase locking means

$$\Phi_x(t)-\Phi_y(t)=\text{constant}. \quad (1)$$

The true synchrony in signals with low signal-to-noise ratio is always buried in a considerable background noise. In order to measure phase synchrony with these signals, two steps are needed: first the instantaneous phase of each signals must be estimated and the second is to provide a statistical criteria to quantify the degree of phase-locking. [37] The instantaneous phase can be calculated by the means of the analytical signal. For arbitrary signal $s(t)$, the analytical signal $z(t)$ is a complex function defined as

$$z(t) = s(t) + j\hat{s}(t)=a(t)e^{j\phi(t)} \quad (2)$$

$$\hat{s}(t) = \frac{1}{\pi}\int_{-\infty}^{\infty} \frac{s(\tau)}{t-\tau} d\tau \quad (3)$$

Where $\hat{s}(t)$ is the Hilbert transform of $s(t)$ and $a(t)$ is the amplitude of the signal. The instantaneous phase of $s(t)$ can be determined in the following way

$$\Phi(t)=\arctan(\hat{s}(t)/(s(t)). \quad (4)$$

When the instantaneous phases are known, the difference of instantaneous phases corresponding to signals $s_x(t)$ and $s_y(t)$ is defined as $\Delta\Phi(t)=\Phi_x(t)-\Phi_y(t)$, and a single-trial phase-locking value for each individual trial is defined as

$$PLV = \left|\langle e^{j\Delta\phi(t)} \rangle_t\right| \quad (5)$$

where the operator $\langle . \rangle_t$ means averaging over time. In the case signals are unsynchronized, PLV=0 and $\Delta\Phi(t)$ follows a uniform distribution. If the signals are completely synchronized, $\Delta\Phi(t)$ is a constant and PLV=1. [37] Usually the signal is filtered with some windowing-method so in that case the PLV-value should be

calculated for each window length and in the end all the PLV-values should be summed together and divided by the number of windows present in order to get the average PLV between the two signals being observed.

4.2 Multivariate Autoregressive Model (MVAR) based analysis

Multivariate autoregressive models can be used to model interactions between multiple regions. Multivariate autoregressive models not only assume instantaneous linear interaction between regions, but also take into account the causal dependence of the present on the past [35]. The MVAR model can be described by the following equation:

$$\sum_{k=0}^{p} \mathbf{\Lambda(k)}\,\mathbf{y}(\mathrm{t}-\mathrm{k}) = \mathbf{e}(\mathrm{t}) \qquad (6)$$

Where **y(t)** is the data vector **y(t)**=[$y_1(t)$, $y_2(t)$,…,$y_n(t)$]$^{\mathrm{T}}$ in time, **e(t)**=[$e_1(t)$,…,e_N]$^{\mathrm{T}}$ is a vector of multivariate zero-mean uncorrelated noise, **Λ(1)**, **Λ(2)**, …**Λ(p)** are NxN matrices of model coefficients and *p* represents the model order [38]. Astolfi et al. (2007) chose *p* in their study by means of the Akaike Information Criterion (AIC) for MVAR processes [39]. The MVAR models thus represent directed influences among a set of regions whose causal interactions are inferred via their mutual predictability from past time points [40]. The MVAR equation can also be expressed on the more simplified form if it is transformed to the frequency domain**.** Equation (7) shows the relationship in the frequency domain:

$$\boldsymbol{\Lambda(f)}\mathbf{y}(\mathrm{f}) = \mathbf{e}(\mathrm{f}) \qquad (7)$$

Where:

$$\mathbf{\Lambda(f)} = \sum_{\mathbf{k=0}}^{\boldsymbol{p}} \mathbf{\Lambda}\,(\mathbf{k})\mathrm{e}^{-\mathrm{j}2\pi\mathrm{f}\Delta\mathrm{tk}} \qquad (8)$$

And Δt is the temporal interval between two samples. The equation (7) can then be rewritten as:

$$\mathbf{y(f)} = \mathbf{\Lambda^{-1}(f)e(f)} = \mathbf{H(f)e(f)} \quad (9)$$

Where **H(f)** is the inverse of the frequency transformed coefficient matrix and **Λ(f)** is the transformation matrix [41]. On the frequency domain we can compute different MVAR measures such as the Directed Transfer Function (DTF), Partial Directed Coherence (PDC) and direct DTF (dDTF). An advantage of MVAR models comparing to the statistical methods (dynamic causal modelling and structural equation modelling) is that no a priori knowledge is required about the connectivity in the network. Furthermore, they allow one to determine the direction of interaction by analogy to the concept of Granger Causality (GC). [35] However, in event related studies the wide sense stationarity requirement does limit the utility of MVAR models, but since they are parametric they can be fit using relatively few samples (with the covariance calculated by averaging across epochs) and non-stationarity then measured using a sliding window [35]. However, these GC based methods are only well applicable when three prerequisites are met: a) the interaction between the signals under observation has to be

well approximated by a linear description, b) the data have to have relatively low noise levels and c) cross-talk between the measurements of interest has to be low [15].

Astolfi et al. (2005) have pointed out that the DTF can recover cortical connectivity patterns under a large range of recording lengths and signal-to-noise ratios [7]. However, the formulation of DTF makes it prone in certain conditions to obtain an incorrect estimation of the paths between cortical areas [38]. Korzeniewska et al. introduced the direct DTF in order to improve the capability of DTF to detect direct and indirect causality pathways [8]. It has been suggested that techniques like dDTF and PDC could overcome this drawback [8]. However, a recent study of Astolfi et al. (2009) in which functional magnetic resonance imaging (fMRI) and EEG were combined presented that the different functional connectivity estimators (DTF, dDTF and PDC) returned essentially the same global picture of connectivity patterns [38]. In the same study it was also shown that the global picture between effective (DTF) and functional (SEM) connectivity methods were also similar, although there were some differences in the connectivity between particular cortical regions. [34] For our knowledge, no studies of MVAR methods have been performed with MEAs.

4.2.1 Directed Transfer Function (DTF)

The directed transfer function is a frequency-domain estimator of causal interaction based on MVAR modelling [41]. The DTF, which represents the causal influence of the cortical waveform estimated in the *j*-th ROI on that estimated in the *i*-th ROI as defined in terms of elements of the transfer matrix **H**, is:

$$\boldsymbol{\theta_{ij}^2}(\mathbf{f}) = \left|\mathbf{H_{ij}}(\mathbf{f})\right|^2 \qquad (10)$$

More frequently used estimate is so-called normalized DTF which enables the results obtained for cortical waveforms with different power spectra to be compared. Normalized spectra can be performed by dividing each estimated DTF by the squared sums of all elements of the relevant row. Normalized DTF can be expressed by the following equation:

$$\boldsymbol{\gamma_{ij}^2}(\mathbf{f}) = \frac{\left|\mathbf{H_{ij}}(\mathbf{f})\right|^2}{\sum_{m=1}^{N}|\mathbf{H_{im}}(\mathbf{f})|^2} \qquad (11)$$

Where N is the number of channels (which may be the number regions of interest in the source domain [41], or the number of sensors in the sensor domain) and $\boldsymbol{\gamma_{ij}(f)}$ indicates the ratio of influence of the cortical waveform estimated in the *j*-th ROI on the cortical waveform estimated in the *i*-th ROI, with respect to the influence of all the estimated cortical waveforms. [38] Normalized DTF values are in the value range of 0 to 1, and the normalization condition in equation (12) is applied.

$$\sum_{n=1}^{N} \boldsymbol{\gamma_{in}^2}(\mathbf{f}) = 1 \qquad (12)$$

One can also calculate the power spectra matrix **S(f)** by using the transfer matrix. If we denote by **V** the variance matrix of the noise **e(f)**, the power spectrum is defined by:

$$\mathbf{S}(\mathbf{f}) = \mathbf{H}(\mathbf{f})\mathbf{V}\mathbf{H} * (\mathbf{f}) \qquad (13)$$

Where the superscript * denotes transposition and complex conjugate [38]. Using **S(f)**, ordinary coherence can be computed as:

$$\mathbf{k_{ij}(f)} = \frac{|S_{ij}(f)|^2}{S_{ij}(f)S_{ij}(f)} \qquad (14)$$

Coherence measures indicate the degree of synchrony between areas *i* and *j*. He et al. (2010) used the ARfit package in the DTF computation function for the estimation of multivariate autoregressive models [42].

4.2.2 Partial Directed Coherence (PDC)

Partial Coherence is another estimator of relationship between a pair of channels, which describes the interaction between areas *i* and *j* when the influence due to all N-2 time series is discounted. It is defined by the following formula:

$$\left|\mathbf{X_{ij}(f)}\right|^2 = \frac{|\mathbf{M_{ij}(f)}|^2}{\mathbf{M_{ij}(f)M_{ij}(f)}} \qquad (15)$$

Where $\mathbf{M_{ij}(f)}$ is the minor performed by removing *i*-th row and *j*-th column from the spectral matrix **S**. [38] In 2001, Baccala introduced the following factorization:

$$\mathbf{X_{ij}(f)} = \frac{\mathbf{\Lambda_i}*\mathbf{(f)V^{-1}\Lambda_j(f)}}{\sqrt{(\mathbf{\Lambda_i}*\mathbf{(f)V^{-1}\Lambda_i(f))(\Lambda_j}*\mathbf{(f)V^{-1}\Lambda_j(f)))}}} \qquad (16)$$

Where $\mathbf{\Lambda_n(f)}$ is the *n*-th column of the matrix $\mathbf{\Lambda(f)}$. From this equation Baccala and Sameshima defined the concept of Partial Directed Coherence (PDC) in 2001. [10] The PDC can be expressed in the following form:

$$\mathbf{\pi_{ij}(f)} = \frac{\mathbf{\Lambda_{ij}(f)}}{\sqrt{\sum_{\mathbf{k=1}}^{\mathbf{N}} \mathbf{\Lambda_{ki}(f)\Lambda_{kj}^*(f)}}} \qquad (17)$$

The PDC from *j* to *i*, $\mathbf{\pi_{ij}(f)}$, describes the directional flow of information from the activity in the ROI $s_j(n)$ to the activity in $s_i(n)$, hence common effects produced by other ROIs $s_k(n)$ on the latter are subtracted, leaving only description that is specifically from $s_j(n)$ to $s_i(n)$. [38] It follows from the normalization condition that PDC takes values between the intervals from 0 to 1. The normalization condition is described by the following way:

$$\sum_{n=1}^{N} |\mathbf{\pi_{ni}(f)}|^2 = 1 \qquad (18)$$

Term $\mathbf{\pi_{ij}(f)}$ represents the fraction of time evolution of ROI *j* directed to ROI *i*, compared to all of *j*'s interactions with other ROIs. [38] Only direct flows between channels can be shown by PDC. In contrast to DTF, PDC is normalized to show a ratio between the outflows from channel *j* to channel *i* to all the outflows from the source channel *j*, so it emphasizes rather the sinks, not the sources. [43] In neurophysiological applications rather sinks, not the sources are of main interest, hence later on the estimator called generalized Partial Directed Coherence (gPDC) was introduced [11], in which normalization factor in the denominator similar to the one used in DTF was proposed. gPDC is given by the following formula [43]:

$$gPDC_{j\to i}(f) = \frac{\mathbf{\Lambda_{ij}(f)}}{\sum_{\mathbf{i=1}}^{\mathbf{k}} |\mathbf{\Lambda_{ij}(f)}|^2} \qquad (19)$$

Schelter et al. (2009) have pointed out that not renormalized PDC has several drawbacks, primarily: (1) PDC is not scale-invariant, because it depends on the units of measurement of the source and target processes, (2) PDC is decreased when multiple signals are emitted from a given source, and (3) PDC does not allow conclusions on the absolute strength of the coupling. Those disadvantages are abated with gPDC. Both gPDC and PDC, similarly with DTF are insensitive to the volume conduction. [44]

4.2.3 Direct DTF (dDTF)

Although the DTF gives very essential information about investigated system, it shows, for a given pair of channels, both indirect and direct propagation within the whole system. In the systems, like in the case of depth electrode recordings, where many coupled structures are communicating with each other along many different pathways, the identification of direct flow is important. Thus, if we know which causal directions are direct, we can simplify the reconstruction of the connections, which means that the signal from channel *i* is not transmitted to channel *j* by a set of transmissions through other channels. [8] In order to distinguish between the cascade and direct flows in DTF, Korzeniewska et al. (2003) introduced the concept of direct DTF (dDTF) [8]. When we know the full frequency DTF (ffDTF), given by:

$$\boldsymbol{\eta_{ij}^2(f)} = \frac{\left|\mathbf{H_{ij}(f)}\right|^2}{\sum_{\mathbf{f}}\sum_{\mathbf{m=1}}^{\mathbf{k}}|\mathbf{H_{im}(f)}|^2} \qquad (20)$$

We can then define the dDTF by multiplying the ffDTF in equation 20 by partial coherence in equation (15). The dDTF from area *j* to area *i* is then defined as:

$$\boldsymbol{\delta_{ij}(f)} = \mathbf{X_{ij}(f)}\boldsymbol{\eta_{ij}(f)} \qquad (21)$$

This function in equation 21 describes only the direct relations between channels. The denominator function (20) does not depend on frequency. [38]

4.2.4 Adaptive Directed Transfer Function (ADTF)

The adaptive DTF (ADTF) is a time-varying multivariate method that has been developed for the estimation of rapidly changing connectivity relationships such as between cortical areas of human brain, while the DTF measure is suitable for the quasi-stationary signals [41]. The DTF has been well used to measure the functional connectivity during a variety of pathological conditions and brains states. However, the DTF method assumes the time invariance of the connectivity and the stationarity of the neural electrical signals among different channels over the time window under study. Such assumptions may not be correct in the abnormal brain signals such as interictal spikes and seizures in epilepsy patients. For that reason, Wilke et al. (2008) introduced an adaptive DTF method through the use of a multivariate adaptive autoregressive model to study the time-variant propagation of seizures and interictal spikes. The study suggested that ADTF method correctly captured the temporal dynamics of the propagation models, while the DTF method couldn't. DTF method even returned false results in some cases. [9] The ADTF is based similarly with DTF estimation on the

modelling of the adaptive MVAR process (AMVAR). The multiple-channel signals are described by the following way:

$$\mathbf{x(t)} = \sum_{\mathbf{i=1}}^{p} \mathbf{\Lambda}\,(\mathbf{i}, \mathbf{t})\mathbf{x}(\mathbf{t} - \mathbf{1}) + \mathbf{e(t)} \quad (22)$$

Where **Λ(i,t)** are the matrices of time-varying model coefficients, **x(t)** is the data vector over time, **e(t)** is the multivariate independent white noise and *p* is the model order. He et al. (2010) obtained time-varying coefficient matrices by using the Kalman filter algorithm [41]. Better description of the algorithm can be found by Arnold et al., 1998 [45]. The transfer function **H(f,t)** can thus be obtained from the time-varying transfer matrix by using the time-varying model coefficients. The ADTF values are then defined as a function of both frequency and time by the following way:

$$\boldsymbol{\gamma}_{\mathbf{ij}}^{\mathbf{2}}(\mathbf{f}, \mathbf{t}) = \frac{|\mathbf{H_{ij}(f,t)}|^{2}}{\sum_{\mathbf{m=1}}^{\mathbf{N}} |\mathbf{H_{im}(f,t)}|^{2}} \quad (23)$$

He at al. (2010) used the MVAAR (multivariate adaptive regressive) tool in TSA (time series analysis) package [46] in the ADTF computation function.

4.3 Cross-correlation (CC) analysis

Cross-correlation (CC) analysis measures the frequency at which one cell fires as a function of time relative to the firing of a spike in another cell [14]. Cross-Correlation analysis and the following three information theory based methods; Mutual Information, Joint-Entropy and Transfer Entropy are all associated to a matrix, the Connectivity Matrix (CM), whose elements (X, Y) correspond to the estimated connection strength between neuronal cell X and Y. [14] Low and high values in the CM are expected to correspond to weak and strong connections. Therefore by using such approach, inhibitory connections could not be detected because they would be mixed with small connection values. By thresholding the CM, it is possible to filter out non-causal and noisy values because they are expected to be small. Nevertheless, a connectivity map is obtained for each threshold value. These connectivity maps, deduced by considering the strongest CM values, display the links which should correspond to the strongest synaptic pathways. [14]

Cross-Correlation function is built by considering the spike trains of two neuronal cells. Mathematically, CC reduces to a simple probability $C_{xy}(\tau)$ of observing a spike in a train Y at time (l+τ), given that there was a spike in another train X at time *t*. The term *τ* is called time lag or time shift. CC function is evaluated considering all pairs of spike trains. Connection strength among neuronal cells can thus be evaluated on the basis of the peak value of CC function. Therefore, the peak values of each CC function is obtained to define CM, so that the highest CC values should correspond to the strongest connections. Moreover, directionality can be deduced from the sign of the corresponding peak latency. [14]

Maccione et al. [47] used recently (2012) CC function for multiscale function connectivity estimation on low-density neuronal cultures recorded by high-density CMOS MEAs which suggested that CC method provided reliable connectivity maps.

4.4 Statistical methods

4.4.1 Structural Equation Modeling (SEM)

Structural Equation Modeling gives a simple approximation to the potentially complex interactions between multiple regions [35]. It has been an established statistical technique in the social sciences for several decades and was introduced to neuroimaging in the early 1990's. It is a hypothesis-driven, multivariate technique that is based on a structural model which represents the hypothesis about the causal relations between several variables. [40] In SEM, the parameters are estimated by minimizing the difference between the observed covariance and those implied by a path or structural model. In neural systems the covariance describes the degree to which the activities of two or more regions are related. [12]

The SEM consists of a set of linear structural equations containing observed parameters and variables defining causal relationships among the variables. Variables in the equation can be exogenous which means that they are independent from the model itself, or they can be endogenous which means that they are dependent from the variables in the model. The SEM describes the causal effects, specifies the causal relationships among the variables and assigns the explained and the unexplained variance. [12]

The structural equation model for these variables is the following:

$$\mathbf{y} = \mathbf{B}\mathbf{y} + \Gamma\mathbf{x} + \boldsymbol{\zeta} \qquad (24)$$

Where

x (n x l) vector of independent (exogenous) variables;

y (m x l) vector of dependent (endogenous) variables;

B (m x m) matrix of coefficients of the endogenous variables;

ζ (m x l) vector of equation errors (random disturbances);

Γ (m x n) matrix of coefficients of the exogenous variables;

ζ is assumed to be uncorrelated with the exogenous variables, and **B** is supposed to have zeros in its diagonal and to satisfy the assumption that (**I**-**B**) is singular, where **I** is the identity matrix.

If **z** is a vector which contains all the *p=m+n* variables, exogenous and endogenous, in the following order: [12]

$$\mathbf{Z}^T = [x \dots x_n y_1 \dots y_m] \qquad (25)$$

The observed covariance can be expressed as

$$\sum_{\text{obs}} = \frac{1}{\text{N}-1} * \mathbf{Z} * \mathbf{Z^T} \qquad (26)$$

Where **Z** is the p x N matrix of the observed variables for N observations. [12]

The covariance matrix implied by the model can be performed by the following way:

$$\sum_{\text{mod}} = \mathbf{E}[\text{zz}^{\text{T}}] = \begin{bmatrix} \mathbf{E}[xx^T] & \mathbf{E}[xy^T] \\ \mathbf{E}[yx^T] & \mathbf{E}[yy^T] \end{bmatrix} \qquad (27)$$

Where

$$\mathbf{E}[yy^T] =$$

$$\mathbf{E}[(\mathbf{I}-\mathbf{B})^{-1}(\Gamma x+\boldsymbol{\zeta})(\Gamma x+\boldsymbol{\zeta})^{\mathrm{T}}((\mathbf{I}-\mathbf{B})^{-1})^{\mathrm{T}}]$$

$$= (\mathrm{I}-\mathrm{B})^{-1}(\Gamma\boldsymbol{\phi}\Gamma^{\mathbf{T}}+\boldsymbol{\Psi})((\mathbf{I}-\mathbf{B})^{-1})^{\mathrm{T}} \quad (28)$$

Since the errors $\boldsymbol{\zeta}$ are not correlated with the x

$$\mathbf{E}[xx^{\mathrm{T}}]=\boldsymbol{\phi} \quad (29)$$

$$\mathbf{E}[xy^{\mathrm{T}}]=((\mathbf{I}-\mathbf{B})^{-1}\boldsymbol{\Gamma\phi})^{\mathrm{T}} \quad (30)$$

$$\mathbf{E}[yx^{\mathrm{T}}]=(\mathbf{I}-\mathbf{B})^{-1}\boldsymbol{\Gamma\phi} \quad (31)$$

The resulting covariance matrix will then be in terms of the model parameters: [12]

$$\sum_{mod}\begin{bmatrix}\boldsymbol{\phi} & ((\mathbf{I}-\mathbf{B})^{-1}\boldsymbol{\phi})^{\mathrm{T}}\\ (\mathbf{I}-\mathbf{B})^{-1}\boldsymbol{\phi} & (\mathbf{I}-\mathbf{B})^{-1}(\Gamma\boldsymbol{\phi}\Gamma+\boldsymbol{\Psi})((\mathbf{I}-\mathbf{B})^{-1})^{\mathrm{T}}\end{bmatrix} \quad (32)$$

Since the number of variables is greater than the number of equations, a priori information about the model has to be provided. This is done by limiting the number of free parameters, i.e., the elements of the matrix B. [35] In order to estimate these parameters, a function of the observed and implied covariance matrices should be minimized. [12]

One disadvantage of SEM is that one is restricted to use structural models of relatively low complexity since models with reciprocal loops and connections often become non-identifiable. [40] The SEM was originally applied for positron emission tomography (PET) and fMRI studies in which dynamic data was not available, so the method hasn't been used much for EEG/MEG data. The method is based on the covariance, therefore it will be affected by linear crosstalk leading to potentially erroneous inferences of network connectivity when applied to EEG or MEG data. [35] However, Astolfi et al. (2005) applied SEM for high-resolution EEG to estimate the cortical connectivity. [12] In their study LISREL [48] was used for the implementation of SEM technique. [12] For our knowledge, no published studies of SEM for MEAs have been performed.

4.4.2 Dynamic Causal Modeling (DCM)

The aim of Dynamic Causal Modeling is to infer the causal architecture of distributed or coupled dynamical systems. [13] It was developed to analyse coupling among brain regions and how that is influenced by experimental changes such as time or context. It has been mainly used for fMRI and event-related potential (ERPs) measured with EEG or MEG. For our knowledge, no published studies of DCM for MEAs have been made. DCM is based on Bayesian model comparison procedure that compares models of how data were generated. Dynamic causal models are constructed by using stochastic or ordinary differential equations (i.e. nonlinear state-space models in continuous time). DCM uses the notion of effective connectivity and it represents a fundamental departure from existing approaches to connectivity because it employs an explicit generative model of measured brain responses that embraces their nonlinear causal architecture. It also takes a very different approach compared for example to autoregressive models and

uses a forward model which explicitly includes long-range connections among neuronal subpopulations underlying measured sources.[13] A single Bayesian inversion also allows one to infer on parameters of the model (i.e. effective connectivity) that mediate functional connectivity.

Whereas DCM assumes a bilinear state space model (BSSM), it covers non-linear interactions – at least partially. However, DCM needs a priori information about the input to the system. It also requires a priori knowledge about the network connectivity being investigated. These priori information about potential connectivity and input to the system may not always be present for example in studies of the resting state. Consequently, it may not be optimal for exploratory analyses. [15]

DCM for event-related potentials is based on a neural mass model, which was developed by David & Friston (2003) as an extension of the model by Jansen & Rit (1995), which uses established connectivity rules in hierarchical sensory systems to compile a network of coupled cortical systems. These rules resemble connections with respect to their laminar patterns of termination and origin and distinguish between i) backward (or top-down) connections originating and terminating in agranular layers, ii) forward (or bottom-up) connections originating in agranular layers and terminating in layer 4 and iii) lateral connections originating in agranular layers and targeting all layers. [40]

In this model, each source or region is modelled as a microcircuit where three neuronal subpopulations are combined in this circuit to supra-/infragranular and granular layers. The neural state equations are summarized in Figure 7. The network receives inputs via input connections which are exactly the same as forward connections and deliver input u to the spiny stellate cells in layer 4. The input u represents afferent activity relayed by subcortical structures and are modelled as two parameterized components, a discrete cosine set (representing variations in input over peristimulus time) and a gamma density which represents an event-related burst of input that is delayed and dispersed by subcortical synapses and axonal conduction. [40] The parameter vector C [13] controls the influence of this input on each source.

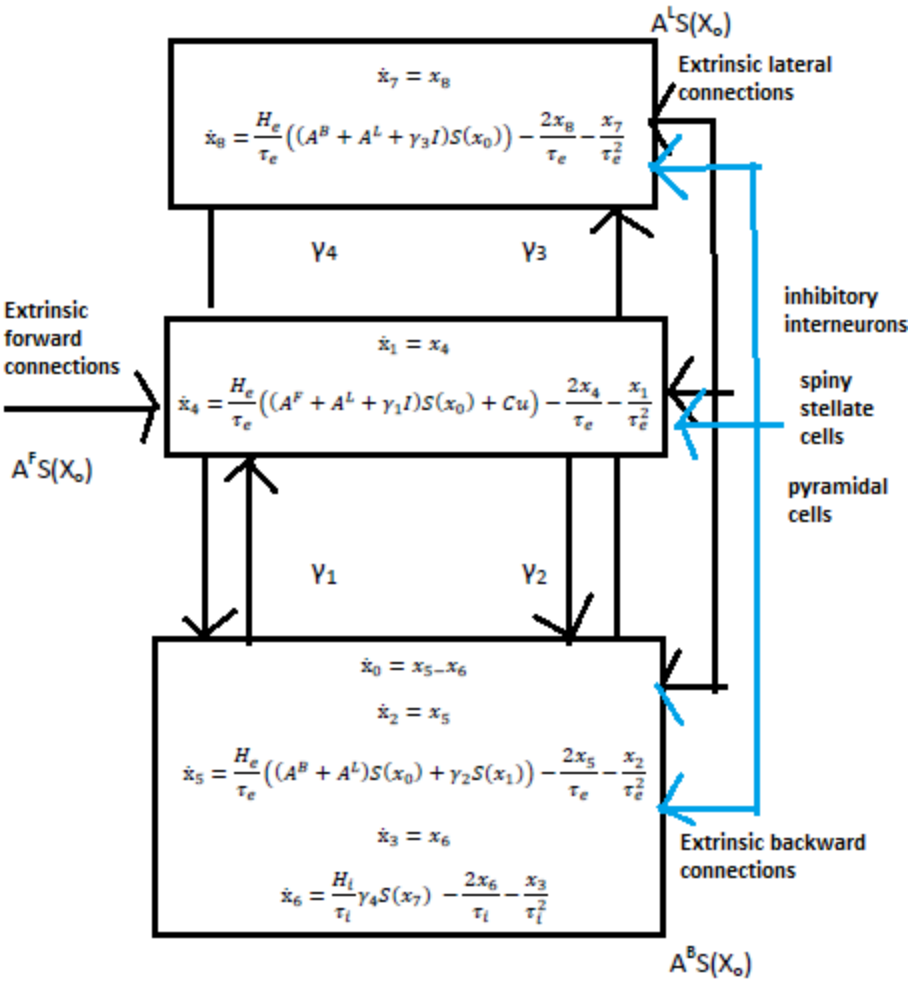

Figure 7. *Schematic of the neural model in DCM for ERPs. The state equations describing the dynamics of a microcircuit representing an individual region (source) are shown in the schema. Each region consists of three populations (inhibitory, spiny stellate and pyramidal interneuronal cells) that are linked by intrinsic connections and have been assigned to infragranular, granular and supragranular layers. Different regions are coupled through extrinsic excitatory connections that follow the laminar patterns of forward, backward and lateral connections.*

The DCM can be specified with the state equations presented in Figure 7 and with a linear output equation

$$\frac{\mathrm{d}x}{\mathrm{dt}} = \mathbf{f}(x, u, \theta) \ , \mathbf{y} = \mathbf{L}x_0 + \varepsilon \qquad (33)$$

Where **L** is a lead field matrix coupling electrical sources to the EEG channels and x_0 represents the transmembrane potential of pyramidal cells. The state equations of DCM for ERPs are much more realistic and complex. As taking an example, the state equation for the inhibitory subpopulation is [40]

$$\frac{\mathrm{dx_7}}{\mathrm{dt}} = x_8 \qquad (34)$$

$$\frac{\mathrm{dx_8}}{\mathrm{dt}} = \frac{\mathrm{H_e}}{\tau_\mathrm{e}}\left((\mathbf{A^B} + \mathbf{A^L} + \gamma_3\mathbf{I})\mathbf{S}(x_0)\right) - \frac{2x_8}{\tau_\mathrm{e}} - \frac{\mathrm{x_7}}{\tau_\mathrm{e}^2} \qquad (35)$$

The parameter matrices $\mathbf{A^L}$, $\mathbf{A^B}$, $\mathbf{A^F}$ refer to lateral, backward and forward connections respectively [40]. The dynamics of neural states are determined by two operators within each subpopulation. The first transforms the average density of presynaptic inputs into the average postsynaptic membrane potential and this is modelled by a linear transformation with inhibitory (*i*) and excitatory (*e*) kernels parameterized by $\mathbf{H}_{e,i}$ and $\tau_{e,i}$. The term $\tau_{e,i}$ represent lumped rate constants (lumped across dendritic tree and dendritic spines) and $\mathbf{H}_{e,i}$ control the maximum postsynaptic potential. The second operator **S** transforms the average potential of each subpopulation into an average firing rate. This is a sigmoid function and is assumed to be instantaneous. Intra-areal interactions among the subpopulations depend on constants $\gamma_{1\ldots4}$. They control the strength of intrinsic connections and reflect the total number of synapses expressed by each subpopulation. In equation (35), the rate of change of voltage as a function of current is expressed on the top line. The second line describes how current changes as a function of current, voltage and presynaptic input from intrinsic and extrinsic sources. [40]

A fully Bayesian approach is required for estimating the parameters from empirical data and it is analogous to that used in DCM for fMRI. In order to test hypotheses about the modelled process (particularly differences in inter-areal connection strengths between different trial types), the posterior distributions of the parameter estimates should be used. A detailed description of Bayesian approach and DCM parameters and their optimization can be found in [13].

4.5 Information theoretic measures

4.5.1 Mutual Information (MI)

Mutual Information is an information theory based method which measures the statistical dependence between two processes. In order to compute MI between two neuronal cells, spike trains should be presented as binary strings. Therefore, time is discretized such each time bin (for example 0.1 ms) represents either the absence or presence of a spike. [14] MI can be evaluated in two different ways depending on the coding mechanism. It can be expressed either as a temporal code, in which also the spike position is considered, or as a simpler rate code (for example ‘1110’ correspond to 3 spikes). [49] Figure 8 shows how the spike trains are can be calculated using binary strings.

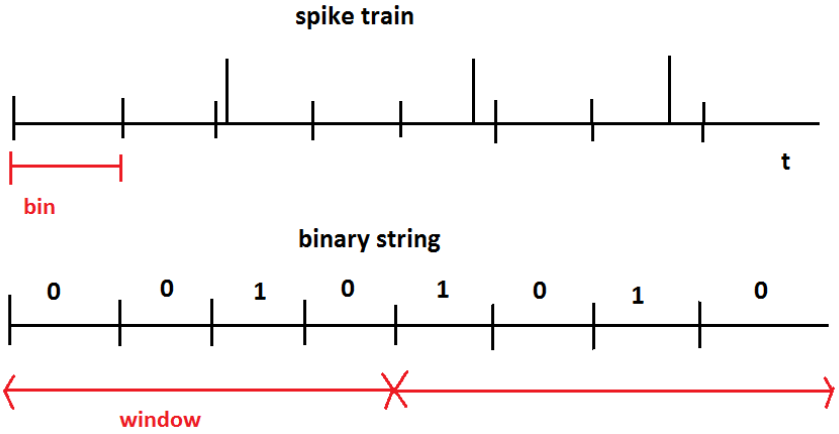

Figure 8. *Binary string is created starting from the spike train. A window is selected to evaluate the TE and to define the MI symbols.*

MI is computed by evaluating joint and single probabilities of the two neuronal cells (X,Y):

$$MI(\mathbf{x},\mathbf{y}) = \sum_x \sum_y p(x,y) * \log_2 \left(\frac{p(x,y)}{p(x)*p(y)} \right) \qquad (36)$$

Where *x*, *y* represent a single event (for example x=2, y=3 spikes). Each joint probabilities p(*x*,*y*), represent the probability of observing *x* spikes emitted by neuronal cell **x**, and *y* spikes by neuronal cell **y** on the same time window. [14] All probabilities can be estimated following the direct method [50]. MI is symmetric with respect to the exchange of the variables **x** and **y**. Therefore, it is not suited to recover information on directionality and causality. Instead, directionality can be determined with the CC function as described in Section 2.6. Figure 9 shows an example where the MI function presents a peak close to time zero.

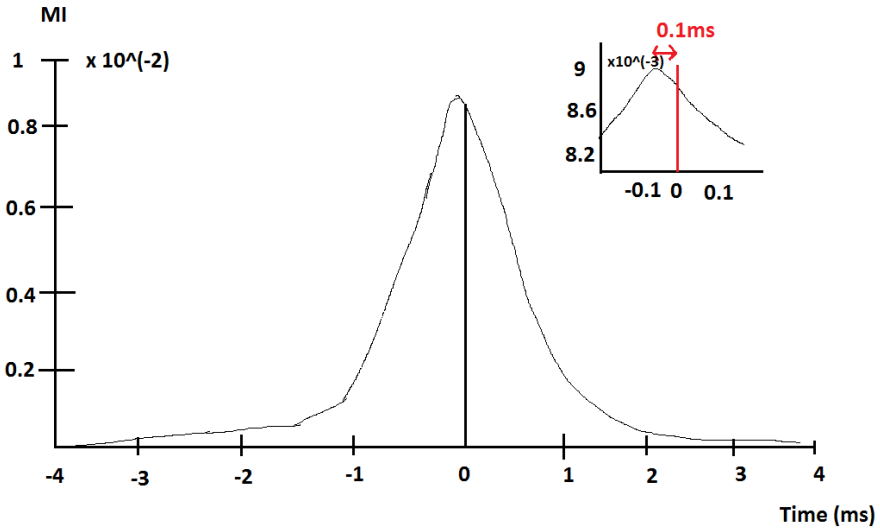

Figure 9. *Mutual Information (spike count approach) function related to a pair of nodes of network model. The inset shows that the MI peak value falls close to the zero time shift (value -0.1 ms).*

4.5.2 Joint-Entropy (JE)

Joint-Entropy is a novel method which was presented in the literature in 2009 by Garofalo's group [14]. It is a linear measure like the cross correlation (CC) and is built by considering the cross inter-spike-intervals (cISI) computed across pairs of neuronal cells. Garofalo et al. suggested that JE is sensitive to the activity patterns showed by the neuronal networks and is able to differentiate the influence of a specific neuronal cell on the activity of another one. For these reasons, the JE measure can be considered as a good alternative for CC function. Moreover, the algorithm which evaluates the JE is faster than both Mutual Information and Transfer Entropy ones which are heavy from a computation calculating point of view. [49]

JE is calculated with the following procedure. Considering **x** as the reference neuronal cell (which actually makes **y** to spike), then for each spike of **x**, a subsequent spike of **y** is considered and cross-inter-spike-intervals are defined as time difference ($cISI=t_Y-t_X$). Example *cISI* spikes are shown in Figure 10.

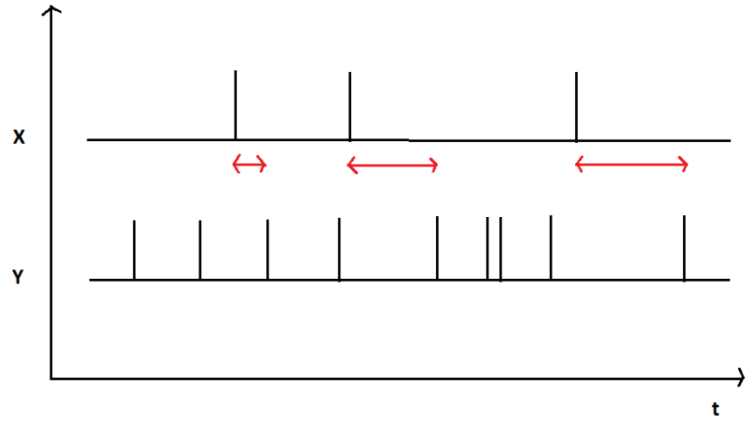

Figure 10. *Cross-inter-spike-intervals (cISI) between neuronal cells* **x** *and* **y** *are highlighted by the red arrows.*

Joint-Entropy (JE) can then be defined as:

$$JE(\mathbf{x},\mathbf{y}) = -\sum_{k=1}^{n} p(cISI_k) * \log_2\big(p(cISI_k)\big) \qquad (37)$$

Where $p(cISI_k)$ is the estimated probability of $cISI_k$. Garofalo et al. defined the cISI so that *cISIs* were binned using a bin size equal to 0.1 ms, and $cISI_k$ was calculated then as *k*binsize.* [14] If **x** and **y** are strongly connected, the *cISI* histogram will show a peak at a specific *cISI* value, and *JE* will be close to zero. Whereas, when **x** and **y** are weakly connected or not connected at all, then the *cISI* will be nearly flat and consequently *JE* will be high. [49] Garofalo et al. [14] computed cISI as follows: for each reference spike (*x*), the nearest subsequent spike (*y*) is considered and if it falls before a new reference spike, then cISI is computed as their time difference, otherwise it is not counted. JE provides asymmetric values and therefore it may be used to infer causality. Unlike the CC and MI methods, the strongest connections in the Synaptic Weight Matrix refer to the lowest JE values. [14]

4.5.3 Transfer Entropy (TE)

Transfer Entropy is an information theoretic measure which allows one to extract causal relationships from time series. It is based on Wiener's definition, which means that a signal **x** is said to cause a signal **y** when the future of signal **y** is better predicted by adding knowledge from the past and present of signal **x** than by using the present and past of signal **y** alone [15]. TE incorporates dynamical and directional information and does not assume any particular model for the interaction between the systems of interests. TE detects not only linear but also non-linear interactions, which becomes an advantage over Granger Causality (GC) based methods which suit only for linear interactions. [15] TE can be calculated both for analogue signals and sparse binary time-series [51].

Transfer Entropy for two observed time series $\mathbf{x_t}$ and $\mathbf{y_t}$ can be defined as:

$$TE(\mathrm{X} \rightarrow \mathrm{Y}) = \sum_{y_{t+u}, y_t^{d_y}, x_t^{d_x}} p(\mathbf{y_{t+u}}, \mathbf{y_t^{d_y}}, \mathbf{x_t^{d_x}}) \log \frac{p(\mathbf{y_{t+u}} | \mathbf{y_t^{d_y}}, \mathbf{x_t^{d_x}})}{p(\mathbf{y_{t+u}} | \mathbf{y_t^{d_y}})} \qquad (38)$$

Where *t* is a discrete valued time-index and *u* denotes the prediction time, a discrete valued time interval. $\mathbf{y_t^{dy}}$ and $\mathbf{x_t^{dx}}$ are d_x- and d_y-dimensional delay vectors. [15] High *TE* values indicate that the time series **x** influences the response of **y**. On the other hand, low *TE* values indicate that $\mathbf{x_t^m}$ has no influence on the transition probabilities of the state of **y**. [14]

There are different estimators to estimate the optimal embedding dimensions for TE [15]. Cao criterion is a method to determine the minimum embedding dimensions of deterministic time series by analysing neighbourhood relations in various dimensions [51]. Ragwitz criterion is an alternative method which optimizes the embedding dimension and embedding delay for deterministic and stochastic data. It predicts the future value of the signal based on estimates of the probability densities of future values of its nearest neighbours after embedding. [51] Even by using these improved estimators, inaccuracies in estimation are still inevitable. Therefore it is necessary to evaluate the statistical significances of TE measures. Common way to do that is to use TE as a statistic measuring dependency of two time series and test against the null hypothesis of independent time series ('absence of causality') by using suitable surrogate data. This means that the surrogate data should be prepared in such a way that the causal dependency of interest is destroyed by constructing the surrogates but trivial dependencies of no interests are preserved. [15]

TE has also some limitations that have to be considered carefully to avoid misinterpretations of results. TE may result false positives when the embedding parameters for the reconstruction of state space are not chosen correctly. Strong non-stationarities in the data infer or make it impossible to average over time to reliably estimate the probability densities on which TE is based. Therefore, TE should only be used on data of sufficient length that show at most weak non-stationarities. One approach to overcome this limitation is by using the trial structure of data sets. Second, TE analysis works better for pairwise analysis. Although a fully multivariate analysis is

conceptually possible, practical data lengths and large computation time restrict its use. Thirdly, TE analysis is difficult to interpret when signals have different physical origin such as an electric field and a chemical concentration. The reason is that even though the signals entering the TE analysis are z-scored to obtain certain normalization, there is no clear physical of distance in the joint space of the signals. [15]

Finally, there are some general limitations related to the concept of causality as defined by Wiener. Therefore, methods based on Wiener's principle such as TE and Granger Causality share the same limitations. [15]

1) There must not be any unobserved common causes that do not enter the analysis, i.e., the description of all system involved has to be causally complete.
2) No causality can be inferred if two systems are related by a deterministic map. This would exclude systems exhibiting complete synchronization.
3) The axiom that the present and past may cause the future but the future may not cause the past. This means that interactions taking place faster than the sampling rate must be missed.

Garofalo et al. compared CC, MI, JE and TE methods in their study [14] which suggested that TE provided the best performances. In that study, MI method showed the worst performances.

4.6 Connectivity analysis software

There exist several software packages for the connectivity analysis. Some are designed mainly for EEG/MEG data analysis such as eConnectome [52] software, whereas the others are designated for MEA data analysis such as SPYCODE [49], MeaTools [53] and MeaBench [54]. Common for those software packages is that most of them are toolboxes, which are designed to work in Matlab environment (SPYCODE, Brain Connectivity toolbox [55], BSMART [56], TRENTOOL [51], FIND [57]). To mention few freely available software, Sections 4.6.1 - 4.6.3 introduce few recently published toolboxes (TRENTOOL, SPYCODE and Brain connectivity toolbox) for connectivity analysis. They all work in Matlab environment.

4.6.1 TRENTOOL (the TRansfer ENtropy TOOLbox)

TRENTOOL (The Transfer Entropy Toolbox) is an open source toolbox to estimate neural directed interactions with transfer entropy developed by Lindner et al. [51] TRENTOOL is implemented as a Matlab toolbox and is available under an open source license (GPL v3). It is closely related to Fieldtrip. TRENTOOL integrates seamlessly with this toolbox by sharing a common data format.

TRENTOOL is designed to use transfer entropy on any kind of time series data. TRENTOOL aims to be user-friendly and makes the computational methods available

for experimental studies although it doesn't provide a graphical user interface. Documentation of all relevant parameters is straightforward and TRENTOOL analysis scripts typically comprise just two or three high level functions and the specification of a handful of analysis parameters. [51]

When using transfer entropy method, several parameters including embedding dimensions and delays, and prediction times have to be estimated from the data before for the method to work well on finite noisy data. In TRENTOOL, parameters for delay embedding are automatically obtained from the data. TRENTOOL also calculates the TE values for each individual prediction time that user has set up and estimates the optimal prediction time based on those results. TE values are estimated by the Kraskov-Stögbauer-Grassberger estimator and then subjected to statistical test against suitable surrogate data. Experimental effect can then be tested on a second level and results can be plotted using Fieldtrip layout formats. [51] A flow chart representing the basic structure of TRENTOOL is presented in Figure 11.

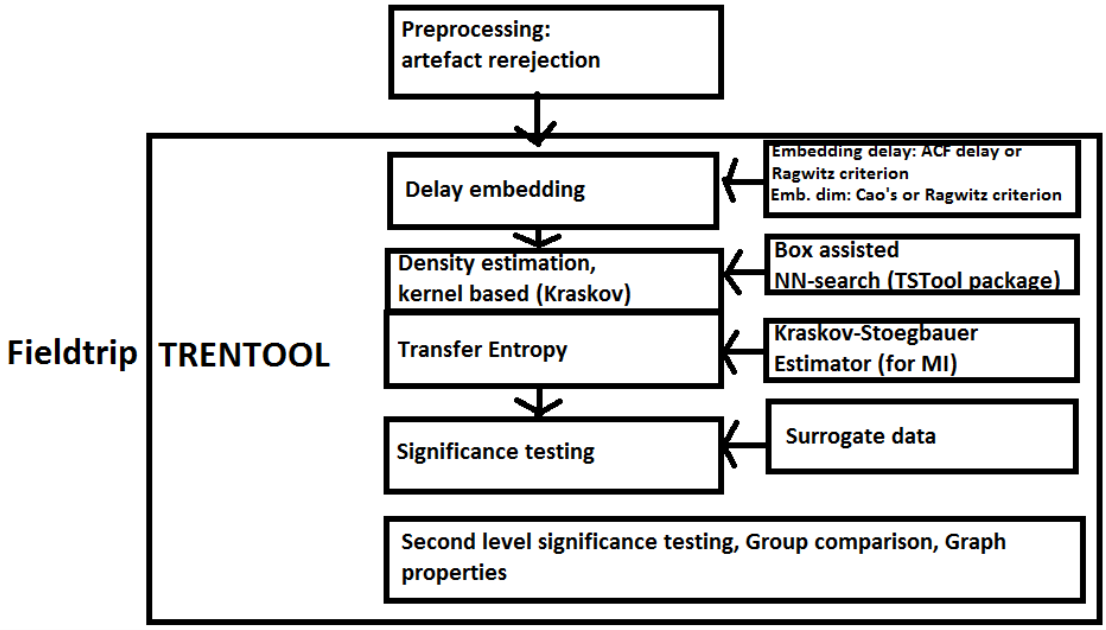

Figure 11. *A flow chart representing the basic structure of TRENTOOL.*

4.6.2 SPYCODE

SPYCODE is a recently developed software package (Bologna et al. 2010) for multi-channel analysis [49]. It has been developed through a user-friendly Graphical User Interface (GUI) for Matlab environment. Although in recent years a number of scientist have been working to develop custom-made tools capable of analysing multi-electrode recorded data, such as MEATOOLS, MEABENCH, FIND and BSMART, those software lack the ability to provide the users with a large number of algorithms for data analysis. They are also not able to manage massive quantities of data. SPYCODE is designed to overcome these limitations. It provides working environment that enables to perform efficient data processing and management since it includes a large number of

standard and advanced signal analysis tools. It also includes novel analyses which are published recently. To provide few examples, SPYCODE includes cross correlation, information theory based methods, extraction of connectivity maps, self-adapting bursts and network burst detection. [49]

The GUI offers a comprehensive menu bar through which the user can choose the analysis to perform. The GUI menu is split into sections by function type. The first level consists of eleven levels, which are named: 'Data Conversion', 'Pre-processing', 'Spike Detection', 'Plot', 'PSTH', 'Spike Analysis', 'Burst Analysis', 'Cross Correlation', 'Additional Tools', 'Multiple Analysis', and 'Help'. The overview of data analysis procedure implemented with SPYCODE is shown in Figure 12. SPYCODE is available for researchers upon request. [49]

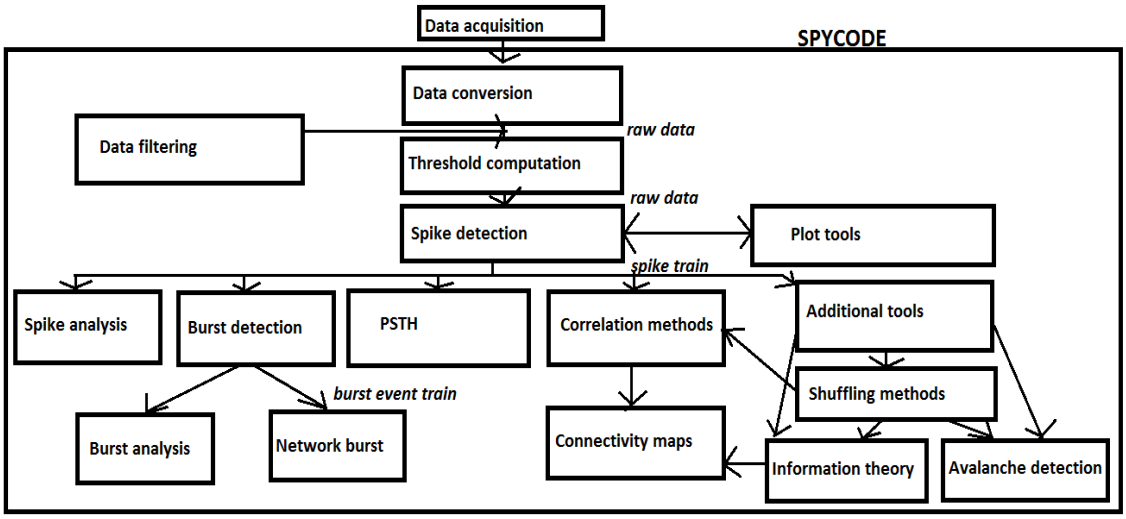

Figure 12. *Overview of data analysis procedure implemented with SPYCODE.*

4.6.3 Brain Connectivity Matlab toolbox

Brain Connectivity is freely available Matlab toolbox, which contains a collection of complex network measures and large-scale neuroanatomical connectivity datasets. It is developed by Mikail Rubinov and Olaf Sporns in 2009 and it has been continually updated [55]. A number of features distinguish it from most other toolboxes. It includes many recently developed network measures, which are discussed in paper [58], but are not yet widely available. It provides also weighted and directed variants for all its measures. Moreover, the toolbox provides functions for network manipulations (such as thresholding) and includes algorithms for generating null-hypothesis networks of predetermined (ordered, random and other) topologies. [58]

The whole list of functions and their definitions can be found on the home page of the toolbox [55], but just to give few examples, this toolbox includes for example the following measures:

- **Degree:** Node degree is the number of links connected to the node
- **Density:** Density gives the fraction of present connections to possible connections

- **Characteristic path length:** The characteristic path length is the average shortest path length in the network
- **And so on.**

In order to use this toolbox for time series data, the data should be first converted in matrix (network) form, for example by computing a correlation or coherence matrix for the time courses and then thresholding. [58] The detailed information can be found in [58] and [59].

5 METHODS AND MATERIALS

5.1 Structure of study

The study is divided into two sections – simulated connectivity signal studies and real MEA data analysis. Four combinations of three signals were constructed for simulation connectivity signal study so that we were able to validate whether the methods correctly identify the known connections. We also provide an example of real MEA data analysis with the same methods and analysis parameters. In real MEA data analysis, the same well of two different pharmacological measurements: bicuculline (excitative) and cnqx+dap5 (inhibitive) and is analysed.

In our study, we concentrated on the analysis of local field potentials (LFPs). Although much effort has been made before on the studies of spiking activity, they only provide information about the outputs of neuronal cells, whereas local field potentials are thought to arise largely from dendritic activity and therefore reflect inputs of neuronal cells. In the LFPs, only the lower fluctuations are preserved and quick fluctuations in the potential difference are filtered out. The quick fluctuations are caused by the short inward and outward currents of the action potential. Therefore the action potentials play no role in the local field potentials. Thus, the LFPs are composed of the more sustained currents in the tissue, i.e., somato-dendritic currents. The LFP is obtained by low-pass filtering the extracellular voltage. We used the same frequency band settings for LFPs as [16] in their study (low-pass filtering below 300 Hz and excluding DC of 50 Hz).

5.1.1 Simulated connectivity signal study

Two signals with good signal-to-noise ratio were chosen for simulation connectivity signal study. Both signals were recorded using a standard electrode (200/30iR-Ti, layout 8x8) MEA layout. Signal 1 has 218 detected spikes and signal 2 has 540 spikes. Both signals are 2 420 000 samples long. The time plots of signal 1 and signal 2 are found in Figures 13 and 14 in Appendix 1. These two signals were used to construct four combinations, each consisting 3 signals. The combinations were constructed in such a way that additional signals were created by adding delays or summation to the original signals. All four combinations are presented below:

Combination 1

Signal 1	Signal 1	Signal 1 (+2ms delay)

Combination 2

Signal 1	Signal 1 (+2ms delay)	Signal 1 (+10ms delay)

Combination 3

Signal 1	Signal 2	Signal 1 + Signal 2

Combination 4

Signal 1	Signal 1 + Signal 2	Signal 1 (+2ms delay) + Signal 2

5.1.2 Real MEA data analysis

Signals were recorded using six-well MEA platforms (6wellMEA200/30iR-Ti-w/o, layout 6x(3x3)). The datasheet of the used 6-well MEA representing the size and locations of electrodes is found on [60]. Two measurements with different pharmacological agents being present were selected for this study. The selected pharmacological measurements were bicuculline and cnqx+dap5. Bicuculline is a GABA antagonists, which inhibits the action of GABA and therefore produces a stimulation effect. Cnqx+dap5 is a pharmacological agent that blocks excitatory receptors and therefore produces an inhibition effect. To enable considerably easy interpretation of the real study results, only the results of well C data (electrodes C1-C9) are presented in this thesis. The amounts of detected spikes for both measurements are shown in Table 1.

Table 1. *The amount of detected spikes for each electrode of C-well in bicuculline and cnqx+dap5 pharmacological measurements.*

	Electrode (signal)	**Amount of detected spikes**
Bicuculline	C1	10477
	C2	463
	C3	30
	C4	7017
	C5	5
	C6	4
	C7	4276
	C8	2169
	C9	184
Cnqx+dap5	C1	1178
	C2	19
	C3	5
	C4	995
	C5	3
	C6	7
	C7	71
	C8	721
	C9	5

5.2 Neuronal cells and cultures

The hESC lines HS181, HS360 and HS362 derived at Karolinska Institutet (Hospital Huddinge, Stockholm, Sweden), and 06/015 derived at Regea (University of Tampere, Tampere, Finland) were used for neuronal differentiation. The derivation, characterization and differentiation of the hESC lines were approved by the ethics committee of the Karolinska Institutet. The ethics committee of the Pirkanmaa Hospital District provided approval for Regea to culture the hESC lines derived at the Karolinska Institutet and to derive and culture new hESC lines. Precise cell culturing information can be found on [31].

5.3 Data acquisition

The MEA dishes were sealed in a laminar flow hood with a semi-permeable membrane (ALA MEA-MEM, ALA Scientific Instruments Inc., Westbury, NY), that is selectively permeable to gases (CO_2, O_2). This was done to keep the cultures sterile prior to recordings. The sealed MEA dishes were then placed into the MEA amplifier (MEA-1060BC, Multi Channel Systems) and allowed to equilibrate for 3 to 5 min before the onset of the recordings. A bandwidth of 1 to 10 kHz and an MEA gain of 1100 were utilized. Signals were sampled at 20 kHz using a data acquisition card controlled through MC_Rack software (both from Multi Channel Systems). A TC02 temperature controller (Multi Channel Systems) was used to maintain the culture temperature at +37℃. Background noise of less than 10 μV_{rms} was allowed. All raw data was stored in the Multi Channel Systems data format for later processing. Spike detection was performed using MC_Rack (Multi Channel Systems) with a threshold of 5.5 times the standard deviation of the noise level. The length of the signals were 2 420 000 samples (=121 s).

5.4 Connectivity analysis

5.4.1 Selection criteria of the connectivity analysis methods

Three neuronal connectivity analysis methods were chosen for this study based on the review made on the Section 2.4. The chosen methods were Phase Lock Value, generalized Partial Directed Coherence and Transfer Entropy. The methods were chosen in order to enable the comparison of the methods of different category. PLV gives undirectional information whereas gPDC and TE offer directional information. PDC is the most widely accepted method of Multivariate Autoregressive models so we decided to use the enhanced and generalized form of it – gPDC. In previous study made by Garofalo et al. [14] it was suggested that TE provides the best and most reliable results of Information Theoretic measures. We were also interested in comparing results

between PDC and TE, as PDC analysis requires the use of a linear stochastic model, whereas TE does not require a model of the interaction. The Table 2 below lists concisely the main differences of the chosen three methods.

Table 2. *A brief comparison of the selected methods of neuronal connectivity analysis.*

Name	Directionality	Stationarity	Linearity	Signal type	Model requirement	Application
PLV	Undirectional information	No stationarity requirement	Linear and non-Linear signals	Continuous	No	Mostly EEG
gPDC	Directional information	For stationary signals	Only linear signals	Continuous	Yes	Mostly EEG
TE	Directional information	Signals should be at most weakly non-stationary	Linear and non-linear signals	Continuous or binary	No	EEG/MEG, fMRI, cultured neuronal populations

5.4.2 Phase Lock Value based analysis

Prior to PLV calculation the data was pre-processed first by low pass-filtering the data below 300 Hz, then decimating the signal from 20 kHz to 1 kHz, and finally notch filter was applied to remove the 50 Hz power line frequency. All the calculations were run in Matlab by constructing the codes which followed the steps presented in Section 4.1. The data were analysed by using a moving-window technique in such a way that the time series were divided into segments of 5000 sampling points each, corresponding to a window length of 5 s at the decimated sampling rate, and windows overlapped by 20%. The most time-consuming part of the algorithm is a fast Fourier transform (FFT) algorithm for the calculation of Hilbert transform, so the computational speed of the algorithm depends of the window length of sampling points.

During the PLV calculation, the following steps were also performed based on the paper by Florian Mormann et al. [61]. Each window was tapered using a cosine half wave (Hanning window) before performing the Fourier transform to avoid the edge effects. Moreover, the Hilbert transform requires integration over infinite time, which cannot be performed for a window of finite length, hence 10% of the calculated instantaneous phase values were discarded on each side of every window.

The threshold values for significance were obtained like suggested in [6]. This was done by creating a surrogate data with phase randomization. The PLV calculation was

then exerted to surrogate data, and those values defined the threshold for significance. The surrogate data was created using surrVFT.m file, which is freely available at the website of eMVAR – Extended Multivariate Autoregressive Modelling Toolbox [62]

5.4.3 Generalized Partial Directed Coherence

Before gPDC analysis, the data was pre-processed by low pass-filtering the data below 300 Hz, then decimating the signals from 20 kHz to 1 kHz and finally removing the 50 Hz by a notch filter. In addition to these steps, data was also detrended and demeaned like suggested in [63]. Detrending is a pre-processing step which removes a best-fitting line (linear trend) from the data. A linear trend basically means a systematic increase or decrease in the data, which can result from sensor drift, for example. Whereas, demeaning is used to remove a constant offset. The result data after demeaning has the same shape as original data but the whole plot is shifted up or down by a constant amount and the average value of the signal will be zero.

The gPDC analysis was performed using AsymPDC Package 1.0 developed by Dr. L.A. Baccala and Dr. K. Sameshima at University of Sao Paolo [64]. This toolbox includes all the necessary steps to estimate the gPDC: MAR model order selection, MAR algorithm and significance analysis. The AIC-criterion was used to estimate the optimal MAR model order and Nutall-Strand algorithm was used for MAR estimation. The diagnostic test of residuals was performed with Portmanteau test, which tests the adequacy of the MVAR model fitting. Portmanteau test detects whether the MAVR model fitting is good or poor, i.e., whether the MVAR model residual null hypothesis is accepted for whiteness for some alpha (1% or 5%). The significance analysis for the PDC results was done with the tools implemented in the toolbox. The significance level in the toolbox was defined like suggested in [65]. Significance level for gPDC null hypothesis testing was set to 5%. The stationarity of the signals were tested using cca_sacf function in Granger Causal Connectivity Analysis Toolbox [63]. Auto-correlation function (ACF) is the cross-correlation of a signal with itself. Stationarity means that the statistical properties of the signal, i.e., its mean and variance do not change over time. A stationary signal will have an autocorrelation function that falls off very quickly close to zero, whereas a non-stationary signal has an autocorrelation function that falls of slowly.

5.4.4 Transfer Entropy

The Transfer Entropy analysis was done with TRENTOOL toolbox, which works in Matlab and is freely available on the home web page of TRENTOOL [66]. Prior to TE analysis, the same first three pre-processing steps were applied like with the two other methods above. First, the data was low pass filtered below 300 Hz, then it was decimated from 20 kHz to 1 kHz, and finally the 50 Hz was removed by a notch filter. In addition, detrending was applied to the signals after the steps above.

The data was first prepared by dividing the signals into several trials like suggested in [51]. We divided the pre-processed signals into 20 trials. The signals were 121 000 samples long after decimation so after cutting them into 20 trials, each set of trial was 15 005 samples long (~15 s). Like presented in equation (38), TE calculation requires the parameters of embedding delay, embedding dimensions and prediction time. Prediction time quantifies the expected interaction delay between the two systems. The embedding delay and dimensions were automatically optimized by Ragwitz criterion in TRENTOOL. Ragwitz criterion is a method which optimizes the embedding dimension and embedding delay for deterministic and stochastic data. The optimal prediction time is also automatically detected after the user has set the prediction range being observed. We set the prediction time range between 1ms – 10ms.

The significance test was also performed using TRENTOOL. The toolbox creates a surrogate data and performs a permutation test between the TE values of the data and the surrogates. Surrogate data is a generated data against which the original data is tested against a null hypothesis. Surrogate data preserve the same autocorrelation, local mean and variance as the original data. Permutation test (also called randomization test) is a type of statistical significance test. In permutation test the distribution of the test statistic under the null hypothesis is obtained by calculating all possible values of the test statistic under rearrangements of the labels on the observed data points. Surrogate type, the number of permutations and alpha parameters were set to default values. Surrogate type was set to trialshuffling (trial(n+1)), number of permutations was set to 190100 and significance level for the permutation test (alpha) was set to 0.05. Additionally, the significance of each signal pair was also analysed using False Discovery Rate (FDR) like suggested in [51]. This technique requires a stronger level of evidence to be observed in order for an individual comparison to be deemed significant.. Finally, the result figures were created using TEplot2D function in TRENTOOL. In the result figures arrow refers to the direction of plausible connection and non-existence of arrows refers that there are no detected connections between the signal pairs.

6 RESULTS

6.1 Simulated connectivity signal study

6.1.1 Phase lock Value

Several sets of signals have been generated as described in Section 5.1.1. All these signal combinations were analysed with PLV-analysis in order to validate how different modifications in signals affect to PLV-results and can they correctly recognize the known connections. It is important to remind that PLV quantifies the overall level of synchronization and doesn't detect any direction of information flow. It is also only sensitive to the phases of the signals, irrespective of the amplitudes of the two signals. It is also bivariate measure, so all calculations have been made between two signals and the properties of the other signals in the combination do not affect the calculations.

The measured PLV-values and the corresponding threshold values for significance are shown in Table 3. The PLV-values refers to average PLV-values between the corresponding signals. As mentioned in Section 5.4.2., the signals were divided into windows corresponding to 5 s each, and then PLV was calculated to each window between the signals. The final PLV-value is then average of PLV-values of all windows between each signal pair. In the Table 3, the bigger value between PLV-value and the corresponding threshold for significance of each signal pair is bolded in order to clearly see, in which cases the PLV-value exceeded the threshold for significance. As the results show, only the signal pair of signal 1 and signal 2 without any modification being made didn't exceed the threshold for significance.

In addition, for each signal pair, the maximum PLV-value and minimum PLV-value were obtained from the PLV-values of each window. The detailed results of each signal combination including the minimum, average and maximum PLV-values are shown in the Figures 15-18 in Appendix 2. To make clear, average PLV-values in Appendix 2 refers to the PLV-values shown in Table 3. The figures in Appendix 2 are constructed in such a way, that the results of each signal pair of the corresponding combination are grouped, and the corresponding minimum PLV, average PLV and maximum PLV-values are then shown in bar graph.

Table 3. *PLV-values of simulated connectivity signal study. The PLV-value and threshold for significance are presented for each signal pair.*

	Signal pairs	**PLV-value**	**Threshold for significance**
Combination 1	Signal 1 <-> Signal 1	**1.0**	0.050
	Signal 1 <-> Signal 1 (+2ms)	**0.338**	0.045
Combination 2	Signal 1 <-> Signal 1 (+2ms)	**0.338**	0.041
	Signal 1 <-> Signal 1 (+10ms)	**0.251**	0.049
	Signal 1 (+2ms)<-> Signal 1 (+10ms)	**0.280**	0.059
Combination 3	Signal 1 <-> Signal 2	0.048	**0.050**
	Signal 1 <-> Signal 1 + Signal 2	**0.593**	0.042
	Signal 2 <-> Signal 1 + Signal 2	**0.612**	0.055
Combination 4	Signal 1 <-> Signal 1 + Signal 2	**0.593**	0.050
	Signal 1 <-> Signal 1 (+2ms) + Signal 2	**0.233**	0.052
	Signal 1 + Signal 2 <-> Signal 1 (+2ms) + Signal 2	**0.532**	0.063

6.1.2 Generalized Partial Directed Coherence

The results of gPDC are shown in Figures 19-22 in Appendix 3. The result figures are observed in the following way. Each signal combination has 3 x 3 (j x i) small figures excluding the diagonal figures which refer to the activity from each signal towards itself. gPDC is asymmetric relation, and the gPDC graphics should be read as if the flow of information is been from the x-axis (j) variable toward y-axis (i) variable. The first variable in i and j refers to the first signal mentioned in the figure title, the second variable in i and j refers to the second signal mentioned in the figure title and finally, the third variable in i and j refers to the third signal mentioned in the figure title. Taking as an example, signal combination 2 in Appendix 3, the figure which is second in the x-axis (j=2) and first in the y-axis (i=1) refers to the information flow from signal 1(+2ms) toward signal 1. The horizontal axis (0-300) in each small figure refers to the frequency in Hz and the vertical axis (0-1) in each small figure refers to the gPDC value. gPDC informs the strength of information flow at specific frequencies. Green line in the figure refers to gPDC value that is not significant and red gPDC values indicate that the gPDC values are significant at those specific frequencies.

The MVAR-model orders for each signal combination estimated by AIC-criterion are listed below:

- Combination 1: model order 127, POOR MVAR model fitting
- Combination 2: model order 168, POOR MVAR model fitting
- Combination 3: model order 1, POOR MVAR model fitting
- Combination 4: model order 77, POOR MVAR model fitting

POOR MVAR model fitting is in the sense of Portmanteau test for residuals, i.e., the MVAR model residual null hypothesis was not accepted for whiteness with alpha 5%. This means that even the optimized model orders were not adequate for gPDC calculation.

In order to fully interpret the results, the results of auto-correlation function for each signal after pre-processing are shown in Figures 23-28 in Appendix 4. The figures show the autocorrelation function (ACF) at specified lags (0-200).

6.1.3 Transfer Entropy

We tested the Transfer Entropy method with a representative set of simulated data which we have control over all parameters such as delay. The TE results of each signal combination are presented in Tables 4-7. It is important to remind that TE detects the directional flow of information so there are separate results for both directions between each signal pair. Each table consists of p-values, average TE-values over 20 trials for each signal pair, presence of the significant connection at alpha level 5%, presence of significant connection after correction for multiple comparisons and estimated optimal prediction time by the TE algorithm. P-values represent the probability of observing Type 1 error (false positive), so low p-values mean that the results are highly accurate. Significant connections at alpha level 5% are listed either as ‘No’, meaning that the TE algorithm did not detect any connections between the signal pair and ‘YES’, that there are detected connection between the signal pair at the prescribed alpha level. The significance of connection after correction for multiple comparisons is presented similarly. It is based on FDR-method which requires more evidence in order the connection to be significant. Finally, the optimal prediction time, which was estimated by the algorithm, is presented in the last column of each table. According to the p-values, it is observed that they are all really small and there is high probability that the detected connections are accurate.

Table 4. *TE results for signal combination 1.*

Signal pairs	**p-values**	**TE-values**	**Significant connection at alpha level 5%**	**Significant connection after correction for multiple comparisons**	**Estimated optimal prediction time**
Signal 1 → Signal 1	**5.2604e-06**	0.0039	YES	YES	6ms
Signal 1 → Signal 1 (+2ms)	**5.2604e-06**	0.0012	YES	YES	7ms
Signal 1 (+2ms) → Signal 1	**5.2604e-06**	0.6745	YES	YES	2ms

Table 5. *TE results for signal combination 2.*

Signal pairs	**p-values**	**TE-values**	**Significant connection at alpha level 5%**	**Significant connection after correction for multiple comparisons**	**Estimated optimal prediction time**
Signal 1 → Signal 1 (+2ms)	**5.2604e-06**	0.0015	YES	YES	7ms
Signal 1 → Signal 1 (+10ms)	**5.2604e-06**	-0.0019	YES	YES	9ms
Signal 1 (+2ms) → Signal 1	**5.2604e-06**	0.6746	YES	YES	2ms
Signal 1 (+2ms)→ Signal 1 (+10ms)	**5.2604e-06**	0.0015	YES	YES	1ms
Signal 1 (+10ms)→Signal 1	**5.2604e-06**	0.6722	YES	YES	10ms
Signal 1 (+10ms)→ Signal 1(+2ms)	**5.2604e-06**	0.6780	YES	YES	8ms

Table 6. *TE results for signal combination 3.*

Signal pairs	**p-values**	**TE-values**	**Significant connection at alpha level 5%**	**Significant connection after correction for multiple comparisons**	**Estimated optimal prediction time**
Signal 1 → Signal 2	**0.0060**	-0.0034	YES	NO	2ms
Signal 1 → Signal 1 + Signal 2	**5.2604e-06**	0.0138	YES	YES	1ms
Signal 2 → Signal 1	**0.1032**	-0.0064	NO	NO	1ms
Signal 2→ Signal 1 + Signal 2	**5.2604e-06**	0.0151	YES	YES	1ms
Signal 1 + Signal 2→Signal 1	**5.2604e-06**	0.0126	YES	YES	1ms
Signal 1 +Signal 2→ Signal 2	**5.2604e-06**	0.0115	YES	YES	1ms

Table 7. *TE results for signal combination 4.*

Signal pairs	**p-values**	**TE-values**	**Significant connection at alpha level 5%**	**Significant connection after correction for multiple comparisons**	**Estimated optimal prediction time**
Signal 1 → Signal 1 + Signal 2	**5.2604e-06**	0.0138	YES	YES	1ms
Signal 1 → Signal 1 (+2ms) + Signal 2	**3.5771e-04**	-0.0014	YES	YES	2ms
Signal 1 + Signal 2→ Signal 1	**5.2604e-06**	0.0126	YES	YES	1ms
Signal 1 + Signal 2→ Signal 1 (+2ms) + Signal 2	**5.2604e-06**	0.0056	YES	YES	1ms
Signal 1 (+2ms) + Signal 2→Signal 1	**5.2604e-06**	0.1333	YES	YES	1ms
Signal 1 (+2ms) + Signal 2→ Signal 1 + Signal 2	**5.2604e-06**	0.1186	YES	YES	1ms

6.2 Real MEA data analysis

6.2.1 Phase Lock Value

Like mentioned in the Section 5.1.2., in the real study analysis section of this thesis we analysed all signals in well C of two different pharmacological measurements: bicuculline and cnqx+dap5. The measured PLV-values for bicuculline and the corresponding threshold values for significance are shown in Table 8, and respectively for cnqx+dap5 measurement in Table 9. The PLV-values refers to average PLV-values between the corresponding signals. As mentioned in Section 5.4.2., the signals were divided into windows corresponding to 5 s each, and then PLV was calculated to each window between the signals. The final PLV-value is then average of PLV-values of all windows between each signal pair. In the Tables 8 and 9, the PLV value is bolded if it exceeded the threshold for significance. The PLV value is in Italic letters, if the PLV-value did not exceed the value for significance. Regarding to the results in Table 8, only the following signal pairs: C1<->C2, C4<->C8 and C7<->C8 did not exceed the threshold for significance in bicuculline measurement of well C. The results in Table 9 show the PLV-values for each signal pair in cnqx+dap5 measurement exceeded the threshold for significance.

Table 8. *PLV-values for each signal pair in well C of bicuculline pharmacological measurement.*

	C2	C3	C4	C5	C6	C7	C8	C9
C1	*0.1541* (0.1568)	**0.2089** (0.0332)	**0.5455** (0.3691)	**0.1430** (0.0289)	**0.1615** (0.0152)	**0.3053** (0.2195)	**0.3767** (0.1946)	**0.1542** (0.0311)
C2		**0.3108** (0.0150)	**0.1592** (0.1466)	**0.1849** (0.0147)	**0.2177** (0.0129)	**0.2603** (0.1407)	**0.1849** (0.1234)	**0.2405** (0.0155)
C3			**0.1575** (0.0320)	**0.3729** (0.0167)	**0.4165** (0.0103)	**0.1836** (0.0204)	**0.2290** (0.0232)	**0.4632** (0.0138)
C4				**0.1060** (0.0330)	**0.1127** (0.0186)	**0.7372** (0.4176)	*0.1669* (0.2879)	**0.1154** (0.0248)
C5					**0.2967** (0.0112)	**0.1260** (0.0205)	**0.1772** (0.0297)	**0.2903** (0.0103)
C6						**0.1367** (0.0256)	**0.1791** (0.0196)	**0.3197** (0.0105)
C7							*0.2091* (0.2871)	**0.1436** (0.0213)
C8								**0.1600** (0.0287)

Table 9. *PLV-values for each signal pair in well C of cnqx+dap5 pharmacological measurement.*

	C2	C3	C4	C5	C6	C7	C8	C9
C1	**0.1826** (0.1630)	**0.3516** (0.0289)	**0.2540** (0.1909)	**0.2587** (0.0379)	**0.2691** (0.0303)	**0.3814** (0.3130)	**0.1976** (0.1313)	**0.2895** (0.0386)
C2		**0.1704** (0.0143)	**0.3849** (0.1852)	**0.1335** (0.0235)	**0.1413** (0.0317)	**0.3804** (0.2027)	**0.1825** (0.1374)	**0.1414** (0.0166)
C3			**0.2454** (0.0369)	**0.4069** (0.0173)	**0.4244** (0.0108)	**0.1922** (0.0401)	**0.3491** (0.0242)	**0.4193** (0.0138)
C4				**0.1954** (0.0240)	**0.2092** (0.0270)	**0.7324** (0.2646)	**0.2618** (0.2221)	**0.1948** (0.0442)
C5					**0.3561** (0.0106)	**0.1663** (0.0252)	**0.2925** (0.0324)	**0.3295** (0.0122)
C6						**0.1760** (0.0317)	**0.3056** (0.0184)	**0.3380** (0.0146)
C7							**0.3408** (0.1900)	**0.1490** (0.0460)
C8								**0.2813** (0.0184)

The results showed connections almost for all signal pairs being observed. Therefore we wanted to further test what kind of PLV-values are present between the signals of different wells in 6-well MEA. Couple example results of larger tests are shown in Figures 29 and 30 in Appendix 5. The Figure 29 shows the PLV values when electrode C4 is the reference in bicuculline measurement, and Figure 30 shows the PLV values when electrode C7 is the reference electrode in cnqx+dap5 measurement. The results indicate that PLV method gives considerably large PLV-values, i.e., significant connections also for electrodes of different wells.

6.2.2 Generalized Partial Directed Coherence

The gPDC results of both pharmacological measurements: bicuculline and cnqx+dap5 are shown in Figures 31 and 32 in Appendix 6. The result figures are interpreted like mentioned in detail in the Section 6.1.2. The results of C-well of bicuculline measurement show that there are some information flow from electrode C7 towards all other electrodes, from electrode C4 towards all other electrodes except electrode C5 and finally, from electrode C1 towards electrodes C1 and C2. Whereas, the results of C-well of cnqx+dap5 measurement indicate that there only some information flow at specific frequencies from electrode C7 towards electrodes C4, C8 and C9. No other activity exists in cnqx+dap5 measurement according to the gPDC results shown in Appendix 6.

The MVAR-model orders for both pharmacological measurements estimated by AIC-criterion are listed below:

- Bicuculline, C-well: model order 160, POOR MVAR model fitting
- Cnqx+dap5: model order 198, POOR MVAR model fitting

In addition, the autocorrelation function test performed for all signals of C-well showed that there exist strong non-stationarities among all signals.

6.2.3 Transfer Entropy

The detailed results of bicuculline and cnqx+dap5 pharmacological measurements of well C are shown in Tables 10 and 11 in Appendix 7. Both measurement results are presented in respective tables similarly with section 6.1.3. The first column of the tables refers to the direction of information flow between channel pair, second column indicates the p-value, and third column refers to the significant connections at alpha level 5%. Fourth column indicates whether there are significant connections after correction for multiple comparisons and the last column tells the estimated optimal prediction time between the signals. The results show that there were no detected significances after correction for multiple comparisons, but the method detected significances at alpha level 5% with the channel pairs shown in Table 12.

Table 12. *Detected significances of bicuculline and cnqx+dap5 pharmaceutical measurements at alpha level 5%. The second column indicates the source electrode and the third column indicates the target electrode of detected significance.*

Measurement	From (source)	To (target)
Bicuculline	C1	C4,C5,C6,C8
	C2	C9
	C3	C2,C5
	C4	C7
	C5	C8
	C6	C5,C7,C9
	C7	C3,C4,C5
	C8	C5
	C9	C2
Cnqx+dap5	C1	C8,C9
	C2	-
	C3	C9
	C4	C2,C7,C9
	C5	C9
	C6	C2
	C7	C2,C4,C5,C6
	C8	C6,C9
	C9	C2,C8

7 CONCLUSIONS AND DISCUSSION

The purpose of this thesis was to review connectivity measures and select few of them with different properties in order to test how applicable they are for MEA data and what kind of information they'll offer. Most of the widely used connectivity estimators have been studied for signals of different origin such as EEG, MEG or fMRI data so a great interest for us was to examine their validity for MEA data. Based on the review section of the methods, we selected Phase Lock Value, generalized Partial Directed Coherence and Transfer Entropy methods for further analysis with our data. PLV is a bivariate measure of phase-coupling, which is applicable both for linear and non-linear signals. By far, PLV has been widely studied on EEG applications [6, 36, 37, 61]. Partial Directed Coherence is maybe the most accepted method of Multivariate Autoregressive Models. It describes the directional flow of information from the activity in the ROI $s_j(n)$ to the activity in $s_i(n)$, hence common effects produced by other ROIs $s_k(n)$ on the latter are subtracted, leaving only description that is specifically from $s_j(n)$ to $s_i(n)$. In our study we used generalized form of PDC, i.e., gPDC which abates few disadvantages that normal PDC has. Unlike normal PDC, gPDC is scale-invariant, it is not decreased when multiple signals are emitted from a given source and finally, gPDC allows conclusions on the absolute strength of the coupling [43, 44]. For our knowledge, most of the MVAR research has focused on EEG analysis and no publications of MVARs for MEA applications have been made. Transfer Entropy (TE) is an information theoretic measure which allows one to extract causal relationships from time series. TE provides directional information and does not assume any model being used. It is applicable also both for non-linear and linear signals. Garofalo et al. [14] pointed out that TE provided the best results of information theoretic measures in their study. In that study, they extracted dissociated cortical neuronal cells from rat embryos and plated then on 60-channel MEAs.

In our study, we concentrated on the analysis of local field potentials (LFPs). Although much effort has been made before on the studies of spiking activity, they only provide information about the outputs of neuronal cells, whereas local field potentials are thought to arise largely from dendritic activity and therefore reflect inputs of neuronal cells. The quick fluctuations are caused by the short inward and outward currents of the action potential. In the LFPs, only the lower fluctuations are preserved and quick fluctuations in the potential difference are filtered out. Therefore the action potentials play no role in the local field potentials. Thus, the LFPs are composed of the more sustained currents in the tissue, i.e., somato-dendritic currents. The LFP is obtained by low-pass filtering the extracellular voltage. We used the same frequency

band settings for LFPs as [16] in their study (low-pass filtering below 300 Hz and excluding DC of 50 Hz).

This study was divided into two parts: simulated connectivity signal study and real MEA signal study. In simulated connectivity signal study we chose two MEA signals with good signal-to-noise ratios. Using these two signals we constructed four sets of three signals by modifying these two original signals by adding delays or summing the signals together. In that way we had full control of certain parameters such as delay being present so we could validate the results more reliably. All the simulated connectivity signal combinations are shown in the Section 5.1.1. Although the main focus of this thesis concentrated on the simulated connectivity signal study section, we wanted to also compare which kind of results these selected methods gave for real signal study. For real signal study we used two pharmacological MEA measurements. The first was with bicuculline pharmacological agent being present, which is a GABA antagonist and inhibits the action of GABA, and therefore produces a stimulation effect. The other was with cnqx+dap5 which is a pharmacological agent being present, that blocks excitatory receptors and therefore produces an inhibition effect. From both of these measurements we analysed the same well C in this thesis. As a measurement data we used measurements of human embryonic stem cell derived neuronal networks *in vitro* on MEAs. The pharmacological data was measured with 6-well MEA, whereas the two signals being picked for simulated connectivity signal study were measured with normal 8 x 8 MEA, because they offered better signal-to-noise ratio than the available data of 6-well MEA.

In simulated connectivity signal study we wanted to explore which kind of information the selected methods will give when we have the full control of the delays being present and how the signals are mixed. To start with the PLV analysis of simulated connectivity signal study, all the obtained results seemed reasonable. The PLV-value between the Signal 1 with itself gave the value of one, which means the full phase coupling. All the other signal pairs gave PLV-values something between zero and one. The significance analysis of PLV claimed that all other PLV-values exceeded the threshold for significance except the signal pair Signal 1 and Signal 2, which was with two totally different signals. In that sense, it seems that PLV method managed to correctly recognize all the signal pairs with phase coupling. Thus the method could recognize the phase coupling even with the delay of 10 ms or when two different signals were summed together.

To continue with the simulated connectivity signal study, gPDC provided incoherent results. For first signal pair it didn't find any significant at any frequency even though it was the same signal twice and then with +2 ms delay. In combination 2 there were some connections on the frequency band of 50-100 Hz and then near 200 Hz. The combination 3 and 4 claimed that there were full connections between all frequencies 0-300 Hz although there were totally different signals present. It seems that the non-stationarity property of the signals caused problems for the gPDC method. MVAR method are only fully applicable and reliable if the analysed signals are fully stationary,

i.e., the statistical properties, for example variance do not vary over time. The autocorrelation function tests clearly showed that none of the signals in simulated connectivity signal study were stationary although the widely used and recommended pre-processing steps were performed. That is most probably the reason why none of the predicted MVAR model orders had good model fitting. Therefore, if the model fitting in MVAR methods is not good, one cannot reliably interpret the results of MVAR method.

To integrate the simulated connectivity signal study results, Transfer Entropy method provided interesting results. Two different significance analyses were performed: significance analysis at alpha level 5% and significant connection after correction for multiple comparisons. Both of these significant analyses were built in TRENTOOL toolbox. From signal 2 toward signal 1 the method claimed no significant connection with either of the significant analyses, whereas from signal 1 toward signal 2 (combination 3) the significance analysis at alpha level 5 % claimed connections but after multiple comparisons test it identified no connections. The results seemed promising in that sense, that from signal 2 toward signal 1 it found no connection and from signal 1 toward signal 2 it did not find connection either after correction for multiple comparison which is more strict significance test. In addition, TE method also calculates the results values for each binary prediction time (for example 1, 2, 3.. ms) that user has set to be analysed. Then the method selects the best fitting prediction time for each signal pair. The obtained results relating to the prediction time results seemed rational, when only the signal pairs from signal 1 toward signal 1 (+2 ms), from signal 1 toward itself and from signal 1 (+2 ms) toward signal 1 (+10 ms) gave clearly different prediction time results than expected. In these cases there might be also strong similarities between the analysed signals with different delays than we set, therefore the method recognized connection with different delay times than expected.

The PLV method in the analysis of C well in bicuculline measurement claimed that there were significant phase coupling between all other signal pairs except with C1 and C2, C4 and C7, and with C4 and C8. In the case of the same well in cnqx+dap5 measurement, significant coupling was present with all signal pairs based on PLV analysis. However, the two example figures in Appendix 5 show that there are also strong phase coupling between signals of different wells in 6-well MEA. We analysed the signals like [16] in their study with the local field potential frequencies below 300 Hz, excluding DC. Based on these results, it is clear that there are some strong distortions present which make obvious false connections between the signals. The signals in the real study clearly have much worse signal-to-noise ratios so it is difficult to recognize correctly the possible connections over the evident strong noise.

In the analysis of gPDC method of real MEA data signals, the same non-stationarity problem was present as with simulated connectivity study signals. The analysed signals were not stationary even after the recommended filtering steps in the literature, so the obtained MVAR model orders for both measurements had poor model order fitting. For that reason, the results of gPDC cannot be interpreted reliably. However it is notable, that gPDC results of bicuculline showed that there were clear directional flows of

information from electrodes C4 and C7 toward all other electrodes with several frequency bands. In the results of PLV, the similar combination C4 and C7 provided the greatest PLV value, i.e., 0.7372. The results of bicuculline also showed some directional flow from electrode C1 towards C2 and C3. In the case of cnqx+dap5 measurement, only some directional flow of information was noticeable from electrode C7 towards electrodes C4, C8 and C9. Still, these results are not fully interpretable, because of the poor model order fitting.

In the analysis of C-well of both pharmacological studies, TE did not detect any significant connections after correction for multiple comparisons. However, with significance analysis at alpha level 5% several connections were detected like shown in the Section 6.2.3. Based on this brief analysis, it is not clear whether these detected connections at alpha level 5% are correct or not. Based on the paper by [51], TE can handle considerably well the noise problem, although TE also requires that signals should be at least partly weakly stationary. In the case of the analysed signals, there were strong amount of noise present and with strong non-stationarities so it is evident that these facts can also infer the results of TE and either false positive or false negative results can occur.

Based on the results discussed before, PLV and TE methods seemed potential for further study in MEA measurements. PLV succeeded to give correct results in simulated connectivity signal study and TE also managed to provide good results with few inaccuracies. Therefore it seems that when the signals have fairly good signal-to-noise ratios, these two methods can be suitable for the analysis of MEA measurements. Both of these measurements are suitable for non-linear signals, which is typically the case in the measurements of neuronal cell cultures. However, the disadvantage of PLV compared to TE is that PLV provides only information about the overall strength of the signal pair being analysed. It does not take into account any causal dependencies and it does not provide any directional information. Usually the measured signals of neuronal cells are affected by several groups of neuronal cells signalling and PLV does not take into account how the neuronal cells between the measurement points have affected the results. TE not only provides directional information but also prediction about the optimal signal delay being present. Both of these properties are important when analysing signals of neuronal cells. It seems that the combination of both PLV and TE can be useful when validating neuronal networks. The results of gPDC showed that MVAR methods can only be applicable when signals are totally stationary either originally or by appropriate filtering. However, methods like gPDC can be very useful for neuronal cell network analysis if the signals are stationary, because it provides directional information over different frequency bands unlike the two other methods. With gPDC, it is possible to explore how signals are connected together on different frequency bands.

The real study results clearly showed that the presence of high noise disturbs the results. With both of pharmacological measurements with 6-well MEA the signal-to-noise ratio was very bad and therefore the methods gave very incoherent results.

Therefore, when there is much noise, we cannot say reliably whether the detected connections are correct or if there are any false positives or false negatives.

It is reasonable to point out that within this thesis it was impossible to test all these three methods with every possible settings and parameters. The purpose of this thesis was mainly just to review which kind of information can be revealed with these methods and do they have potential for further analysis on MEA signals.

This thesis did not test how settings like signal/trial length affects to the results of each method? Methods should also be tested for example with narrower frequency bands, and explore how those affects to the results? We used the referred filtering settings of other relevant papers, so it is also evident that different pre-processing steps can be potential for further research. It would be also interesting to know why the available 6-well MEA data had so high noise levels. Was the problem on the properties of 6-well MEA layout itself or on the measurement environment? It is clear, that further research is needed in order to validate these methods in detail for MEA measurements. Especially Transfer Entropy method seems very potential for further research in MEA measurements.

REFERENCES

[1] S.M. Potter, T.B. DeMarse, ‘’A New Approach to Neural Cell Culture for Long-Term Studies’’, *Journal of Neuroscience Methods*, vol.110, no.1-2, pp.17-24, Sept. 2001. http://dx.doi.org/10.1016/S0165-0270(01)00412-5

[2] J.A. Thomson, J. Itskovitz-Eldor, S.S. Shapiro, M.A. Waknitz, J.J. Swiergel, V.S. Marshall, J.M. Jones, ‘‘Embryonic Stem Cell Lines Derived From Human Blastocysts’’, *Science 6*, vol.282, no.5391, pp.1145-1147, Nov.1998. http://dx.doi.org/10.1126/science.282.5391.1145

[3] J. Ban, P. Bonifazi, G. Pinato, F.D. Broccard, L. Studer, V. Torre, M.E. Ruaro, ‘‘Embryonic Stem Cell-derived Neurons Form Functional Networks in vitro’’, *Stem Cells*, vol.25, no.3, pp.738-749, Nov.2006. http://dx.doi.org/10.1634/stemcells.2006-0246

[4] M. Chiappalone, A. Vato, L. Berdonini, M. Koudelka-Hep, S. Martinoia, ‘‘Network Dynamics and Synchronous Activity in Cultured Cortical Neurons’’, *Int, J. Neural Syst*, vol.17, no.2, pp.87-103, Apr.2007. http://dx.doi.org/10.1142/S0129065707000968

[5] X. Li, W. Zhou, S. Zeng, M. Liu, Q. Luo, ‘‘Long-term Recording on Multi-electrode Array Reveals Degraded Inhibitory Connection in Neuronal Network Development’’, *Bionsensors and Bioelectronics*, vol.22, no.7, pp.1538-1543, Feb.2007. http://dx.doi.org/10.1016/j.bios.2006.05.030

[6] J.P. Lachaux, E. Rodriguez, J. Martinerie, F.J. Varela, ‘’Measuring Phase Synchrony in Brain Signals’’, *Human Brain Mapping*, vol.8, no.4, pp.194-208, Nov.1999. http://dx.doi.org/10.1002/(SICI)1097-0193(1999)8:4<194::AID-HBM4>3.0.CO;2-C

[7] L. Astolfi, F. Cincotti, D. Mattia, C. Babiloni, F. Carducci, A. Basilisco, P.M. Rossini. S. Salinari, L. Ding, Y. Ni, B. He, F. Babiloni, ‘’Assessing cortical connectivity by linear inverse estimation and directed transfer function: simulations and applications to real data’’, *Clinical Neurophysiology*, vol.116, no.4, pp.920-932, Apr.2005. http://dx.doi.org/10.1016/j.clinph.2004.10.012

[8] A. Korzeniewska, M. Manczak, M. Kaminski, K.J. Blinowska, S. Kasicki, ‘’Determination of information flow direction between brain structures by a modified directed transfer function method (dDTF)’’, *J Neurosci Methods*, vol. 125, no.1-2. pp.195-207, May 2003. http://dx.doi.org/10.1016/S0165-0270(03)00052-9

[9] C. Wilke, L. Ding, B. He, ‘‘Estimation of Time-varying Connectivity Patterns Through the Use of an Adaptive Directed Transfer Function’’, *IEEE Trans Biomed Eng*, vol.55, no.11, pp.2557-2564, Nov.2008. http://dx.doi.org/10.1109/TBME.2008.919885

[10] L.A. Baccala, K. Sameshima, ‘’Partial Directed Coherence: A New Concept in Neural Structure Determination’’, *Biological Cybernetics*, vol.84, no.6, pp.463-474.May 2001. http://dx.doi.org/10.1007/PL00007990

[11] L.A. Baccala, D.Y. Takahashi, K. Sameshima, ‘‘Generalized Partial Directed Coherence’’, *Proceedings of the 15th International Conference on Digital Signal Processing. IEEE*, Cardiff, Jul.2007, pp.163-166. http://dx.doi.org/10.1109/ICDSP.2007.4288544

[12] L. Astolfi, F. Cincotti, C. Babiloni, F. Carducci, A. Basilisco, P.M. Rossini, S. Salinari, D. Mattia, S. Cerutti, D.B. Dayan, L. Ding, Y. Ni, B. He, F. Babiloni, ‘’Estimation of the Cortical Connectivity by High-Resolution EEG and Structural Equation Modeling: Simulations and Application to Finger Tapping Data’’, *IEEE Transactions on Biomedical Engineering*, vol.52, no.5, pp.757-768, May 2005. http://dx.doi.org/10.1109/TBME.2005.845371

[13] O. David, S.J. Kiebel, L.M. Harrison, J. Mattout, J.M. Kilner, K.J. Friston, ‘’Dynamic Causal Modeling of Evoked Responses in EEG and MEG’’, *Neuroimage*, vol.3, no.4, pp.1255-1272, May2006. http://dx.doi.org/10.1016/j.neuroimage.2005.10.045

[14] M. Garofalo, T. Nieus, P. Massobrio, S. Martinoia, ‘‘Evaluation of the Performance of Information Theory-Based Methods and Cross-Correlation to Estimate the Functional Connectivity in Cortical Networks’’, *PLoS ONE*, vol.4, no.8, Mar.2009. http://dx.doi.org/10.1371/journal.pone.0006482

[15] R. Vicente, M. Wibral, M. Lindner, G. Pipa, ‘’Transfer Entropy – a Model-Free Measure of Effective Connectivity for the Neurosciences’’, J Comput Neurosci, vol.30, no.1, pp.45-67, Feb.2011. http://dx.doi.org/10.1007/S10827-010-0262-3

[16] G. Kreiman, C. P. Hung, A. Kraskov, R. Q. Quiroga, T. Poggio, J.J. DiCarlo, ‘’Object Selectivity of Local Field Potentials and Spikes in the Macaque Inferior Temporal Cortex’’, *Neuron*, vol.49, no.33, pp.433-445, Feb.2006. http://dx.doi.org/10.1016/j.neuron.2005.12.019

[17] E. Haug, O. Sand, V. Ø.V. Sjaastadt, *Ihmisen Fysiologia*, 1-2th Edition, Helsinki, Finland, WSOY, 1999,526 p.

[18] A. Friedman, ‘’Introduction to Neurons’’, *in Tutorials in Mathematical Biosciences*, Mathematical Biosciences Institute, The Ohio State University, USA. [online] Available: http://www.springerlink.com/content/dr9jmp21qqae3bav/fulltext.pdf [cited 14.8.2012]

[19] *Neuron*, Wikipedia [online] Available: http://upload.wikimedia.org/wikipedia/commons/b/bc/Neuron_Hand-tuned.svg [cited 02.05.2013]

[20] A.R. Damasio, *The Scientific American Book of the Brain*, 1th Edition, Scientific American, Lyons Press, 2001, 340 p

[21] G. Deco, V.K. Jirsa, P.A. Robinson, M. Breakspear, K. Friston, ‘The Dynamic Brain: From Spiking Neurons to Neural Masses and Cortical Fields’, Plos Computation Biology, vol. 4, no. 8, Aug. 2008. http://dx.doi.org/10.1371/journal.pcbi.1000092

[22] L. Ylä-Outinen. ‘’Functionality of Human Stem Cell Derived Neuronal Networks - Biomimetic environment and characterization’’, Ph.D Dissertation, Department of Biotechnology, University of Tampere, Finland, 2012. http://urn.fi/urn:isbn:978-951-44-8756-9

[23] A.F. Johnstone, G.W. Gross, D.G Weiss, O.H. Schroeder, A. Gramowski, T.J. Shafe, ‘’Microelectrode arrays: a physiologically based neurotoxicity testing platform for the 21st century’’, *Neurotoxicology*, vol.31, no.4, pp.331-350, Aug.2010. http://dx.doi.org/10.1016/j.neuro.2010.04.001

[24] A. Rolletschek, P. Blyczuk, A.M. Wobus, ‘’Embryonic stem cell-derived cardiac, neuronal and pancreatic cells as model systems to study toxicological effects’’, *Toxicology letters*, vol.149, no.1-3, pp. 361-369, Apr.2004. http://dx.doi.org/10.1016/j.toxlet.2003.12.064

[25] J.E. Kim, M.L O’Sullivan, C.A. Sachez, M. Hwang, M.A. Israel, K. Brennand, T.J. Deerinck, L.S. Goldstein, F.H. Gage, M.H Ellisman, A. Gosh, ’’Investigating synapse formation and function using human pluripotent stem cell-derived neurons’’, *Proc Natl Acad Sci*, vol.108, no.7, pp.3005-3010, Jun.2010. http://dx.doi.org/10.1073/pnas.1007753108

[26] O. Lindvall, Z. Kokaia, ‘’Stem cells for the treatment of neurological disorders’’, *Nature 441*, vol.441, pp.1094-1096, Jun.2006. http://dx.doi.org/10.1038/nature04960

[27] O. Lindvall, Z. Kokaia, ‘‘Stem cells in human neurogenerative disorders – time for clinical translation?’’, *J Clin Invest*, vol.120, no.1, pp.29-40, Jan.2010. http://dx.doi.org/10.1172/JCI40543

[28] Invitrogen. LifeTechnologies. *Introduction to Cell Culture*. [online] Available: http://www.invitrogen.com/site/us/en/home/References/gibco-cell-culture-basics/introduction-to-cell-culture.html [cited 20.8.2012]

[29] G. Vunjak-Novakovic, R.I. Freshney, *Culture of Cells for Tissue Engineering*, 1st Edition, Wiley, 2006. http://dx.doi.org/10.1002/0471741817

[30] D. Purves, G.J. Augustine, D. Fitzpatrick, W.C. Hall, A.-S. Lamantia, J.O. McNamara, L.E. White, *Neuroscience*, 4th Edition, Sunderland, MA, Sinauer Associates Inc.

[31] T.J. Heikkilä, L. Ylä-Outinen, M.A. Tanskanen, R. Suuronen, J.E. Mikkonen, J.A.K. Hyttinen, S. Narkilahti, ‘’Human embryonic stem cell-derived neuronal cells from spontaneously active neuronal networks in vitro’’, *Experimental Neurology*, vol.218, no.1, pp.109-116, Jul.2009. http://dx.doi.org/10.1016/j.expneurol.2009.04.011

[32] M. Taketani, M. Baudry, *Advances in Network Electrophysiology*, Springer, 2006. 478 p.

[33] *Microelectrode Array (MEA) Manual*, Multichannel systems, 2013, [online] Available: http://www.multichannelsystems.com/sites/multichannelsystems.com/files/documents/manuals/MEA_Manual.pdf [cited 3.8.2012]

[34] L. Astolfi, F. De Vico Fallani, F. Cincotti, D. Mattia, M.G. Marciani, S. Salinari, J. Sweeney, G.A. Miller, B. He, ‘’Estimation of Effective and Functional Cortical Connectivity From Neuroelectric and Hemodynamic Recordings’’, *IEEE Transactions on Neural Systems and Rehabilitation Engineering*, vol.17, no.3, pp.224-233, June 2009. http://dx.doi.org/10.1109/TNSRE.2008.2010472

[35] F. Darvas and R.M. Leahy, ‘’Functional Imaging of Brain Activity and Connectivity with MEG’’, *in Handbook of Brain Connectivity*, 1st Edition, Springer, 1999, pp.201-220.

[36] E. Gysels, P. Celka, ‘’Phase Synchronization for the recognition of mental tasks in a brain-computer interface’’, *IEEE Trans. Neural. Syst. Rehabil.Eng*., vol.12, no.4, pp. 406-15, Dec.2004. http://dx.doi.org/10.1109/TNSRE.2004.838443

[37] Y. Wang, B. Hong, X. Gao, S. Gao, ‘’Phase Synchrony Measurement in Motor Cortex for Classifying Single-trial EEG during Motor Imagery’’, *Proceedings of the 28th IEEE EMBS Annual International Conference*, New York City, USA, Aug.-Sept 2006, pp.75-78. http://dx.doi.org/10.1109/IEMBS.2006.259673

[38] L. Astolfi, F. Cincotti, D. Mattia, M.G. Marciani, L.A. Baccala, F. de Vico Fallani, S. Salinari, M. Ursino, M. Zavaglia, L. Ding, J.C. Edgar, G.A. Miller, B. He, F. Babiloni, ‘’Comparison of Different Cortical Connectivity Estimators for High-Resolution EEG Recordings’’, *Human Brain Mapping*, vol.28, no.2, pp.143-157, Feb.2007. http://dx.doi.org/10.1002/hbm.20263

[39] H. Akaike, ‘’A New look at Statistical Model Identification’’, *IEEE Trans Automat Control*, vol.19, no.6, pp.716-723, Dec.1974. http://dx.doi.org/10.1109/TAC.1974.1100705

[40] K.E. Stephan, K.J. Friston, ‘’Models of Effective Connectivity in Neural Systems’’, *in Handbook of Brain Connectivity*, Understanding Complex Systems, Springer, Berlin, 2007, pp.303-327.

[41] B. He, Y. Dai, L. Astolfi, F. Babiloni, H. Yuan, L. Yang, ‘’eConnectome: A Matlab Toolbox for Mapping and Imaging of Brain Functional Connectivity’’, *Journal of Neuroscience*, vol.195, no.2, pp.261-269, Feb.2011. http://dx.doi.org/10.1016/j.jneumeth.2010.11.015

[42] T. Schneider, A. Neumaier, ‘’Algorithm 808: Arfit-a Matlab Package for the Estimation of Parameters and Eigenmodes of Multivariate Autoregressive Models’’, *ACM Trans Math Softw*, vol.27, no.1, pp.58-65, Mar.2001. http://dx.doi.org/10.1145/382043.382316

[43] K.J. Blinowska, ‘’Review of the Methods of Determination of Directed Connectivity from Multichannel Data’’, *Med Biol Eng Comp*, vol.49, no.5, pp.521-529, May.2011. http://dx.doi.org/10.1007/s11517-011-0739-x

[44] B. Schelter, J. Timmer, M. Eichler, ‘’Assessing the Strength of Directed Influences Among Neural Signals Using Renormalized Partial Directed Coherence’’, *J Neurosci Methods*, vol.179, no.1, pp.121-130, Apr. 2009. http://dx.doi.org/10.1016/j.jneumeth.2009.01.006

[45] M. Arnold, W.H.R. Miltner, H. Witte, R. Bauer, C. Braun, ‘’Adaptive AR Modeling of Nonstationary Time Series by Means of Kalman Filtering’’, *IEEE Transactions of Biomedical Engineering*, vol.45, no.5, pp.553-562, May.1998. http://dx.doi.org/10.1109/10.668741

[46] A. Schlögl, *Time Series Analysis - a Toolbox for the use with Matlab*. 1996-2002. [online] Available: http://biosig-consulting.com/matlab/tsa/

[47] A. Maccione, M. Garofalo, T. Nieus, M. Tedesco, L. Berdondini, S. Martinoia, ‘’Multiscale Functional Connectivity Estimation on Low-Density Neuronal Cultures Recorded by High-Density CMOS Micro Electrode Arrays’’, *Journal of Neuroscience Methods*, vol.207, no.2, pp.161-171, Jun.2012. http://dx.doi.org/10.1016/j.jneumeth.2012.04.002

[48] K. Jöreskog, D. Sörbom, (2002, Dec.) *LISREL 8.53*. Scientific Software International, Inc.,[online]. Available: http://www.ssicentral.com

[49] L.L. Bologna, V. Pasquale, M. Garofalo, M. Gandolfo, P.L. Baljon, A. Maccione, S. Martinoia, M. Chiappalone, ‘’Investigating Neuronal Activity by SPYCODE Multi-Channel Data Analyzer’’, *Neural Networks*, vol.23, no.6, pp.685-697, Aug.2010. http://dx.doi.org/10.1016/j.neunet.2010.05.002

[50] A. Borst, F.E. Theunissen, ‘’Information Theory and Neural Coding’’, *Nature Neuroscience*, vol.2,no.11, pp. 947-957, Nov.1999. http://dx.doi.org//10.1038/14731

[51] M. Lindner, R. Vicente, V. Priesemann, M. Wibral, ‘’TRENTOOL: A Matlab Open Source Toolbox to Analyze Information Flow in Time Series Data With Transfer Entropy’’, *BMC Neuroscience* , vol.12, no.119. http://dx.doi.org/10.1186/1471-2202-12-119

[52] Biomedical Functional Imaging and Neuroengineering laboratory, University of Minnesota, *eConnectome*, [online] Available: http://econnectome.umn.edu/ [cited 13.07.2012]

[53] *MEATools*. MATLAB tools for the analysis of multi-neuronal data recorded with multi-electrode arrays. Version 2.8. [online] Available: http://material.brainworks.uni-freiburg.de/research/meatools/ [cited 13.07.2012]

[54] *MEABench*. Wagenaar’s MEABench: Multi-electrode data acquisition and analysis. [online] Available: http://www.its.caltech.edu/~daw/meabench/ [cited 13.07.2012]

[55] *Brain Connectivity Toolbox*. [online] Available: https://sites.google.com/a/brain-connectivity-toolbox.net/bct/Home [cited 13.07.2012]

[56] *BSMART: A Matlab/C Toolbox for Analyzing Brain Circuits*. [online] Available: http://www.brain-smart.org/ [cited 13.07.2012]

[57] *FIND – Finding Information in Neuronal Data. An open-source analysis toolbox for multiple-neuron recordings and network simulations.* [online] Available: http://find.bccn.uni-freiburg.de/?n=Main.HomePage [cited 13.07.2012]

[58] M. Rubinov, O. Sporns, ''Complex Network Measures of Brain Connectivity: Uses and Interpretations'', NeuroImage, *Computational Models of the Brain*, vol.52, no.3, pp.1059-1069, Sep.2010. http://dx.doi.org/10.1016/j.neuroimage.2009.10.003

[59] D. Zhou, W.K. Thompson, G. Siegle, ''Matlab Toolbox for Functional Connectivity, *NeuroImage*, vol.47, no.4, pp.1590-1607, Oct.2009. http://dx.doi.org/10.1016/j.neuroimage.2009.05.089

[60] *60-6wellMEA datasheet*, Multichannel systems [online] Available: http://www.multichannelsystems.com/sites/multichannelsystems.com/files/documents/data_sheets/MEA_Layout_60-6wellMEA_Datasheet.pdf

[61] F. Mormann, K. Lehnertz, P. David, C.E. Elger, ''Mean Phase Coherence as a measure for phase synchronization and its application to the EEG of epilepsy patients'', *Physica D: Nonlinear Phenomena*, vol.144, no.3-4, pp.358-369, Oct.2000. http://dx.doi.org/10.1016/S0167-2789(00)00087-7

[62] *surrVFT.m file*, in eMVAR – Extended Multivariate Autoregressive Modelling Toolbox. [online] Available: http://www.science.unitn.it/~nollo/research/sigpro/eMVAR.html [cited 2.4. 2013]

[63] A.K. Seth, ''Granger Causal Connectivity Analysis: A Matlab Toolbox for Granger causal connectivity analysis'', *J Neurosci Methods*, vol.186, no.2, pp.262-273. http://dx.doi.org/10.1016/j.jneumeth.2009.11.020

[64] K. Sameshima. L.A. Baccala. AsymPDC Package 1.0, User Guide. [online] Available: http://www.lcs.poli.usp.br/~baccala/pdc/ [cited 2.4.2013]

[65] B. Schelter, M. Winterhalder, M. Eichler, M. Peifer, B. Hellwig, B. Guschlbauer, C.H. Lücking, R. Dahlhaus, J. Timmer, ''Testing for Directed Influences Among Neural Signals Using Partial Directed Coherence'', *Journal of Neuroscience Methods*, vol.152, no.1-2, pp.210-219, Apr.2006. http://dx.doi.org/10.1016/j.jneumeth.2005.09.001

[66] *TRENTOOL – the Transfer Entropy Toolbox for the Fieldtrip data format*. [online] Available: http://www.trentool.de/ [cited 3.4.2013]

APPENDIX 1: SIMULATED CONNECTIVITY STUDY SIGNALS

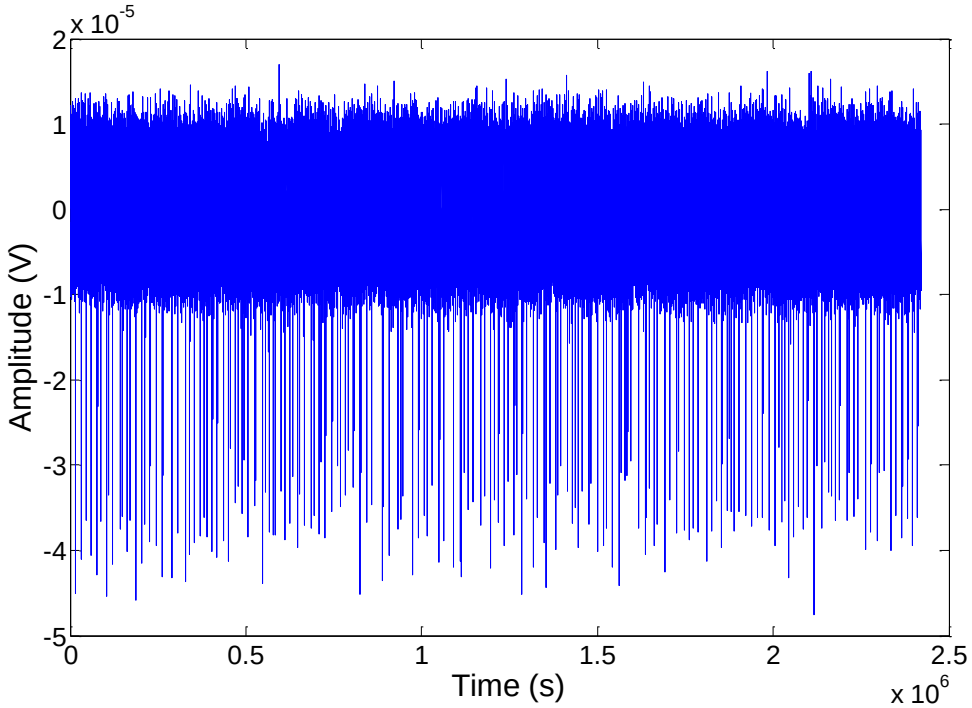

Figure 13. *The time series of Signal 1 in simulated connectivity signal study.*

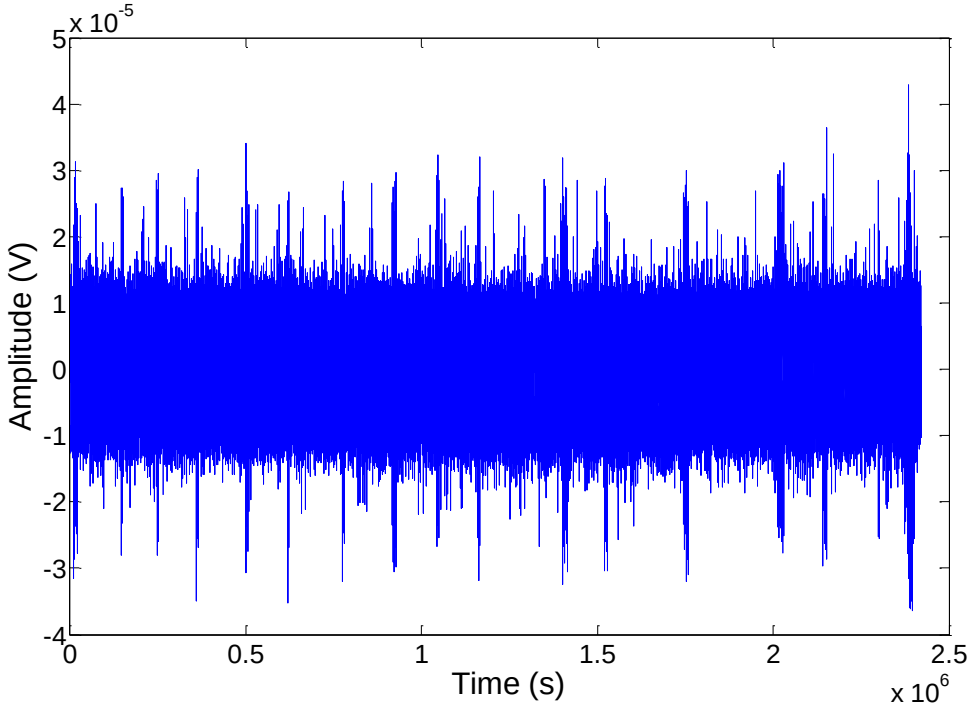

Figure 14. *The time series of Signal 2 in simulated connectivity signal study.*

APPENDIX 2: GRAPHS OF PLV-VALUES OF SIMULATED CONNECTIVITY SIGNAL STUDY

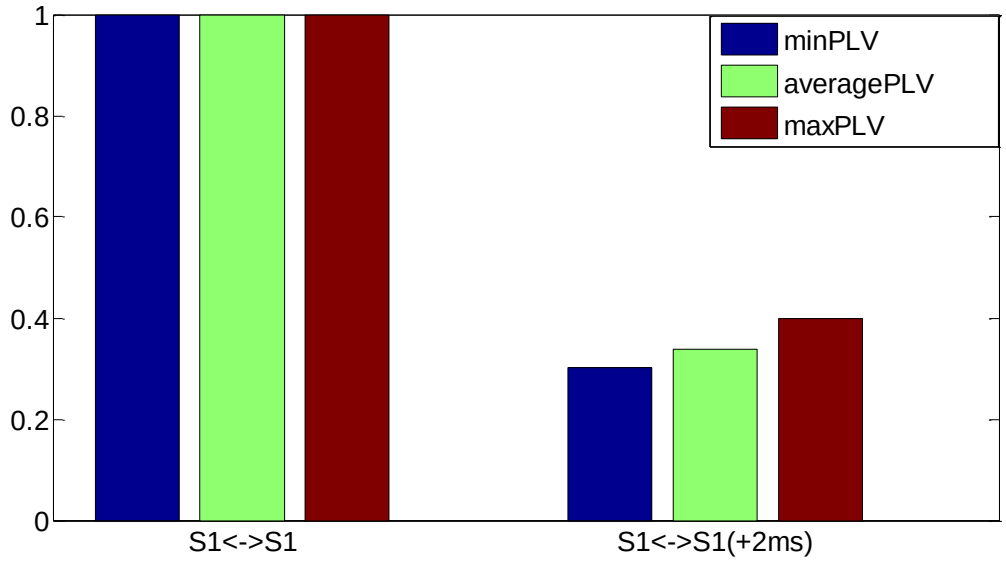

Figure 15. *PLV results of combination 1 in simulated connectivity signal study. Red bars show the Minimum PLV values, green bars refer to the average PLV values and red bars indicate the maximum PLV values.*

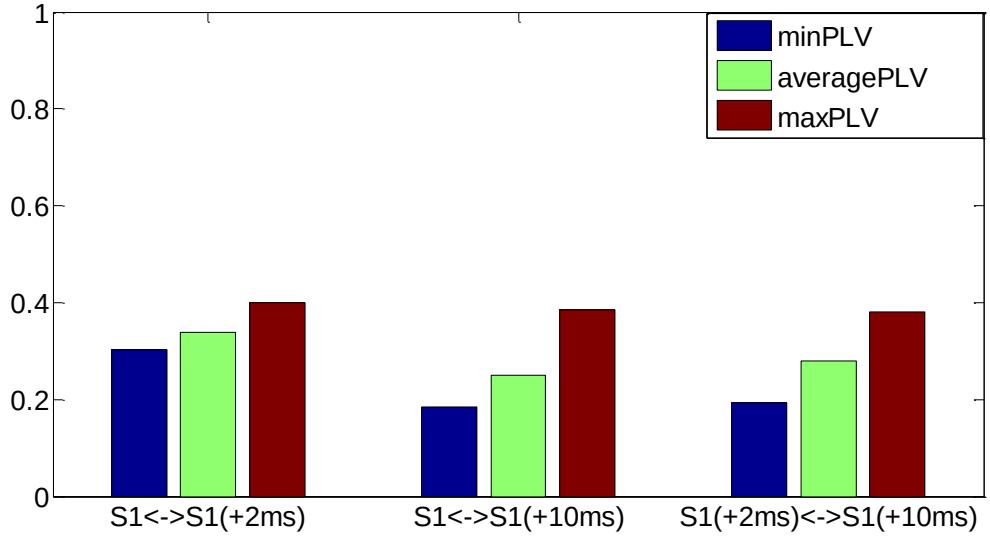

Figure 16. *PLV results of combination 2 in simulated connectivity signal study.*

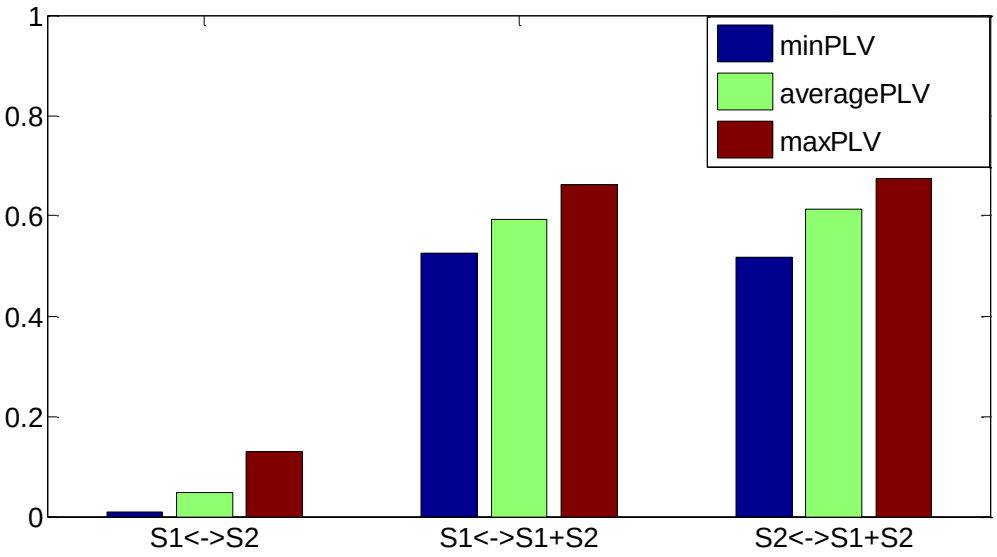

Figure 17. *PLV results of combination 3 in simulated connectivity signal study.*

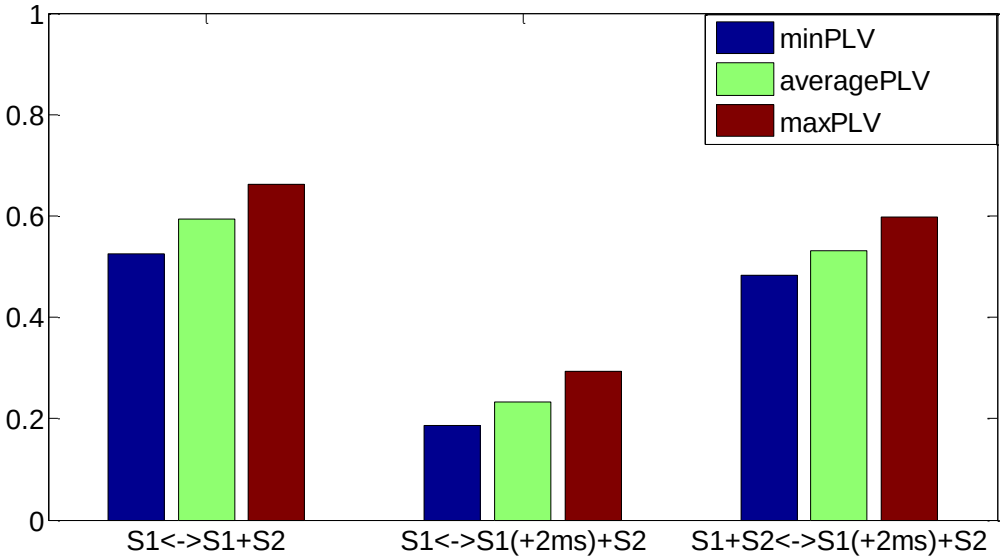

Figure 18. *PLV results of combination 4 in simulated connectivity signal study.*

APPENDIX 3: gPDC RESULTS OF SIMULATED CONNECTIVITY SIGNAL STUDY

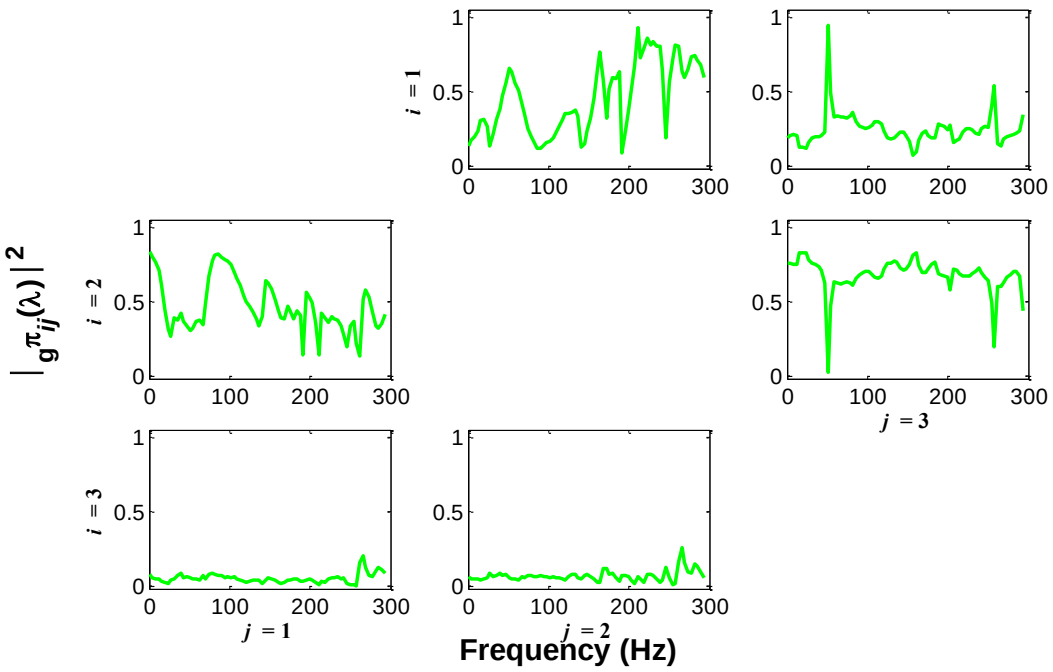

Figure 19. *gPDC results of combination 1(S1 S1 S1(+2ms)) in simulated connectivity signal study. gPDC graphics should be read as if the flow of information is been from the x-axis (j) variable toward y-axis (i) variable. The horizontal axis (0-300) in each small figure refers to the frequency in Hz and the vertical axis (0-1) in each small figure refers to the gPDC value. The alpha level was set to 5% and model order was estimated to be 127.*

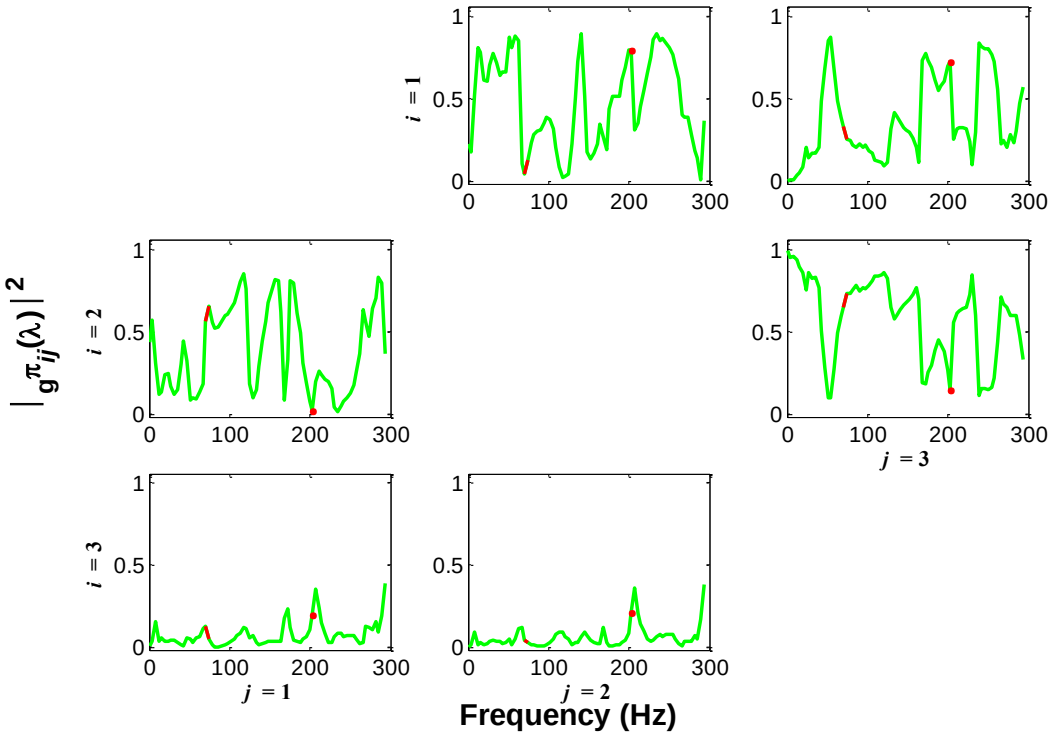

Figure 20. *gPDC results of combination 2(S1 S1(+2ms) S1(+10ms)) in simulated connectivity signal study. The alpha level was set to 5% and model order was estimated to be 168.*

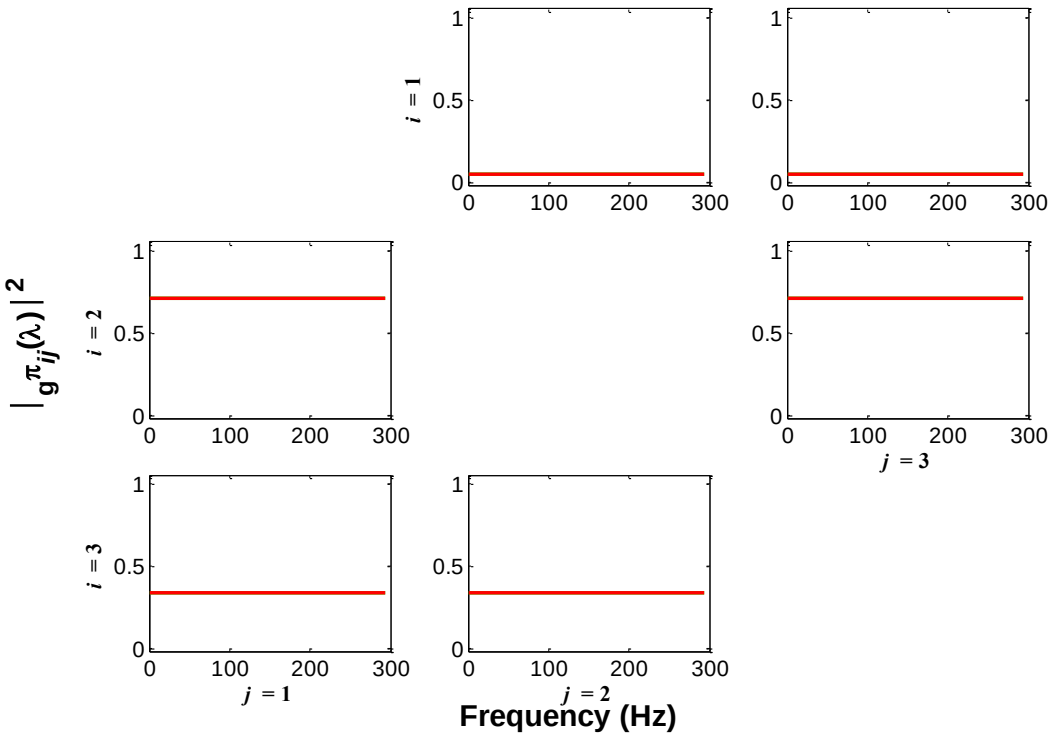

Figure 21. *gPDC results of combination 3(S1 S2 S1+S2) in simulated connectivity signal study. The alpha level was set to 5% and model order was estimated to be 1.*

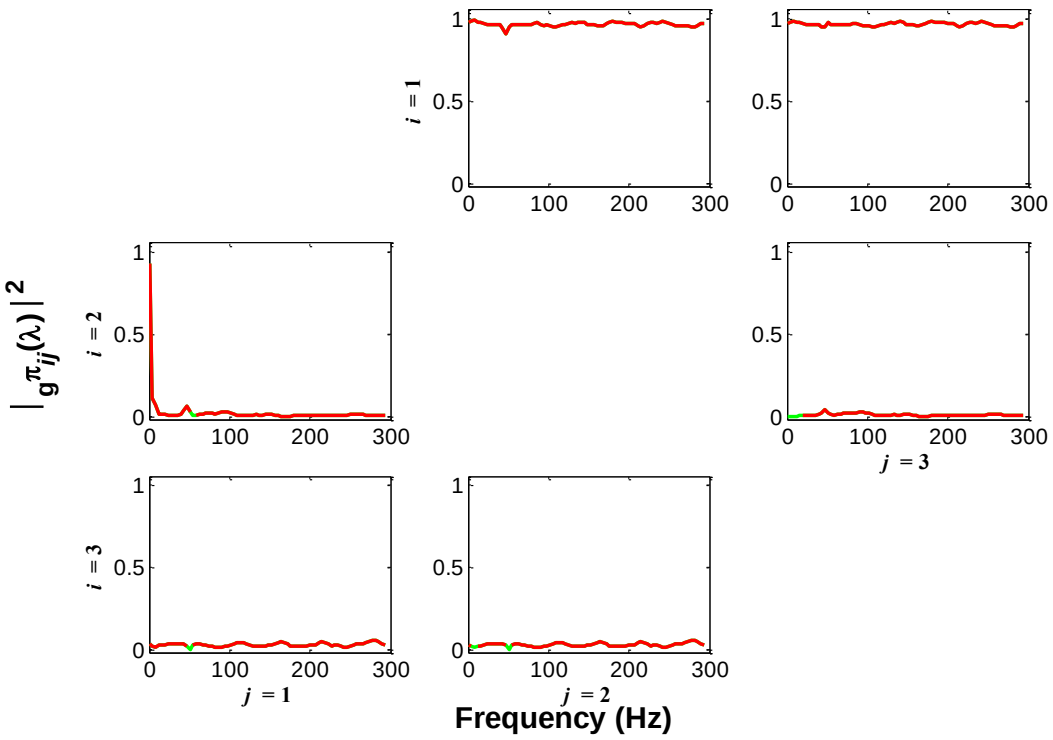

Figure 22. *gPDC results of combination 4 (S1 S1+S2 S1(+2ms)+S2)in simulated connectivity signal study. The alpha level was set to 5% and model order was estimated to be 77.*

APPENDIX 4: AUTOCORRELATION FUNCTIONS OF SIMULATED CONNECTIVITY SIGNAL STUDY

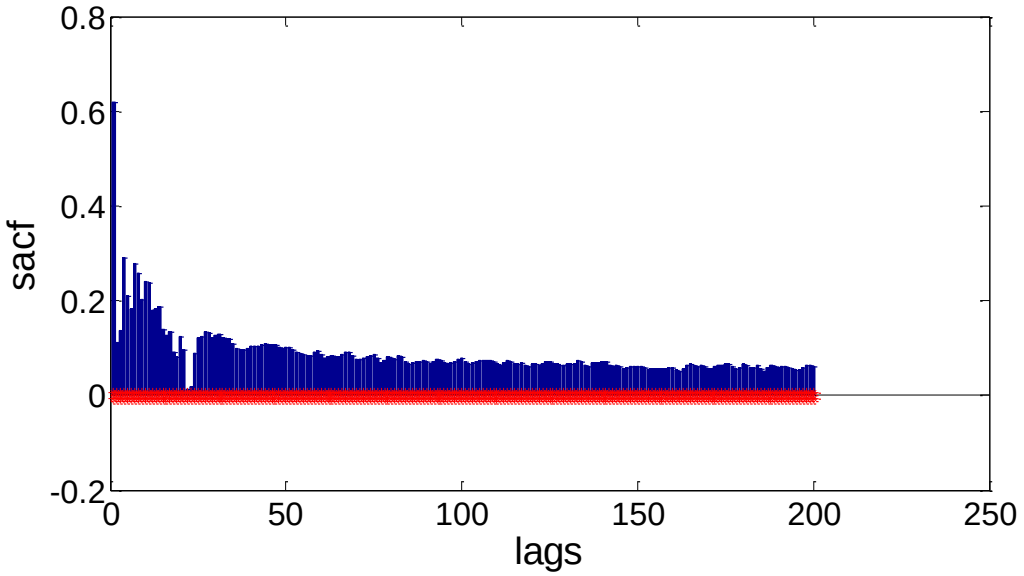

Figure 23. *Autocorrelation function of signal 1 in simulated connectivity signal study. Y-axis shows the autocorrelation function with respect to the amount of lags in x- axis.*

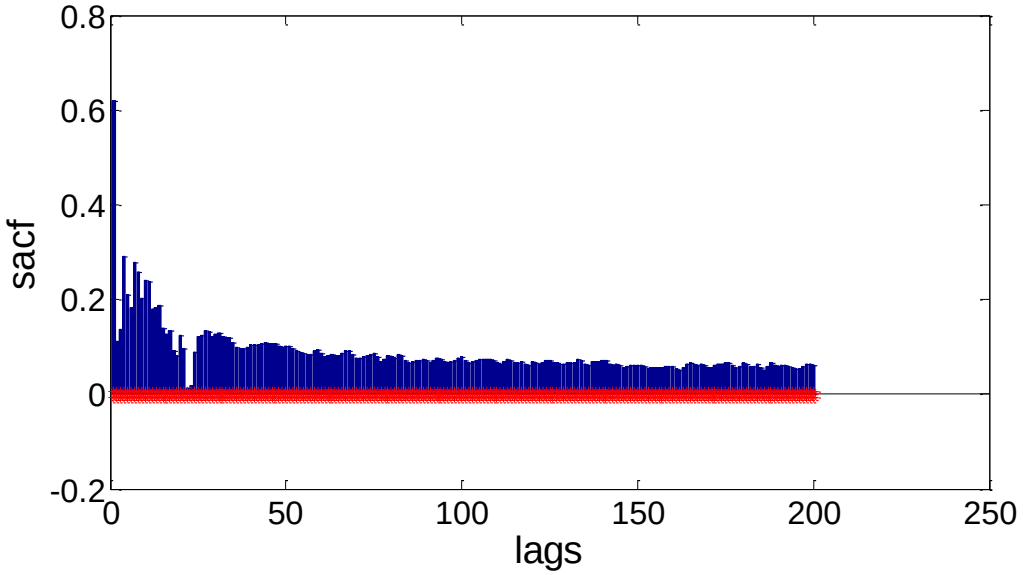

Figure 24. *Autocorrelation function of signal 1(+2ms) in simulated connectivity signal study.*

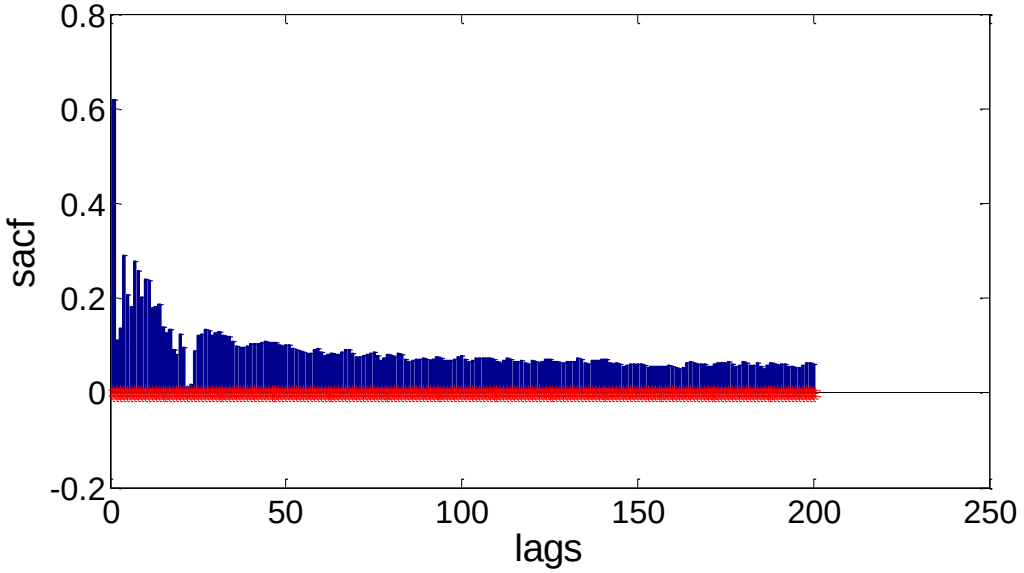

Figure 25. *Autocorrelation function of signal 1(+10ms) in simulated connectivity signal study.*

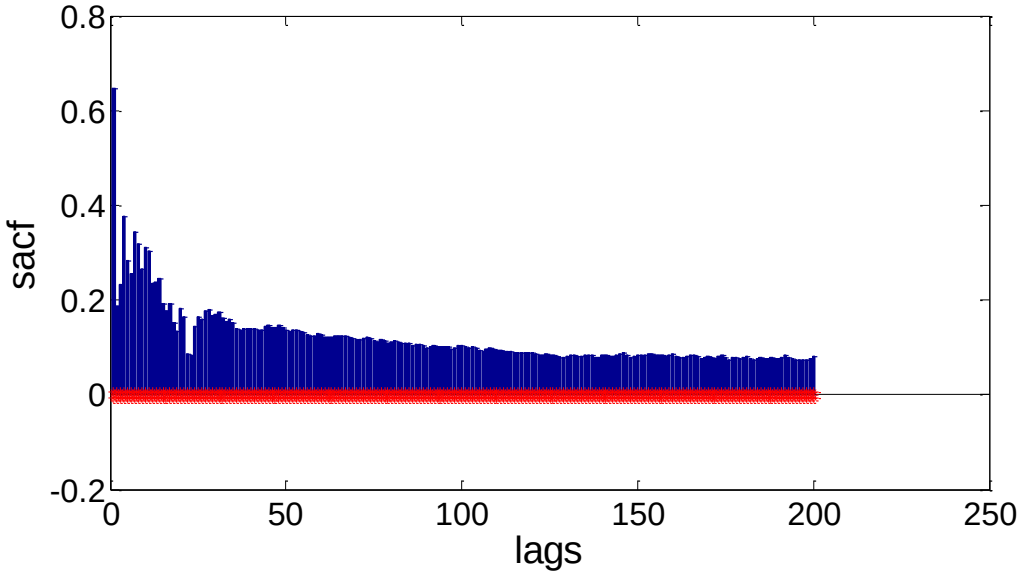

Figure 26. *Autocorrelation function of signal 2 in simulated connectivity signal study.*

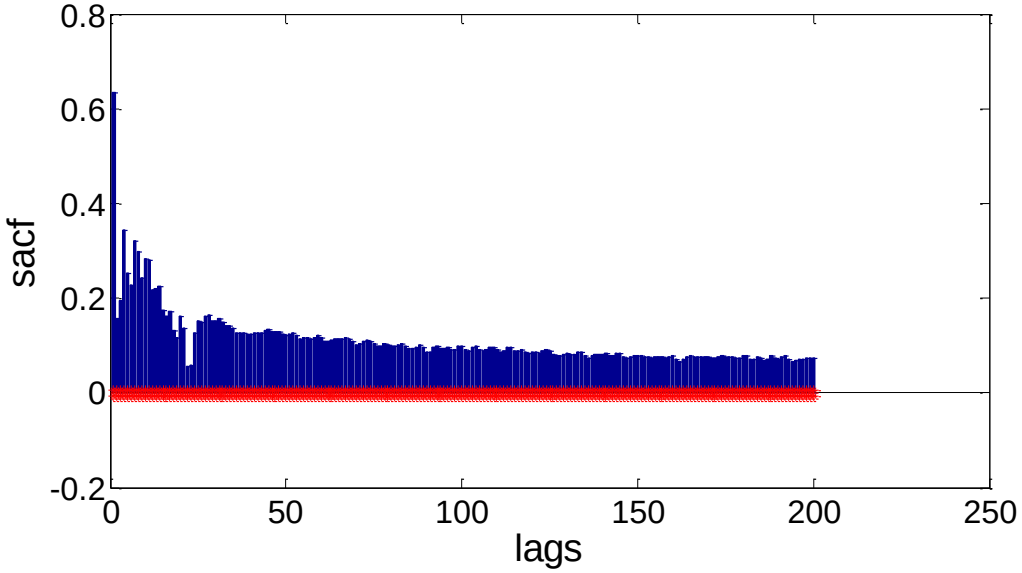

Figure 27. *Autocorrelation function of signals 1 and 2 summed together in simulated connectivity signal study.*

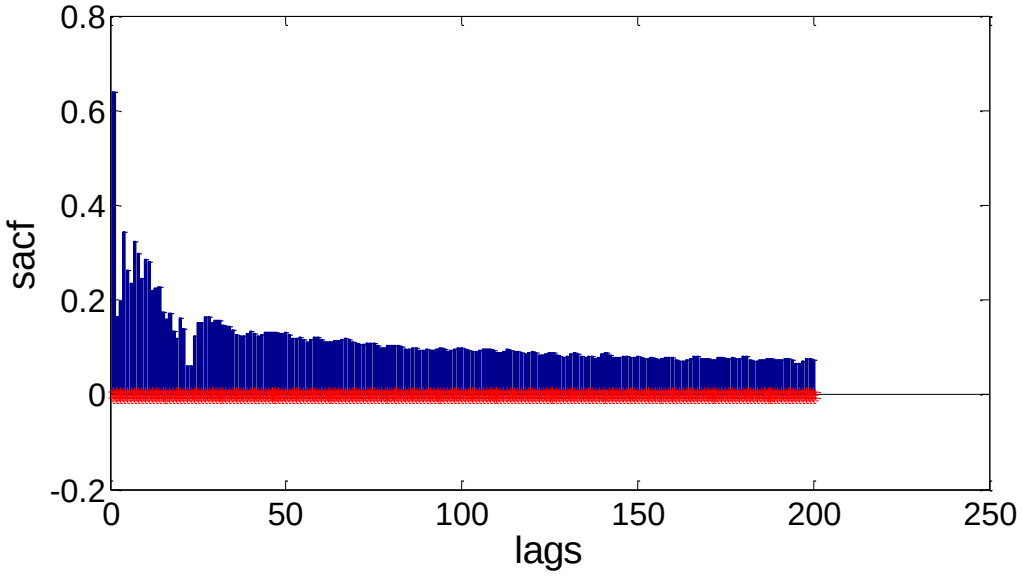

Figure 28. *Autocorrelation function of signals 1(+2ms) and 2 summed together in simulated connectivity signal study.*

APPENDIX 5: PLV RESULTS OF REAL MEA SIGNAL STUDY

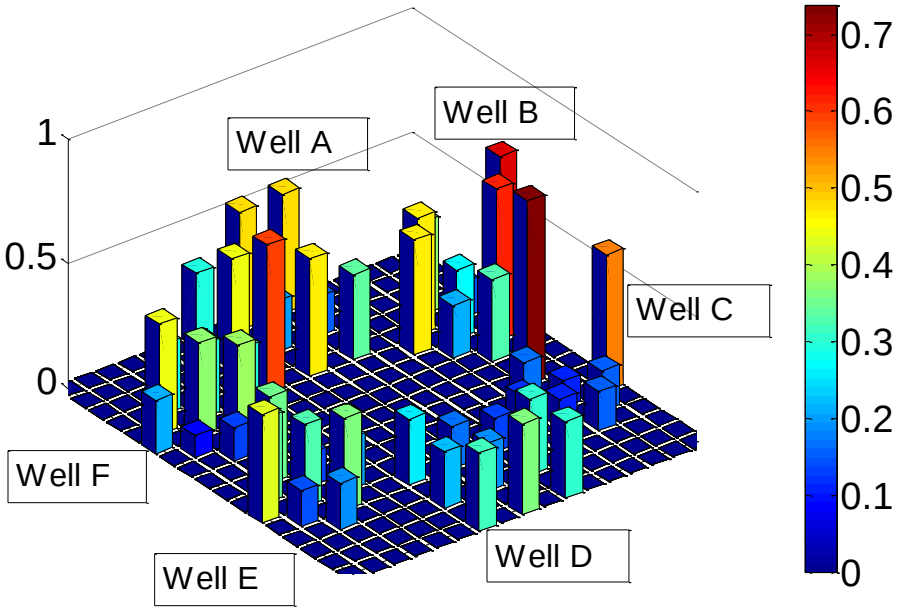

Figure 29. *PLV values for reference channel C4 in bicuculline pharmacological measurement.*

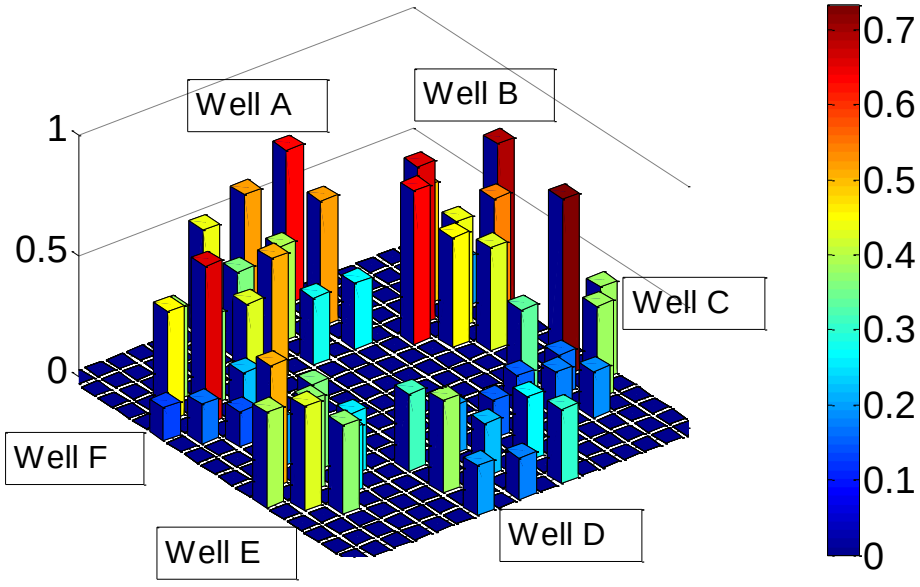

Figure 30. *PLV values for reference channel C4 in cnqx+dap5 pharmacological measurement.*

APPENDIX 6: gPDC RESULTS OF REAL MEA SIGNAL STUDY

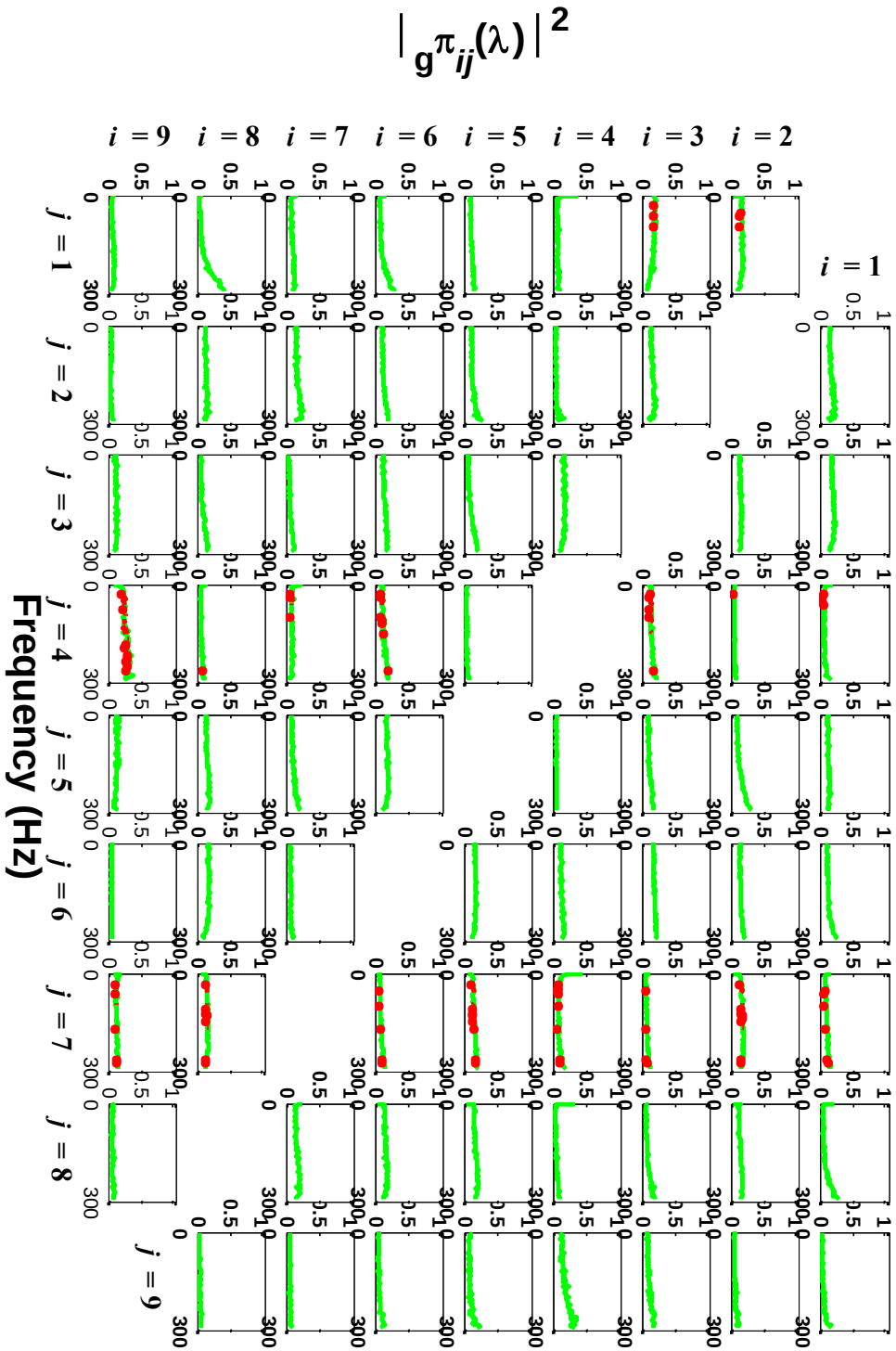

Figure 31. *gPDC results of C well in bicuculline pharmacological measurement.*

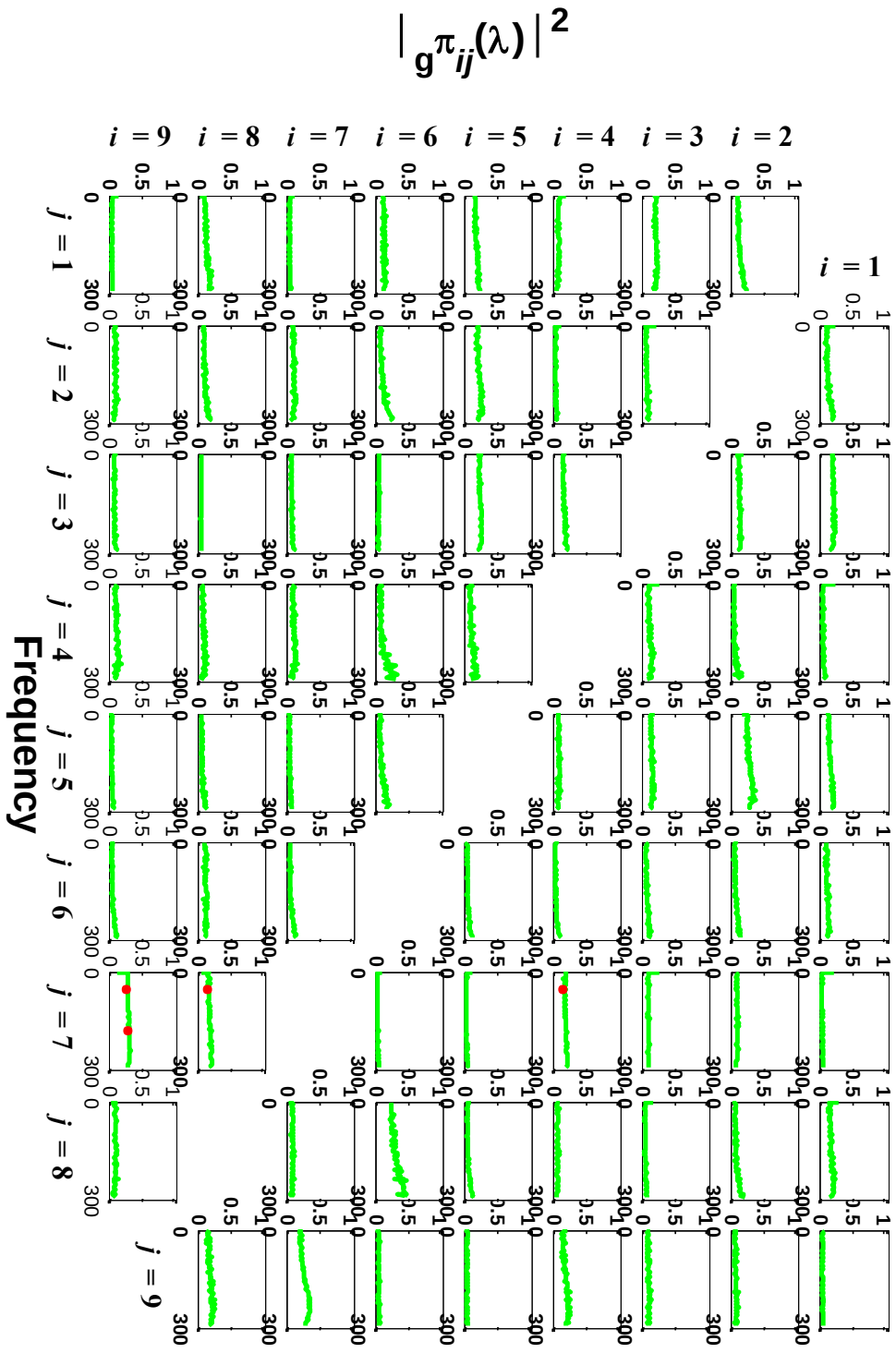

Figure 32. *gPDC results of C well in cnqx+dap5 pharmacological measurement.*

APPENDIX 7: TE RESULTS OF REAL MEA SIGNAL STUDY

Table 10. *Transfer Entropy results of bicuculline pharmacological measurement.*

Signal pairs	p-values	TE-values	Significant connection at alpha level 5%	Significant connection after correction for multiple comparisons	Estimated optimal prediction time
C1->C2	0.0673	0.0112	0	0	1
C1->C3	0.2220	0.0008	0	0	10
C1->C4	0.0078	-0.0745	**1**	0	2
C1->C5	0.0443	-0.0009	**1**	0	5
C1->C6	0.0375	-0.0007	**1**	0	10
C1->C7	0.0598	-0.1112	0	0	3
C1->C8	0.0099	0.0133	**1**	0	6
C1->C9	0.0885	0.0036	0	0	6
C2->C1	0.6950	-0.0153	0	0	8
C2->C3	0.1595	-0.0016	0	0	1
C2->C4	0.2464	-0.0176	0	0	5
C2->C5	0.2065	-0.0027	0	0	7
C2->C6	0.0501	-0.0022	0	0	5
C2->C7	0.6068	-0.0172	0	0	6
C2->C8	0.3247	-0.0069	0	0	7
C2->C9	0.0194	-0.0014	**1**	0	9
C3->C1	0.1265	-0.0042	0	0	6
C3->C2	0.0187	-0.0004	**1**	0	8
C3->C4	0.4174	-0.0120	0	0	5
C3->C5	0.0311	-0.0018	**1**	0	10
C3->C6	0.0901	-0.0035	0	0	1
C3->C7	0.0599	-0.0066	0	0	10
C3->C8	0.2712	-0.0050	0	0	9
C3->C9	0.0749	-0.0024	0	0	2
C4->C1	0.1699	-0.0902	0	0	2
C4->C2	0.1328	0.0110	0	0	6
C4->C3	0.0765	-0.0001	0	0	8
C4->C5	0.2122	-0.0008	0	0	1
C4->C6	0.0713	-0.0023	0	0	3
C4->C7	0.0003	-0.0602	**1**	0	2
C4->C8	0.1705	-0.0230	0	0	7

Table 10. *Transfer Entropy results of bicuculline pharmacological measurement. (Cont'd.)*

C4->C9	0.2056	0.0018	0	0	9
C5->C1	0.2195	-0.0041	0	0	5
C5->C2	0.1362	-0.0045	0	0	9
C5->C3	0.3400	-0.0033	0	0	2
C5->C4	0.4573	-0.0127	0	0	10
C5->C6	0.2967	-0.0031	0	0	5
C5->C7	0.3234	-0.0084	0	0	3
C5->C8	0.0314	-0.0057	**1**	0	8
C5->C9	0.0949	-0.0023	0	0	2
C6->C1	0.1417	-0.0035	0	0	1
C6->C2	0.2133	-0.0041	0	0	4
C6->C3	0.1117	-0.0038	0	0	7
C6->C4	0.4079	-0.0129	0	0	4
C6->C5	0.0064	-0.0027	**1**	0	5
C6->C7	0.0472	-0.0064	**1**	0	9
C6->C8	0.3769	-0.0059	0	0	10
C6->C9	0.0462	-0.0042	**1**	0	2
C7->C1	0.5444	-0.0880	0	0	4
C7->C2	0.1239	0.0111	0	0	3
C7->C3	0.0116	-0.0011	**1**	0	4
C7->C4	0.0128	-0.0572	**1**	0	2
C7->C5	0.0068	0.0012	**1**	0	5
C7->C6	0.1294	0.0018	0	0	9
C7->C8	0.0572	-0.0042	0	0	1
C7->C9	0.2503	0.0013	0	0	5
C8->C1	0.3813	-0.0443	0	0	3
C8->C2	0.1148	0.0056	0	0	9
C8->C3	0.0858	-0.0014	0	0	2
C8->C4	0.4567	-0.0508	0	0	5
C8->C5	0.0189	-0.0013	**1**	0	10
C8->C6	0.2261	-0.0025	0	0	10
C8->C7	0.2235	-0.0396	0	0	8
C8->C9	0.3897	-0.0021	0	0	7
C9->C1	0.0602	-0.0050	0	0	5
C9->C2	0.0276	-0.0041	**1**	0	3
C9->C3	0.2752	-0.0031	0	0	2
C9->C4	0.0925	-0.0093	0	0	2
C9->C5	0.1985	-0.0029	0	0	7
C9->C6	0.1684	-0.0041	0	0	10
C9->C7	0.2324	-0.0087	0	0	7
C9->C8	0.1298	-0.0051	0	0	5

Table 11. *Transfer Entropy results of cnqx+dap5 pharmacological measurement.*

Signal pairs	p-values	TE-values	Significant connection at alpha level 5%	Significant connection after correction for multiple comparisons	Estimated optimal prediction time
C1->C2	0.1545	0.0044	0	0	2
C1->C3	0.0636	-0.0006	0	0	3
C1->C4	0.0911	-0.0300	0	0	8
C1->C5	0.1667	0.0002	0	0	3
C1->C6	0.0660	-0.0003	0	0	6
C1->C7	0.4791	-0.0335	0	0	1
C1->C8	0.0315	0.0093	**1**	0	8
C1->C9	0.0091	0.0005	**1**	0	1
C2->C1	0.3721	-0.0036	0	0	9
C2->C3	0.1293	-0.0018	0	0	9
C2->C4	0.3931	-0.0081	0	0	1
C2->C5	0.1552	-0.0026	0	0	4
C2->C6	0.1326	-0.0039	0	0	4
C2->C7	0.0501	-0.0082	0	0	4
C2->C8	0.3551	-0.0030	0	0	9
C2->C9	0.3249	-0.0040	0	0	4
C3->C1	0.1187	-0.0044	0	0	6
C3->C2	0.2383	-0.0034	0	0	8
C3->C4	0.0631	-0.0036	0	0	8
C3->C5	0.0689	-0.0013	0	0	2
C3->C6	0.0515	-0.0040	0	0	1
C3->C7	0.1160	-0.0037	0	0	1
C3->C8	0.3439	-0.0056	0	0	7
C3->C9	0.0271	-0.0028	**1**	0	8
C4->C1	0.7138	-0.0205	0	0	5
C4->C2	0.0262	0.0115	**1**	0	3
C4->C3	0.5049	-0.0021	0	0	3
C4->C5	0.2186	-0.0014	0	0	8
C4->C6	0.1122	-0.0012	0	0	6
C4->C7	0.00002	0.0012	**1**	0	2
C4->C8	0.2292	0.0124	0	0	8
C4->C9	0.0489	-0.0011	**1**	0	9
C5->C1	0.1149	-0.0033	0	0	2
C5->C2	0.1187	-0.0022	0	0	4
C5->C3	0.0958	-0.0021	0	0	4

Table 11. *Transfer Entropy results of cnqx+dap5 pharmacological measurement. (Cont'd.)*

C5->C4	0.1387	-0.0039	0	0	4
C5->C6	0.3123	-0.0026	0	0	6
C5->C7	0.2098	-0.0055	0	0	4
C5->C8	0.0748	-0.0034	0	0	4
C5->C9	0.00004	0.0002	**1**	0	1
C6->C1	0.3513	-0.0055	0	0	2
C6->C2	0.0203	-0.0008	**1**	0	10
C6->C3	0.2283	-0.0056	0	0	7
C6->C4	0.1284	-0.0036	0	0	2
C6->C5	0.1280	-0.0037	0	0	6
C6->C7	0.0730	-0.0047	0	0	6
C6->C8	0.2066	-0.0013	0	0	4
C6->C9	0.1712	-0.0040	0	0	2
C7->C1	0.5205	-0.0102	0	0	7
C7->C2	0.0272	0.0110	**1**	0	6
C7->C3	0.4226	-0.0011	0	0	1
C7->C4	0.0224	-0.0367	**1**	0	3
C7->C5	0.0203	-0.0008	**1**	0	8
C7->C6	0.0147	-0.0015	**1**	0	9
C7->C8	0.1841	0.0128	0	0	8
C7->C9	0.1251	-0.0013	0	0	7
C8->C1	0.3145	-0.0098	0	0	3
C8->C2	0.1998	0.0003	0	0	5
C8->C3	0.1356	-0.0018	0	0	10
C8->C4	0.6141	-0.0219	0	0	6
C8->C5	0.4215	-0.0025	0	0	8
C8->C6	0.0407	-0.0035	**1**	0	1
C8->C7	0.8252	-0.0225	0	0	2
C8->C9	0.0030	-0.0008	**1**	0	5
C9->C1	0.1759	-0.0060	0	0	6
C9->C2	0.0347	-0.0030	**1**	0	2
C9->C3	0.0948	-0.0016	0	0	8
C9->C4	0.1699	-0.0047	0	0	4
C9->C5	0.2406	-0.0043	0	0	9
C9->C6	0.2072	-0.0038	0	0	9
C9->C7	0.0607	-0.0022	0	0	4
C9->C8	0.0300	-0.0022	**1**	0	4